UNIVERSITY OF CALIFORNIA
RIVERSIDE

Polydiacetylene-Based Colorimetric Sensors for Plant Diagnostics

A Dissertation submitted in partial satisfaction
of the requirements for the degree of

Doctor of Philosophy

in

Bioengineering

by

Jessica Tsai Wen

June 2016

Dissertation Committee:
Dr. Hideaki Tsutsui, Chairperson
Dr. Valentine Vullev
Dr. Caroline Roper

The Dissertation of Jessica Tsai Wen is approved:

Committee Chairperson

University of California, Riverside

ACKNOWLEDGEMENTS

First and foremost, I would like to express my deepest gratitude for my advisor, Dr. Hideaki Tsutsui, for his unwavering guidance as my research mentor. Under his direction, I have learned how to become a true scientific researcher, both inside and outside of the laboratory. Specifically, he has taught me the significance of producing quality research results for scientific contribution, and the importance of communicating my research successfully, through written journal articles and proposals as well as oral presentations. He was the first person I knew from the Bourns College of Engineering at UCR. He took me in as a master's student despite my non-traditional career goals, and has stood by me through my ups, downs, and all of my odd transitions in-between. He has been constructive and supportive throughout the entirety of my graduate school experience and has been paramount in my success. I would not be who I am or where I am today without him.

I would like to give special thanks to my committee members, Dr. Valentine Vullev (Dept. of Bioengineering) and Dr. Caroline Roper (Dept. of Plant Pathology). More than a committee member, Dr. Vullev has also been my graduate student advisor. He has never failed to provide me with the advice and encouragement that I needed to stay on track and has always made time to have conversations with me despite his busy schedule. I have learned a lot from the wisdom he shares through his worldly experiences and I could not be more grateful to have his guidance both in research and in life.

I am also deeply indebted to Dr. Roper for her expertise and advice in the field of plant pathology. My research would not have been possible without her intellectual

contributions and assistance in the laboratory through her graduate students. Our discussions regarding the design of my sensors for plant diagnostics have molded their development and I am greatly appreciative for her steady and open communication with us.

I would additionally like to express my gratitude towards my laboratory colleagues Mr. Carlos Castro, Mr. Brent Kalish, and Mr. Daniel Nampe for their invaluable contributions to my work. I have become a better researcher through working with them and they have kept me sane these past years. Furthermore, I would like to thank my colleagues from collaborating laboratory groups, Ms. Jillian Larsen (Vullev Lab, Dept. of Bioengineering), Ms. Elizabeth Luscher (Springer Lab – Plant Cell Biology), Mr. Brian Ingel (Roper Lab, Dept. of Plant Pathology), and Mr. Polrit Viravathana (Roper Lab, Dept. of Plant Pathology). Their assistance and expertise in their fields has been instrumental in the progression of my research.

In addition, I would like to thank Dr. Dan Borchardt for his training in the use of NMR instrumentation, Mr. Douglas Holt for his guidance with growing corn, and Mr. Hung Duy Lai for his assistance with our maize plants in the greenhouse.

This work has been supported by the Bill and Melinda Gates Foundation through the Grand Challenges Explorations Program (grant #: OPP1059995) and the UCR Research and Economic Development Collaborative Seed Grant. Access to NMR facilities was provided by the UC Riverside Analytical Chemistry Instrumentation Facility. Greenhouse space was provided through the UC Riverside Department of Agricultural Operations. Studies from Chapters 4 and 6 have been previously published

in *Sensors and Actuators, B: Chemical* (doi: 10.1016/j.snb.2016.03.118) and the *Journal of Laboratory Automation* (doi: 10.1177/2211068214551826) respectively.

DEDICATION

This dissertation is dedicated to my parents, Chris and Tina Wen, my brothers and sister, Jeff, Christina and Alston, and my 啊公 (grandpa). Thank you for being my rock, my motivation and never doubting me.

ABSTRACT OF THE DISSERTATION

Polydiacetylene-Based Colorimetric Sensors for Plant Diagnostics

by

Jessica Tsai Wen

Doctor of Philosophy, Graduate Program in Bioengineering
University of California, Riverside, June 2016
Dr. Hideaki Tsutsui, Chairperson

The Food and Agriculture Organization of the United Nations (FAO) estimates that 98% of the world's reported 870 million undernourished people reside in developing countries, where nearly 15% of the population are undernourished. In these regions, smallholder farmers are dominant factors in meeting food demands. Therefore, in order to alleviate recurrent food shortages worldwide, low-cost and robust solutions must be provided to protect and prevent the loss of smallholder crop yield. This research reports on the development of *in vitro* and *in vivo* diagnostic devices for in-field crop diagnostics. In particular, we employ chromatic polydiacetylenes in the fabrication of analyte-sensitive strips for plant testing *in vitro*. Specifically, two sets of strips were developed that exhibited blue to pink/red transitions when incubated in solutions containing plant nutrient, Zn^{2+}, or xylem-limited bacterium, *X. fastidiosa* respectively. These strips demonstrated one-step, equipment-free detection appropriate for resource-limited settings. Additionally, a poof-of-concept *in vivo* detection platform was evaluated and

subsequently, injectable poydiacetylene liposome sensors were designed for specific colorimetric detection of apoplast-colonizing bacterium *P. stewartii*. An *in vivo* detection system would provide continuous monitoring of plant pathogen transmission for early detection of crop diseases. Such a platform would be ideal for disease prevention and management on smallholder farms by eliminating the need for user-initiated testing for disease diagnostics. Both of our *in vitro* and *in vivo* detection systems provide great potential to improve in-field plant diagnostics in low-resource settings.

TABLE OF CONTENTS

List of Figures

List of Tables

CHAPTER 1:

INTRODUCTION

1. SIGNIFICANCE

With the world population expected to exceed 9 billion by the year 2050, the need to increase food production by 50-70% over the next few decades has become one of the most pressing issues of this century [2-4]. One key approach involves the development of new technologies to improve crop protection and yields from smallholder farms, which have played a historically significant role in meeting global food demands [1]. Particularly, one solution to increase smallholder yields is to facilitate the early detection of crop diseases [5]. More specifically, the introduction of low-cost, in-field sensing devices would offer rapid diagnostic information in low-resource settings and enable effective crop management strategies, especially for smallholder farmers.

Early diagnosis of plant diseases can prevent the spread of disease to the remaining crop. Standard methodologies in plant diagnostics range from the physical examination of symptoms to the use of molecular diagnostics such as enzyme-linked immunosorbent assay (ELISA) or polymerase chain reaction (PCR) [6, 7]. ELISA and PCR offer high sensitivity and specificity; however, both of these approaches require expensive laboratory facilities and trained operators. On the other hand, physical examination can only offer a diagnosis well past the onset of pathogenic infection. Ideal diagnostic tools would provide disease information early and without the need for bulky equipment.

Plant pathogenic bacteria are a one of the major causes of crop diseases both pre- and post-harvest [5]. In particular, these pathogens can be characterized by the type of plant tissue they colonize [8]. Specifically, endogenous bacteria colonize the phloem or

xylem tissues of plants [9]. Such bacterial pathogens are often restricted to these tissues due to their environmental requirements for proliferation [8, 9]. Contrastingly, exogenous bacteria primarily colonize the apoplast of plant tissue [9, 10]. These bacteria are found in the intercellular spaces of plant organs including the leaves [10]. In the development diagnostic tools for plant pathogenic bacteria, it is critical to acknowledge the spatial movement of the pathogen in the host organism to design devices suited for their detection. This research focuses on the fabrication of detection platforms for both endogenous and exogenous bacteria. In particular, endogenous bacterium, *Xylella fastidiosa,* and exogenous bacterium, *Pantoea Stewartii,* were detected as model pathogens for each type of bacterial pathogen respectively.

More specifically, these studies employ the colorimetric properties of polydiacetylenes (PDA) for the development of *in vitro* and *in vivo* tools for plant diagnostics. For the *in vitro* platform, we report 'dipstick' type sensor strips for naked-eye detection of plant nutrient, Zn^{2+}, and xylem-limited bacterium, *X. fastidiosa* (Chapters 3 and 4). The strip is composed of a self-assembled PDA coated on an inert membrane. Interactions between a detection probe conjugated to the PDA and target analyte in solution caused changes in strip color that were readily discernable by the naked eye (Figure 1.1A).

Additionally, we report the ongoing development of an *in vivo* detection system for of apoplast-colonizing bacterium, *P. stewartii*, the causal agent of Stewart's wilt in sweet corn [11] (Chapters 5 and 6). This proposed platform employs a minimally invasive, needleless syringe infiltration procedure [12] to introduce and immobilize

pathogen-responsive PDA liposomes into the maize leaf intercellular space (Figure 1.1B). The success of this approach will enable continuous monitoring of pathogen levels *in vivo* for early disease diagnosis that is readily visible to the naked eye.

2. FIGURES

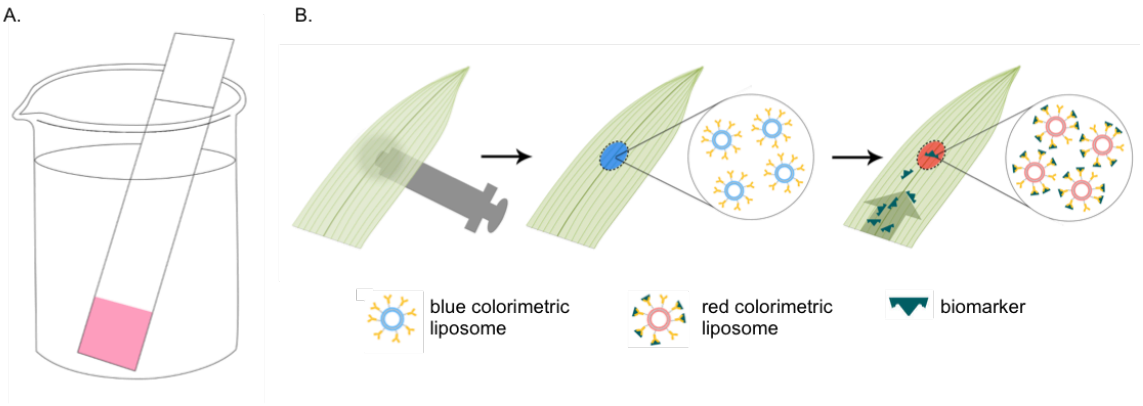

Figure 1.1. Research overview. (A) Diagnostic strips dipped in solutions of processed diseased plant materials results in blue (not shown) to pink/red color changes discernable by the naked eye. The colored region is coated with detection probe-conjugated PDA. (B) Schematic process of *in vivo* lateral flow pathogen detection by injected PDA liposomes conjugated with detection probe.

References

[1] The State of Food Insecurity in the World 2012, Food and Agriculture Organisation of the United Nations (FAO), Rome, 2012.

[2] Declaration of the World Summit on Food Security, Food and Agriculture Organisation of the United Nations (FAO) Rome, 2009.

[3] T. Lang, D. Barling, Food security and food sustainability: reformulating the debate, *Geogr J*, 178(2012) 313-26.

[4] D. Tilman, K.G. Cassman, P.A. Matson, R. Naylor, S. Polasky, Agricultural sustainability and intensive production practices, *Nature*, 418(2002) 671-7.

[5] R.N. Strange, P.R. Scott, Plant disease: a threat to global food security*, Phytopathol*, 43(2005) 83-116.

[6] A.S. Nezhad, Future of portable devices for plant pathogen diagnosis, *Lab Chip*, 14(2014) 2887-904.

[7] S. Sankaran, A. Mishra, R. Ehsani, C. Davis, A review of advanced techniques for detecting plant diseases, *Comput and Electron Agr*, 72(2010) 1-13.

[8] G.A. Beattie, Plant-associated bacteria: survey, molecular phylogeny, genomics and recent advances, Plant-associated bacteria, Springer 2007, pp. 1-56.

[9] J. Bové, M. Garnier, Phloem-and xylem-restricted plant pathogenic bacteria, *Plant Sci*, 164(2003) 423-38.

[10] J.R. Alfano, A. Collmer, Bacterial pathogens in plants: life up against the wall, The *Plant Cell*, 8(1996) 1683-1698.

[11] M.C. Roper, Pantoea stewartii subsp. stewartii: lessons learned from a xylem‐dwelling pathogen of sweet corn, *Mol Plant Pathol*, 12(2011) 628-37.

[12] J.T. Wen, C. Castro, H. Tsutsui, In Planta Microsphere-Based Lateral Flow Leaf Biosensor in Maize, *J Lab Autom*, 20(2015) 500-505.

CHAPTER 2:

POLYDIACETYLENES

Abstract

The unique chromatic properties of polydiacetylenes have generated much popularity for their use in biosensing applications over the past three decades. In particular, their biochromic characteristics have facilitated the development of label-free biological and chemical detection systems. These range from colloidal suspension of liposome sensors to films, hydrogels, and printed ink. In this chapter, we review the wide range of techniques employed in the development of polydiacetylene sensors and summarize methods to modify, characterize and analyze polydiacetylene-based sensing systems. Additionally, we discuss the recent direction of polydiacetylene materials, outside of sensing applications, as versatile tools for biomedicine and tissue engineering.

1. INTRODUCTION

Polydiacetylenes (PDA) are an amphiphilic class of polymers with highly conjugated backbones that have become increasingly attractive as biosensing materials due to their unique optical and chromatic properties. PDA materials provide a number of advantages attributable to their ease of formation under self-assembly systems. Additionally, the polymerization of diacetylenes (DA) to form PDA commonly occurs via photoreaction. This allows for high purity during synthesis by eliminating un-wanted byproducts frequently produced by chemical initiators. The chromatic properties of PDA arise from its highly structured alternating ene–yne backbone. Upon UV or γ- irradiation, monomers polymerize to appear optically blue and non-emitting. Exposing blue PDA to environmental changes results in a shift in its absorption spectrum from low to high energy resulting in the appearance of optically red PDA that also exhibits red fluorescence. PDA materials have been reported to undergo blue to red transitions in response to various environmental perturbations including changes in pH [1, 2], temperature (thermochromism) [3-5], mechanical stress (mechanochromism) [6, 7], and molecular binding events (affinochromism/biochromism) [8, 9].

The specific biochromism demonstrated by PDA is due to their chemical adaptability. In particular, the hydrophilic heads of DA monomers are easily modified to facilitate their interaction with target molecules. Specifically, by conjugating functional detection probes onto these head groups, chromatic PDA signals in response to specific detection of biomolecules can be generated. PDA systems conjugated with antibodies [10-13], aptamers [14-17], proteins [12, 18, 19], and various functional groups [20, 21]

have been demonstrated. Due to their built-in chromatic conversion, PDA platforms forego the need for costly secondary labels and detection instruments. This extensive adaptability of PDA furthers its potential in label-free biosensing systems.

Since the initial development of PDA films by Wegner in 1969 [22], PDA materials have been prepared in a variety of forms and composed as mixtures with other lipid constituents [23]. Currently, PDA is most commonly synthesized as self-assembled bilayer liposomes in aqueous solutions [13, 20, 24-26]. Recent developments in PDA biosensors have given rise to the immobilization of PDA liposomes on solid substrates, such as microbeads [27] and cellulose membranes [28, 29]. More recent applications have incorporated PDA with host matrices, including sol-gel materials [10, 30-32], fibrous scaffolds [33], graphene sheets [34], and polyvinylidene fluoride membranes [12, 35]. The use of fluorescent red-phase PDA has also been explored in highly sensitive microarray assays and microfluidic chip sensors [15, 36]. The properties and applications of PDA materials have been reviewed and discussed over the years [36-44]. However, as PDA technology progresses, researchers continue to establish a wide array of methods to synthesize and design PDA platforms, and there is a need to tabulate these approaches to better facilitate advancement and prepare new researchers interested in PDA technologies. In this strategic review of PDA materials, we discuss the fundamental properties of PDA and organize the diverse methods of PDA synthesis. This includes compiling the various approaches in conjugating functional materials to PDA and the role of adding external constituents into PDA materials. Additionally, we summarize current techniques used to characterize and quantify color change in PDA sensors. Finally, we

review some of the most recent platforms for PDA systems. This review is targeted for researchers of all scientific backgrounds as both an introduction to and an update on the current state of PDA materials. Due to previous in-depth discussion of PDA sensors as Langmuir-Blodgett (LB) films [41], these will not be discussed in detail here.

2. POLYDIACETYLENES

2.1 Brief History

The first investigation into PDA materials was carried out by Wegner in 1969 [22]. In his initial studies Wegner achieved photopolymerization of bis-(*p*-toluene sulfonate) to create purple DA crystals that transitioned to red after UV polymerization [45]. The application of PDA materials as biosensors was pioneered largely by Charych and colleagues in the early 1990's [9, 40, 46-50]. Most notably, Charych and colleagues demonstrated the blue to red color transitions of sialic acid-conjguated PDA in response to the binding of influenza virus [9]. These early investigations into PDA for biosensing materials resulted in the synthesis of a number of chromatic DAs ranging in color from blue to orange; however 10, 12-pentacosadiynoic acid (PCDA) and 10, 12-tricosadiynoic acid (TCDA) were favored for their stable blue to red color transitions when polymerized in response to molecular binding events [40] (Figure 2.1A). PCDA and TCDA are currently most widely used in PDA applications and are commercially available.

2.2 Properties of Polydiacetylenes

PDA is photosynthesized via 1,4 addition of the diacetylenic moiety of DA monomers by UV irradiation (Figure 2.1B). Due to their amphiphilic structure, DA monomers will naturally align in solution as a result of van der Waals' interactions between the hydrophobic alkyl chains [37, 51]. This is favorable because proper packing and alignment of the DA moiety is required for polymerization to occur [52-54]. Upon 254 nm UV irradiation, PDA supramolecules appear deep blue (A_{max} ~640 nm). The appearance of color in polymerized PDA materials is a result of optical π-π* absorption in the alternating ene-yne conjugated polymer backbone [37, 55]. The exertion of external stimuli to the backbone results in an irreversible shift in absorbance from low to high energy, resulting in the appearance of red-phase PDA (A_{max} ~540 nm) [37].

The mechanism of transition from blue-phase to red-phase PDA remains to be fully elucidated. It is proposed that after photopolymerization, the resulting blue-phase PDA backbone is prevented from adopting a fully relaxed configuration due to geometric restrictions imposed by the hydrophilic head groups. The exertion of environmental stimuli causes fluctuations in the head group configuration thereby disrupting the planarity of the conjugated backbone via rotational changes about the C-C bonds [37, 41] (Figure 2.2). This shifts the π-orbital overlaps causing a blue-shift in the absorption spectrum of the PDA backbone. Red-phase PDA is perceived to be more thermodynamically stable than blue-phase PDA resulting in the irreversible character of PDA transitions [37, 56-58]. This proposed mechanism of transition is supported by the observation of engineered reversible PDA materials, in which the DA head groups are

modified with pendant side-chains to increase H-bonding between head groups after polymerization [59, 60]. This modification stabilized the initial blue-phase configuration of PDA head groups, allowing the backbone to return to blue-phase planarity upon release of external stimuli (e.g., heat and pH treatment) [56]. While the development of reversible PDA materials is another desirable aspect for biosensing solutions, the present review focuses on irreversible PDA materials.

Red-phase PDA exhibits intense fluorescence properties that are not observed in blue-phase PDA. The reason for this is suggested to be an energy shift in the lowest excited state from the blue-phase to the red-phase. In the blue-phase, the lowest excited state exhibits A_g symmetry, a dipole-forbidden transition. In the red-phase, the lowest excited state exhibits B_u symmetry, which allows for radiative decay resulting in fluorescence [37, 61, 62]. Red-phase PDA will emit red fluorescence with emission peaks at approximately 560 and 640 nm [63].

The unique chromogenic and fluorogenic properties of PDA make it a desirable material for biosensing applications. Specifically, its internal "switch" to give a visual output via blue to red color transitions in response to external stimuli make PDA materials especially attractive for user-friendly, in-field, diagnostic applications. This characteristic of PDA enables the production of one-step detection devices, foregoing the need for secondary labels to visualize analyte detection. The additional property of PDA materials to transition from a non-fluorescent to fluorescence-emitting state further lends potential for the development of highly sensitive sensors (e.g., microarrays [15, 64]) and

possibilities for signal amplification (e.g., Resonance Energy Transfer (RET) applications [65, 66]).

3. SYNTHESIS OF POLYDIACETYLENES FOR BIODETECTION

PDA polymers are commonly synthesized from commercially available PCDA and TCDA monomers. In the advancement of PDA technologies, researchers have explored a vast range of methods to tailor PDA materials and enhance their properties. A few examples include approaches to increase their detection sensitivity, biomimetic properties (for PDA liposomes), and to incorporate PDA into various material forms. In this section, we discuss the methods by which researchers have tailored PDA materials for biosensing. For a detailed discussion of the synthesis of PDA films and liposomes, readers are referred to a comprehensive review by Reppy and Pindzola (2007) [41]. The present article instead focuses on PDA modifications to enhance biodetection.

3.1 Synthesis of Polydiacetylene Liposomes

Many recent advancements involve the manipulation of PDA liposomes that are synthesized in colloidal suspension. Due to their amphiphilic nature, DA monomers will form self-assembled bilayer liposomes in aqueous solution. A general procedure for the preparation of PDA liposomes involves first dissolving the DA monomers, along with any other lipid constituents desired, in chloroform to create an even distribution of monomers. If no additives are desired or only one type of DA monomer is being used,

this step may be omitted. Chloroform is then evaporated, often in vacuum, by N_2 airstream, or via rotary evaporation. The resulting mixture is resuspended in deionized water or aqueous buffer and dispersed via sonication at above 60°C, the phase transition temperature (T_m) of DAs. The resulting solution is commonly filtered through a porous membrane to remove any aggregates. In order to promote liposome stability and alignment of the DA backbone, the colloidal suspension is stored at 4°C for at least 4 h. The opaque solution is then irradiated under 254 nm UV light resulting in the appearance of a blue PDA polymer solution. PDA liposome solutions commonly range from 0.5 to 2 mM total lipid concentration, as higher concentrations can cause the liposomes to precipitate out of solution [41].

3.2 Modifications of Polydiacetylenes for Biodetection

While PDA materials are naturally responsive to environmental stimuli, researchers have explored various modifications in order to adapt and enhance the polymer for specific detection of biomolecules (Table 2.1). In this subsection, we review a number of these approaches.

3.2.1 Lipid Doping

The addition of other lipids, most commonly phospholipid dimyristoylphosphocholine (DMPC), to PDA mixtures to form phospholipid/PDA liposomes was first demonstrated by Jelinek and colleagues in the early 2000s [24, 67-71]. In such composite liposomes, DMPC was found to form sub-domains within the PDA membrane and did not inhibit polymerization. While initial investigations of

DMPC/PDA liposomes were for their biomimetic properties in studies involving cell membrane interactions [25], subsequent reports highlighted their use in biodetection. Taking advantage of hydrophobic ionophores with specific ion selectivity, Jelinek and colleagues successfully incorporated ionophores into the phospholipid domain of the of the DMPC/PDA liposomes. Subsequent addition of ions to DMPC/PDA liposome solutions resulted in specific interactions between ions and ionophores embedded into the lipid membrane causing a color response visible to the naked eye [69].

Jelinek and colleagues further demonstrated the feasibility of this method through reports of specific interactions between antibodies with epitopes embedded into phospholipid domains of DMPC/PDA liposomes [68], and again with specific protein interactions with embedded calixarenes (Figure 2.3) [23]. The same group also employed unmodified DMPC/PDA composites as bacterial sensors [72, 73]. The design of these sensors benefits from the interaction between bacterial endotoxins and the membrane phospholipids. Although this non-specific approach cannot distinguish detection of specific bacterial strains, color transitions in the liposome-laden agar scaffolds were observed in the presence of both gram-negative and gram-positive bacteria [73].

Additional investigations into DMPC/PDA liposomes suggest that they enhance the properties of PDA sensors [13, 74]. Su *et al.* [13] reported that DMPC/PDA liposomes composed of 40% DPMC exhibit up to 35% higher sensitivity of antigen detection by conjugated anti-human immunoglobulin (h-IgG) antibody-conjugtated PDA as compared to liposomes containing 0% DMPC, as determined by percent Color Response (CR) (Section 4.2.1). Similarly, a report by Kim *et al.* [74] found that

liposomes composed of 20-40% DMPC displayed expedited color transitions as compared to lower DMPC percentages in the detection of *E. coli*. Notably, both studies indicated that liposome morphology at 40% DMPC resembles flat sheets rather than circular liposomes (Figure 2.4). Studies investigating the morphology changes of 4:6 DMPC/PDA materials have reported varying morphologies, including circular liposomes, flat sheets, and fibers [13, 41, 47, 75]. A discussion of these is available elsewhere [41].

The mechanism by which DMPC doping increases sensitivity of PDA materials is unknown and has yet to be fully investigated. A number of reports indicated an increase in the flexibility of phospholipid/PDA composite materials due to interruptions in the rigid PDA backbone [25, 70, 71, 76]. Particularly, it is proposed that the insertion of DMPC along the PDA backbone disrupts hydrogen bonding between PDA head groups. This results in a less rigid PDA structure, which enables more sensitive blue to red transitions upon biomolecular recognition events [13, 74].

While DMPC remains the most widely used dopant in PDA composite materials, several studies further explored additional phospholipids such as dimyristoylphosphoethanolamine (DMPE) [14, 77-80] and dimyristoylphosphoglycerol (DMPG) [77-80], among others [72, 81, 82]. Whereas a number of recent studies incorporated such additional phospholipids to increase the biomimetic properties of PDA liposome membranes for the purpose of studying cell membrane interactions [77, 79, 81], Deming and colleagues have highlighted the preferential interaction of certain amino acids for particular phospholipids. For example, Lysine and Leucine induced more sensitive color transitions when exposed to DMPG/PDA and DMPE/PDA liposomes as

compared to DMPC/PDA [80]. Similarly, Jelinek and colleagues have recently determined lipid-dependent sensitivities in PDA fingerprinting platforms for bacterial detection [72]. Specifically, films made with three different lipids DMPC/PDA, 1-α-dioleoylphosphatidylethanolamine (DOPE)/PDA, and 1-palmitoyl-2-oleoyl-sn-glycero-3-[phospho-rac-(1-glyc-erol)] (POPE)/PDA each resulted in a distinct color transition when exposed to certain strains of bacteria (Figure 2.5). Such findings suggest the significance of the dopant lipid head groups in biodetection assays and indicate yet another approach to tailor PDA materials for more specific and sensitive biomolecular interactions.

Lipid Doping Conclusions. The use of PDA composite materials has been employed most commonly for their biomimetic properties in studies investigating cell membrane interactions [41]. However, Jelinek and colleagues have demonstrated the advantages of phospholipid/PDA liposomes for biosensing assays through the incorporation of hydrophobic biodetection molecules (e.g., ionophores, calixarenes) into the phospholipid region of the composite membranes. Additionally, both Deming and colleagues and the Jelinek group have observed lipid-dependent sensitivities in PDA sensors by certain target molecules [80, 82]. Furthermore PDA composed of 40% DMPC have reported increased sensitivities in antibody-conjugated liposomes [13]. All of these characteristics are advantageous for promoting higher sensitivities in target detection, and are significant to acknowledge for the prevention of false-positive signals due to non-specific interactions. Nevertheless, more investigation is required into the mechanisms by which phospholipid subdomains in PDA composite materials affect PDA transitions for biodetection.

3.2.2 Covalent Modifications

PDA conjugates have been investigated for biomolecular detection since initial studies by Charych and colleagues, in which the modification of DA monomers with sialic acid via carboxylic ester synthesis was reported in the detection of the influenza virus [9]. In this subsection, we discuss the general techniques used to conjugate functional biomaterials to PDA and review a number of strategic approaches to increase detection sensitivity through covalent modifications.

3.2.2.1 Polydiacetylene intermediates. The modification of PDA materials commonly refers to the conjugation of functional compounds onto the hydrophilic head groups of PCDA and TCDA monomers. Specifically, carboxylic ester synthesis from the carboxylic acid moiety of the DA monomer and an amine group on the biodetection probe (e.g., antibody, aptamer, functional group, etc.) occurs via activation of the carboxylic acid with N-hydroxysuccinimide (NHS) and ethyl(dimethylaminopropyl) carbodiimide (EDC) [83]. While the conjugation of biodetection probes can follow immediately after the conversion of DA monomers to the succinimidyl ester, an alternative is to synthesize and store the activated DA intermediate, DA-NHS, for further use. A general procedure for the synthesis of DA-NHS involves reaction of the DA monomers with excess NHS and EDC in dichloromethane for 2 h at room temperature. Next, removal of the organic solvent (dichloromethane) by evaporation is followed by extraction using ethyl acetate. The resulting DA-NHS monomer is a white solid (Figure 2.6).

More recently, Kim and colleagues have reported studies incorporating the addition of linker or spacer molecules to DA intermediates [15, 16, 84]. In these reports, 2,2'-(ethylenedioxy)bis(ethylamine) (EDEA) [16] and ethoxy ethanol [84] were conjugated after the synthesis of DA-NHS and before the conjugation of biodetection probes. Interestingly, further investigation by Kim and colleagues into the effect of alkyl spacer moieties on color transformations of PDA materials determined that the sensitivity between color transitions decreased with increasing alkyl spacer length (Figure 2.7) [85]. This result is supported by the current proposed mechanism of color transitions (Section 2.2), in which increasing alkyl spacer lengths is associated with an increase in van der Waals' interactions between monomer side-chains, thereby stabilizing the blue phase through restricting rotations in the PDA backbone.

Kim and colleagues have further explored an alternative to DA-NHS intermediates by investigating DA-epoxy conjugates due to the known stability of epoxy groups under proper storage and their ability to readily react with amine groups [15, 64, 84]. Accordingly, their results suggest that DA-epoxy provides higher stability as compared to DA-NHS intermediates. These reports from such explorations into the effects of additional linkers between conjugated detection probes and the PDA membrane surface as well as the use of alternative intermediates for probe conjugation are significant for both increasing detection sensitivities and revealing properties behind PDA color transformations.

3.2.2.2 Functional materials. The functionalization of DA monomers with biomolecular detection probes including antibodies [10-13], aptamers [14-17], proteins

[12, 18, 19] and others [8, 20, 21, 86-89] have been reported. Generally, these involve the spontaneous reaction of DA-NHS esters with an amine group on the detection probe in aqueous solution, followed by a step to remove unreacted molecules. Methods of conjugation vary at the time point in which conjugation occurs. For example, in a study by Jung *et al.* [14], thrombin aptamers were conjugated to previously prepared, unpolymerized DA-NHS monomers in excess and unreacted monomers are removed by centrifugal filtration. DA monomers functionalized with thrombin aptamer were then mixed with non-functionalized lipids for PDA liposome formation. Alternatively, another approach by the same group [10] converted unpolymerized DA to succinimidyl esters as self-assembled liposomes and removed unreacted NHS by centrifugation. Anti-phosphinothricin acetyltransferase (PAT) antibodies were then reacted with the DA-NHS liposomes in solution. Unconjugated antibodies were additionally removed via centrifugal filtration and unreacted esters were quenched with ethanolamine. Indeed, a different method by Lee *et al.* [16] described the conjugation of potassium aptamers in excess onto unpolymerized, self-assembled DA-NHS liposomes. Unbound aptamers were then removed by dialysis.

The relationship between the percent of probe-conjugated DAs from total matrix lipids is significant but not well understood. In early investigations, Charych and colleagues determined that for optimal detection of influenza virus, PDA film sensors were fabricated with 5-10% sialic acid-conjugated PDA [24, 46]. This is additionally reflected in Jung *et al.* [14], in which the optimal percentage of thrombin aptamer-conjugated DA was reported at 6.7%. Contrastingly, Park *et al.* [12] indicated that optical

transformations were most sensitive to streptavidin when biotin-conjugated DA monomers were at 20-40%. Alternatively, Lee *et al.* [15] reported the fabrication of mercury(II) sensors with 80% of aptamer-conjugated DA. These varied findings indicate that more examination is needed to elucidate the relationship between percentage of probe-conjugated DA and sensor sensitivity.

The conjugation of functional groups to PDA head groups has also been investigated as methods to enhance biodetection. Specifically, amine-terminated ($-NH_2$) PDA materials have been reported for non-specific detection of negatively charged biomolecules [21, 86-88]. Alternatively, Chung and colleagues have investigated the use of functional groups to prevent non-specific binding [12]. In their report, amine-terminated, hydroxyl-terminated (-OH), and naturally occurring carboxylic acid-terminated (i.e., polymerized TCDA) PDA were studied for non-specific interactions with bovine serum albumin (BSA). They showed that PDA composed of TCDA-OH exhibited the least amount of non-specific interactions with BSA proteins due to the electrically neutral and hydrophilic properties of the hydroxyl functional group in phosphate buffered saline (PBS, pH=7.4). This report indicates an approach to enhance the signal to noise ratio of PDA biosensors by minimizing non-specific binding.

Covalent Modifications Conclusions. Covalent modification of PDA head groups is a staple in the field of PDA biosensors. In particular, the direct conjugation of biodetection probes (e.g., antibodies, aptamers, etc.) onto the carboxylic acid head groups of PDA monomers facilities specific colorimetric detection of target biomolecules. However, there is much more to consider in this arena, including the possible effects of

linkers or spacers on detection sensitivity and even alternative intermediates (i.e., DA-epoxy vs. DA-NHS) for probe conjugation. Additionally, the percent of probe-conjugated DA and the chemical properties of matrix DA are also significant to enhance the sensitivity and decrease non-specific interactions in PDA sensors. The adaptability of PDA is one of its most advantageous properties for biosensing applications; nevertheless more investigations are needed to fully understand the effects of such modifications in order to truly optimize the PDA materials for biodetection.

4. CHARACTERIZATION OF POLYDIACETYLENES

4.1 Properties

Following the synthesis of PDA materials, it is necessary to determine the basic properties of the synthesized polymer in order to characterize and confirm successful modifications. In this subsection we discuss a few of the methods currently employed to characterize PDA materials.

4.1.1 Color

In order to characterize the color properties of PDA, it is common to measure the absorbance spectra of the material in the visible spectrum (Figure 2.8A). Specifically, UV-Vis spectroscopy measurements are done using a spectrophotometer. Blue-phase PDA are associated with an absorbance maximum at approximately 640 nm and a vibronic shoulder peak at 600 nm [13, 37]. Alternatively, red-phase PDA materials are

characterized by a shift in absorbance peak to approximately 540 nm [37]. The intermediate purple phase, distinct from a mixture of blue- and red-phase PDA, is associated with a peak at approximately 600 nm. It is speculated that this peak is related to the secondary absorbance peak associated with blue-phase PDA at the same wavelength [30, 40, 41, 90-92]. The peak absorbance values are commonly used to quantify blue to red transitions of PDA materials through the colorimetric response (CR) value (Section 4.2.1).

Due to the intense fluorogenic properties of red-phase PDA (Figure 2.8B), another way to contrast the blue and red phase is through measuring the fluorescence spectra using a fluorometer. The red phase is characterized by emission peaks at 560 and 640 nm (Figure 2.8C), while the blue phase exhibits no fluorescence properties [63]. Accordingly, measuring photoluminescence or fluorescence intensity of the material is yet another option (Figure 2.8D) [16]. As a result, it is possible to indirectly quantify blue to red color transitions as a measurement of fluorescence intensity of the material [36, 42].

4.1.2 Size and Morphology

It is important to understand the morphology of synthesized PDA materials in order to confirm consistent reproducibility as well as observe physical changes associated with molecular binding onto material surfaces and color transitions. In this subsection we review a few of the most frequent methods used to determine PDA morphology.

Dynamic light scattering (DLS) is frequently employed to determine the size of synthesized liposomes, which regularly vary with preparation methods. In particular, we

have determined that liposome size is inversely correlated with sonication time in the preparation process (Figure 2.9). Other factors that we speculate to influence liposome size include sonication type (probe vs. bath), power (watts), and volume of sample. Such details are often overlooked but may be necessary for consistencies in reproducing materials.

To observe the surface and shapes of PDA materials, transmission electron microscopy (TEM) [93] and scanning electron microscopy (SEM) [77] are prevalently used (Figure 2.10). While both are sufficient for their purpose, higher resolution TEM is often preferred over SEM when observing nanoscale liposomes. SEM and TEM images are frequently viewed after the synthesis of the PDA material and compared before and after molecular binding events. With the recent popularity of using substrates coated with PDA liposomes, atomic force microscopy (AFM) has also been employed to confirm and characterize the depositing of such materials. However, due to the destructive nature of AFM, blue to red color transformations are commonly observed as a result of the procedure [37].

4.1.3 Molecular Structure

With the constant modification and adaptation of PDA materials for specific functions, it is important to confirm successful conjugations by examining the molecular structure of synthesized PDA materials. ^{1}H nuclear magnetic resonance (NMR) is widely used to verify the synthesis of DA conjugates, in which the characteristic properties of hydrogen atoms in response to a magnetic field can confirm the presence of specific

compounds. Accordingly, DA conjugates can be verified by comparing peaks in their ^{1}H NMR spectra (Figure 2.11).

Another approach to examine the structure of PDA materials is through Fourier transform infrared spectroscopy (FTIR), in which the presence of bonds between specific atoms can be deduced (Figure 2.12). While FTIR is advantageous in confirming the presence of certain compounds, it can also be used to investigate changes in the strength of hydrogen bonds between PDA head groups [56, 59]. This is significant since intermolecular bonding between head groups is assumed to be the key reason for chromatic transitions in PDA materials.

Properties Conclusions

The characterization of materials is one of the most fundamental aspects in the fabrication of devices. The above described methods to characterize PDA materials are only a few of which are commonly used by researchers. Other methods of characterization [23, 76, 94-99] have been employed by a number of studies investigating PDA materials but are not discussed here. A thorough understanding of chemical characterization techniques would be helpful for those interested in the field of PDA biosensors.

4.2 Analysis of Optical Properties

Quantifying the sensitivity of a biosensor is a critical aspect to evaluate the efficiency of that application. In this subsection we discuss current methods to quantify the optical transitions in PDA materials.

4.2.1 Colorimetric Response

The colorimetric response (CR), developed by Charych and colleagues, is the standard method of quantifying blue to red color transitions in PDA sensors [40]. In particular, the wavelength at which the absorbance maxima occur in the blue phase (~640 nm) and red phase (~540 nm) of the sensor are subject to focus. The exact wavelengths used vary depending on the absorbance spectrum of the specific PDA material being investigated. The %CR value is determined first by calculating the percent blue, *PB*, in which:

$$PB = \frac{A_{blue}}{A_{blue} + A_{red}} \times 100\%$$

where A_{blue} is the absorbance value at the wavelength at which the absorbance maximum occurs for the blue phase and A_{red} is the equivalent absorbance value for the red phase. From here, the %CR value is determined as:

$$CR = \frac{\left(PB_0 - PB_f\right)}{PB_0} \times 100\%$$

where PB_0 is the initial percent blue of a baseline. The reasoning for this systematic approach is that any environmental factors affecting absorbance values will likely affect A_{blue} and A_{red} equally and will minimize alterations in overall detection [41].

4.2.2 Digital Colorimetric Analysis

In their analysis of a PDA film for the sensing of membrane-active compounds, Kolusheva, Jelinek and colleagues have developed an approach that quantifies the red-green-blue (RGB) values of scanned images [100]. This quantification approach has gained recent popularity especially for analyzing fabricated PDA films [27-29, 100-103].

Volinsky *et al.* [100] derived this digital colorimetric analysis (DCA) method from Pratt [104], in which the red chromaticity level, *r*, is defined as:

$$r = \frac{R}{R + G + B}$$

For PDA materials, Volinsky *et al.* further extrapolated the equation to quantify the blue to red transitions as a red chromatic shift (RCS) value:

$$\% \, RCS = \frac{r_{sample} - r_0}{r_{max} - r_0} \times 100\%$$

where r_{sample} is defined as the average chromaticity level from all pixels in the sample PDA image, r_0 is defined as the average red chromaticity level of a PDA image prior to treatment, and r_{max} is defined as the average red chromaticity level of a PDA image with maximum blue to red transition (i.e., positive control). Volinsky *et al.* further compared the results of their DCA study with a parallel CR analysis, and indicated a close correlation between the two data sets (Figure 2.13). Currently, CR remains the most widely used approach to quantify blue to red color transitions of PDA materials, especially liposomes. Nevertheless, the DCA approach is advantageous in that high quality images of samples are sufficient for analysis and is an easier option for the analysis of PDA films or strips.

4.2.3 Fluorescence Emission

Alternative PDA-sensing technologies take advantage of the environmentally induced "turn-on" of fluorescence properties in PDA materials, in which the detection sensitivity of the sensor is simply measured by fluorescence intensity before and after molecular binding events [36]. The major advantage for this approach is the high

sensitivity in fluorescence measurement systems that allow for the detection of small changes in emission as compared to changes in absorbance or RGB values. However, the drawback to this methodology is that the need for such fluorescence instruments for analysis may limit the application of these types of sensors in low-resource settings.

Analysis Conclusions

Currently there are two methods to analyze blue to red color transitions of PDA sensors. CR developed by Charych and colleagues during their initial investigations of PDA sensors, remains the predominant approach. However, the recent development of DCA by Kolusheva, Jelinek and colleagues provides a simpler approach of analysis without the need for spectrophotometric instruments. Alternatively, the exploration of fluorescent-based PDA sensors offers a highly sensitive method for biodetection quantified by the intensity of fluorescence emission.

5. RECENT ADVANCES IN POLYDIACETYLENE APPLICATIONS

The incorporation of PDA in a vast array of material forms has been previously reviewed, from PDA films and self-assembled monolayers [41], colloidal solutions [24], and fluorescence microarrays [36]. While the bulk of this article has focused on PDA as biosensors, in this section, we discuss a few of the most recent and unconventional material forms currently investigated that are not limited to the field of biosensing applications.

5.1 Paper-Based Polydiacetylene Sensors

One of the greatest advantages of PDA materials is for the fabrication of label-free, chromatic sensors. This is desirable because PDA platforms enable one-step, colorimetric detection of analyte without the need for costly secondary labels. To further the advancement of low-cost PDA sensors, researchers have incorporated PDA materials as paper-based sensors. These sensors are advantageous for in-field or point-of-care settings due to their stability, ease of transport, inexpensive fabrication, and user-friendly platform without the need for external reagents or laboratory instruments. In this subsection, we review reports of paper-based PDA sensors.

Notably, Wacharasindhu and colleagues have reported the specific colorimetric detection of volatile organic compounds (VOCs) using PDA-coated filter paper [28]. Specifically, eight types of PDA were tested for their sensitivity against VOC vapors, including commercially available PCDA and TCDA. Dots from unpolymerized DA solutions of uniform size were created on filter paper using an automatic pipette and were tested by attachment of the coated filter paper on the inner lid of a chamber containing various VOCs. DCA analysis indicated that DA monomer 6,8-nonadecadiynioic acid exhibited the greatest sensitivity, exhibiting distinct chromatic transitions when exposed to 18 different VOCs. This is an improvement from their previous work, reporting non-specific VOC detection [29]. Significantly, the VOC-sensing devices were reported to be stable in a refrigerator over the span of several months.

The fabrication of paper-based, VOC-detecting PDA sensors has been further adapted by Yoon *et al.* [105] onto conventional printer paper via inkjet printing. In this

investigation, VOCs both in the vapor phase and the liquid phase were detected by UV-irradiated polymers of 5,7-dodecdiyne-1,12-diol bis[((butoxycarbonyl)methyl)urethane] (4BCMU). Varied results between VOC detection from liquid and vapor exposure were observed only in tetrahydrofuran (THF), DCM (a.k.a. methylene chloride), and chloroform. Interestingly, liquid-phase detection of THF, DCM, and chloroform, along with vapor-phase detection of chloroform, resulted in blue to red to yellow chromatic transitions that reverted to red phase upon removal from VOC. Notably when in the yellow-phase, poly-4BCMU exhibits green fluorescence (instead of red fluorescence), excitable at 488 nm (Figure 2.14).

Alternatively, Wang *et al.* [34] demonstrated the use of stacked, PDA-coated graphene films or "paper" for the detection of VOC vapors. Notably, unmodified PCDA was used for this study. The thickness of the fabricated graphene films was reported to be ~1-40 μm, and the structure was observed by scanning tunneling microscopy. The exposure of PDA/graphene films to four VOCs gave distinct color transitions.

While the paper-based PDA sensors have generally been limited to either temperature [60, 106] (previously reviewed by Jelinek *et al.* [39]) or volatile compound detection [28, 29, 34, 105, 107], Yu and colleagues have recently reported the specific detection of Pb^{2+} ions in a paper-based assay fabricated from a nanofibrous membrane [108, 109]. In their most recent study, Yu and colleagues functionalized PCDA monomers with glycine (Gly) for specific interactions with Pb^{2+}. A polyacrylonitrile (PAN) nanofibrous membrane (NFM) was then fabricated with embedded PCDA-Gly and SiO_2 nanoparticles (NPs), in which SiO_2 NPs increased the surface area of the

material for higher exposure of PCDA-Gly to sample solutions. The structures of membranes with 0 to 1 wt% of SiO_2 NPs were observed with field emission SEM. Exposure of the different membranes to varying concentrations of Pb^{2+} demonstrated that PCDA-Gly PAN NFMs composed of 0.5 wt% SiO_2 NPs exhibited the highest sensitivity to low concentrations of Pb^{2+}, with a limit of detection at 0.24 μM.

Paper-based PDA materials have great potential applications for low-resource or in-field settings due to their long-term stability and ease of use without the need for external reagents or laboratory instruments. While there are currently very few reports of paper-based PDA sensors, and even less for targets in aqueous solution, their continued development is promising for applications in the developing world.

5.2 Polydiacetylenes for Drug Delivery

The advancement of drug delivery systems for anticancer therapies and their ability to selectively target tumor cells has gained popular attention over traditional non-selective treatments such as chemotherapy and radiation [110]. Due to their biocompatible properties, self-assembled liposomes composed of phospholipids have long been investigated as encapsulating agents for such drug delivery systems [111-113]. Challenges in liposome-mediated drug delivery include long-term sustainability of the liposome and controlled-release of the therapeutic agent. In particular, liposomes are easily disassembled in acid/base environments or in the presence of surfactants; additionally, liposome-cell fusion is also an area of concern [112]. Previous

investigations have determined that one solution is to use polymerized liposomes, which have much more stable morphologies in a range of molecular environments [114-116].

PDA liposomes have been recently recognized in the field of drug delivery systems for their nontoxicity [117] and photo-induced polymerization without the use of toxic initiators [44]. Furthermore, the ease of chemical modification to PDA head groups along with the control over their degree of polymerization via mixed phospholipid/PDA liposomes have made PDA attractive for drug delivery systems in the past decade. In this subsection, we discuss some of recent advances in PDA for anti-cancer drug delivery.

Qin *et al.* [118] has fabricated PDA liposomes for "remote controlled" drug delivery that instantaneously release encapsulated reagents upon trigger by a laser (Figure 2.15). Specifically, partially polymerized liposomes (PPLs) composed of two DAs and a phospholipid were functionalized with gold nanoparticles (GNPs). Notably, the report of laser-induced liposome release of embedded drug via GNPs was previously studied by Wu et al [119], in which the use of near infrared (NIR) pulse lasers caused release of liposomes due to raised temperatures in the GNPs. First PPL-GNPs were loaded with fluorescence dye, calcein, to observe the retention ability of the PDA liposomes. After 3 days at 40 °C, it was reported that negligible leakage occurred. Next, to evaluate the laser-induced release of liposome-encapsulated reagent, PPL-GNPs were loaded with radioactive Tc-99m mebrofenin. Upon irradiation of 10 x 6 ns pulses of laser, PPL-GNPs were measured to release approximately 70% of their content. Finally, PPL-GNPs were loaded with anti-cancer drug, doxorubicin and exposed to breast cancer cells *in vitro*. After laser irradiation, it was shown that only ~20% of cancer cells were viable.

Significantly, control studies with treatment of cancer cells with unloaded PPL-GNPs determined that laser treatment did not affect the viability of the cancer cells, indicating that the significant drop in cell viability was indeed a result of doxorubicin release from PPL-GNPs.

While other *in vitro* studies of PDA drug delivery liposomes have been reported [112, 120, 121], Mackiewicz *et al.* [122] described an *in vivo* study with the use of PDA micelles for both imaging and drug delivery. In particular, micelles composed of PCDA monomers functionalized with poly(ethylene glycol) (PEG, 2000 Da (PEG2000)) were selected and evaluated. Characterization by DLS indicated that the average diameter of micelles were approximately 10 nm overall. To investigate the viability of PDA micelles for the delivery of hydrophobic imaging agents, PDA-PEG2000 micelles were loaded with NIR lipophilic carbocyanine dye (DiR) and injected into mice with subcutaneous breast cancer tumors. NIR imaging confirmed that PDA-PEG2000-encapsulated DiR accumulated at the tumor site, whereas non-encapsulated DiR accumulated in the liver. Finally, the anti-cancer agent, paclitaxel (PTX) was loaded into PDA-PEG2000 micelles and studied for their drug delivery capabilities *in vivo*. After 2 months, tumors treated with PTX-loaded PDA micelles showed reductions in volume by a factor of 4.5. As a comparison, tumors treated with commercially available Taxol exhibited reductions in tumor volumes by a factor of 3.3. Significantly, it was also reported that PTX-loaded PDA micelles were stable at 4 °C after storage for two months and PTX retained its cytotoxicity within micelles.

While the current use of PDA materials in drug delivery systems does not take advantage of its putative chromatic properties, it is important to observe materials beyond their most apparent properties in order to fully take advantage of their capabilities. For example, traditional PDA sensors have all been designed for *in vitro* applications. However, such investigations into PDA materials for drug delivery systems have highlighted their non-toxic, biocompatible properties which give rise to another potential for the design of *in vivo* PDA sensors similar to one we have proposed [123].

5.3 Polydiacetylenes for Tissue Engineering

Over the last decade, there has been an increasing interest in the use of peptide amphiphiles in the field of regenerative medicine as building blocks for the fabrication of tissue scaffolds [124-126]. While synthetic polymeric hydrogels have long been the focus of tissue engineering applications, their limits in the control of pore size, fiber diameter, and shape have posed significant challenges in the field [127]. Alternative approaches, such as electrospinning and phase separation are similarly restricted by lack of morphological controls at the molecular level [33]. Peptide amphiphiles offer significant advantages in their potential to self-assemble into supramolecular structures, including one-dimensional monolayers [128], two-dimensional β-sheets [129], and three-dimensional nanotube fibers [130, 131]. This is done via high controls at the molecular level through mixed peptide amphiphiles and modifications to the hydrophilic head groups and alky chains. However, one of the major challenges in this approach is the poor mechanistic stability of unpolymerized peptide amphiphiles [128]. Additionally,

chemically cross-linked polymers often involve the use of toxic agents and unwanted by-products [125].

Accordingly, investigations into photopolymerized peptide-diacetylenes have advanced the potential for peptide amphiphiles in tissue engineering applications. While the potential for PDA materials for biosensing applications has been extensively discussed, their recent applications in tissue scaffolds remain largely obscure. In this subsection, we review a number of recent reports exploring the use of PDA-peptides in tissue scaffolds for tissue engineering.

The first report of PDA in tissue engineering was published in 2006 by Tirrell and colleagues, in which a TCDA-fatty acid monolayer exhibiting varying concentrations of conjugated cell-adhesion peptides fabricated on an LB film was investigated [128]. The cell-adhesion peptide used in this study was glycine-arginine-glycine-aspartic acid-serine-proline (GRGDSP), a peptide sequence well-known for its mouse fibroblast adhesion properties. AFM analyses of the composite TCDA-fatty acid and TCDA-GRGDSP at varying mole concentrations of the latter confirmed the adjustability of monomer packing.

Further investigation of the TCDA-fatty acid/GRGDSP film studied the adhesion potential of mouse fibroblasts. Specifically, mixed films with TCDA-GRGDSP at mole percentages from 0% to 75% were compared. Cell adhesion assays were performed by treating PDA surfaces with a defined number of cells for 60 m and counting the number of cells attached per surface area. The resulting analysis of these assays indicated that films composed of 10% TCDA-GRGDSP exhibited the highest percentage of adherent

cells. Significantly, optical micrographs of PDA films from initial cell seeding, mechanical removal of cells, and re-seeding of cells confirmed that PDA films were viable for reuse.

This initial two-dimensional study by Tirrell and colleagues was a significant demonstration of the viability of PDA materials for cell adhesion that was further investigated by Frauenrath and colleagues in the formation of three-dimensional scaffolds composed of oligopeptide-functionalized PDA that formed β-sheets in solution [129]. In this communication, TEM and SEM micrographs of their functional PDA confirmed its self-assembly into controlled helical fibrils composed of β-sheet aggregates. Importantly, the formation of β-sheets instead of liposomes enabled fibrous morphologies appropriate for the composition of tissue scaffolds.

The realization of PDA scaffolds for tissue engineering has been pioneered by Stupp and colleagues [132]. In their report, top-down lithography protocols were employed using peptide-conjugated PDA to fabricate an array of tissue scaffolds with highly controlled micropatterning for the study of human mesenchymal stem cells (hMSCs). Specifically, the study takes advantage of the photopolymerizable properties of PDA materials to create rigid scaffolds with high mechanical integrity. Stupp and colleagues demonstrated the ability to fabricate nanostructures with controlled microtextures including channels, pores, posts, and double-layer topographies to a resolution of 5 μm (Figure 2.16). They similarly adopted mixed PDA composed of matrix and peptide-conjugated PDA for cell adhesion. The adhesion peptide used in this study was arginine-glycine-aspartic acid-serine (RGDS) and it was determined that scaffolds

consisting of 80% PDA-RGDS were optimal for adhesion of hMSCs. From their investigations, Stupp and colleagues were able to distinguish morphologies to which hMSCs aggregated and differentiated. This significant study has demonstrated the great potential for the fabrication of tissue scaffolds with highly controlled micropatterned textures using PDA materials.

Voelcker and colleagues have most recently fabricated lysine-conjugated PDA tissue scaffolds for hMSCs [33]. In this report, the researchers demonstrated the ability to change the hydrophobic and hydrophilic properties of the lysine-PDA monomers by masking and un-masking lysine side chains using Fmoc and Boc protecting groups. This aspect of tissue scaffold production is significant in controlling its wettability, which is an important factor for cell adhesion. Specifically, five polymers with increasing hydrophilicity were investigated. Notably, cell adhesion was most efficient on the highly hydrophilic polymers, but cell proliferation was more favorable on the more hydrophobic polymers.

The developing field of PDA materials for tissue engineering is one in which much more exploration is needed. The most recent advances by Stupp and Voelcker demonstrate great potential for PDA tissue scaffolds; however, further investigations might take advantage of the chromatic properties of PDA materials in determining cell properties. Some examples include the detection of cell signals to indicate specific stem cell differentiation or cell stress/apoptosis. Additionally, future investigations in the fabrication of biodegradable PDA scaffolds, through mixed amphiphile/PDA composites

or side chain modifications, would also be advantageous in the field of implantable biomaterials.

6. FUTURE DIRECTIONS FOR POLYDIACETYLENE MATERIALS

Since their first preparation nearly a half-century ago, PDA materials have attracted much attention from researchers for their remarkable optical properties. In this review, we discussed the basic properties of PDA materials and the currently accepted theories behind their exceptional environmentally induced color transitions and fluorogenic "turn-on" characteristic. For the benefit of researchers from all fields, we reviewed some general procedures then highlighted more recent explorations into methods for PDA synthesis and modification. The latter include PDA-epoxy intermediates and the use of modified functional groups (e.g., -OH, $-NH_2$, -COOH) on matrix constituents to promote non-specific binding of biomolecules. We also discussed the most common characterization methods for PDA and compared CR, the traditional approach to quantify color transitions, with DCA, an alternative approach developed by Kolusheva, Jelinek, and colleagues. Finally, we reviewed advancing platforms for PDA materials, including paper-based PDA sensors for low-resource settings, PDA systems for drug delivery, and PDA nanostructures for tissue engineering.

As PDA technology advances and continues to branch into diverse applications, it is critical to investigate and understand the underlying mechanisms behind its chromatic properties. While the development of new sensor types and novel applications are

exciting aspects to the field, the full potential of PDA materials cannot be realized without a fundamental understanding of its properties.

Future explorations of PDA applications may combine its conventional appeal as sensors with the advantages of its biocompatible properties. Even more, with the recent developments of reversible PDAs (not discussed here), advancements in the above suggested field of *in vivo* sensors has great potential for applications in medicine, horticulture and agriculture to monitor, diagnose and even treat diseases in humans, animals, and plants alike. Alternatively, the advancement of low-cost and stable paper-based PDA sensors are ideal for low-resource applications and may be coupled with smartphone-based systems for in-field quantitative analyses.

As the field of PDA materials garners more attention in the scientific world, PDA applications will continue to expand and increase in quality and sensitivity. Already, many reports demonstrate the design of PDA-based systems comparable to, or even better than, currently accepted standards. Eventually, with the current rate of developments, practical application of PDA systems will be available and accessible to both research and commercial sectors across the globe.

7. FIGURES

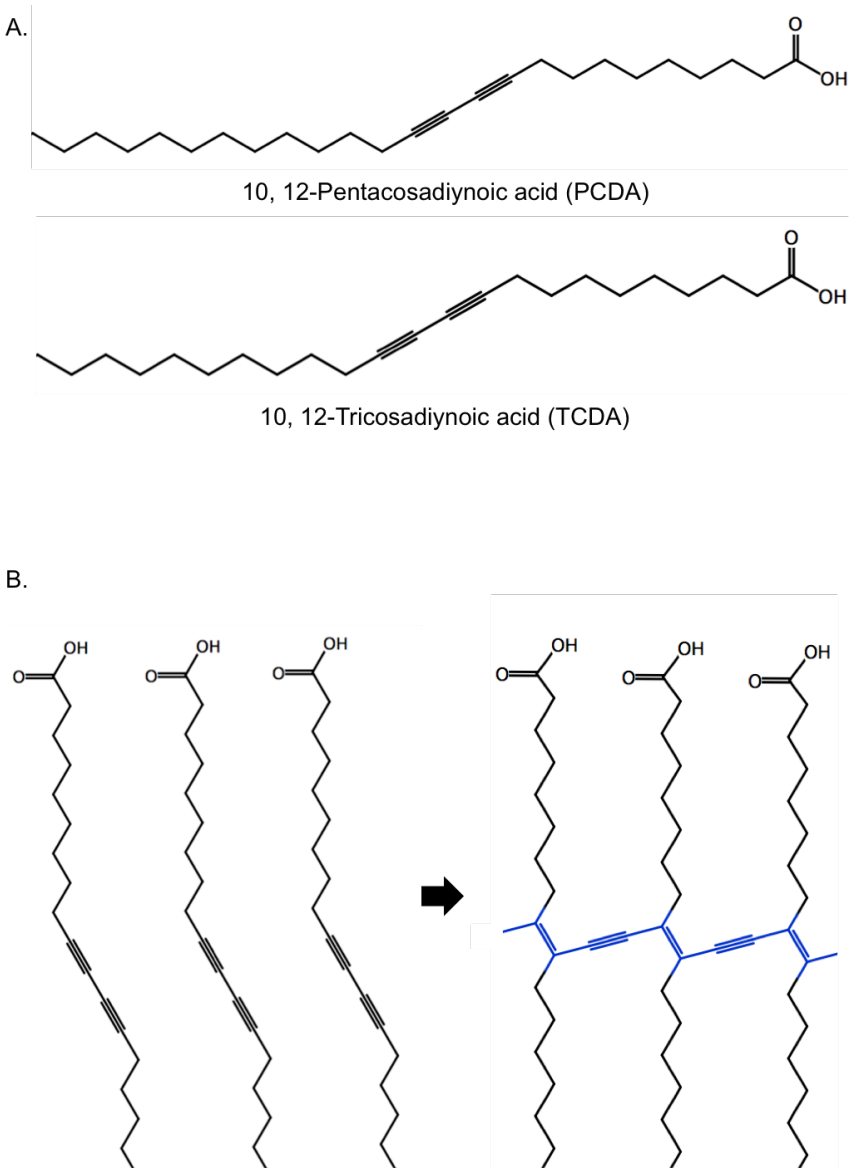

Figure 2.1. Molecular structure of diacetylenes. (A) Structure of commercially available diacetylenes PCDA and TCDA. (B) polymerization of diacetylenes via 1,4 addition.

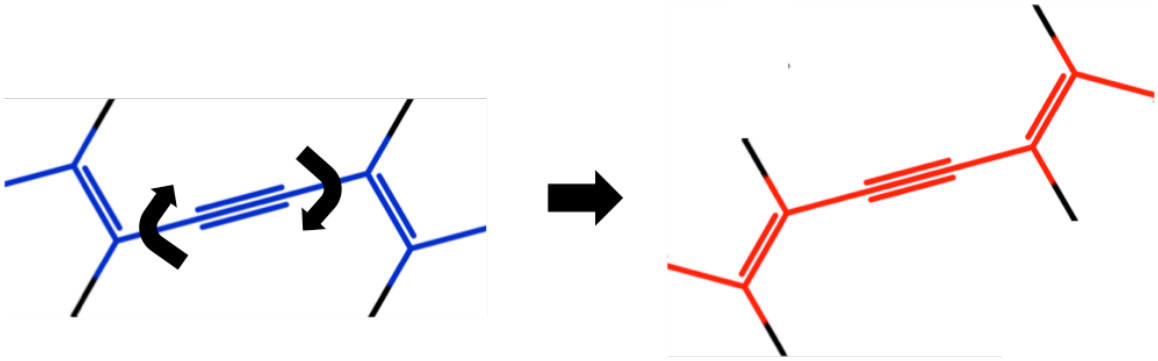

Figure 2.2. Slight rotations in the PDA backbone result in the conversion from blue phase to red phase.

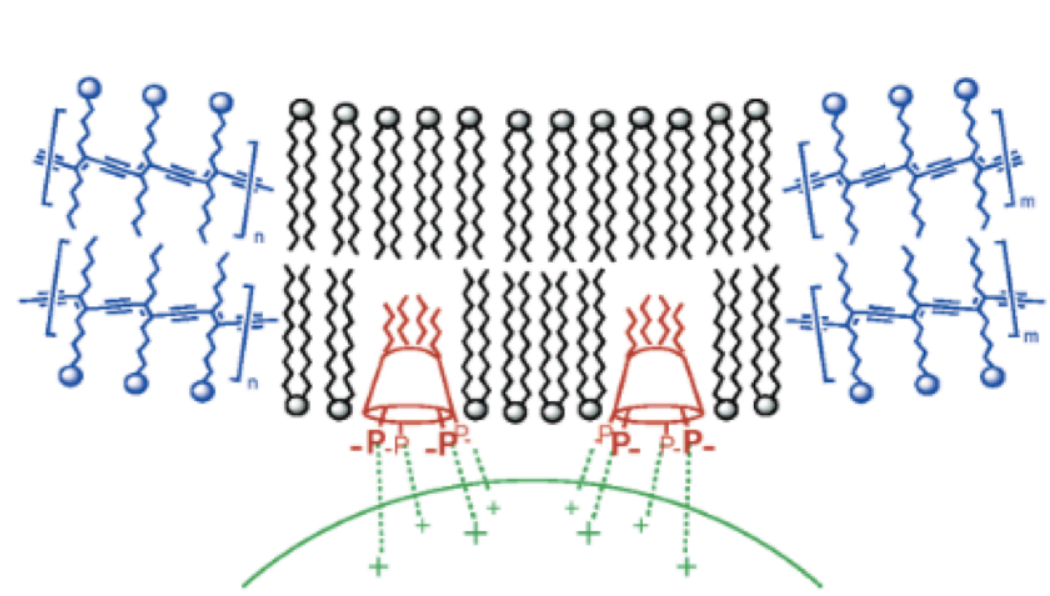

Figure 2.3. Phospholipid doping of PDA results in a mixed liposome membrane composed of phospholipid (black) and PDA (blue) subdomains. The embedding of membrane proteins into the phospholipid domains can act as receptors for target analytes. Reproduced with permission from ref. 23, Copyright (2006), *American Chemical Society*.

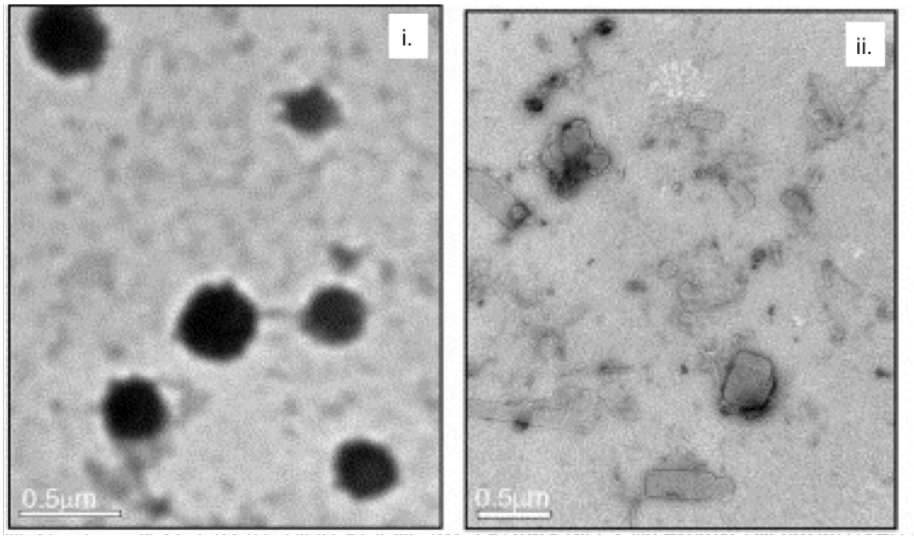

Figure 2.4. TEM images of DMPC/PDA with 0% DMPC (left) and 40% DMPC (right). Adapted with permission from ref. 13, Copyright 2004, *Elsevier B.V*.

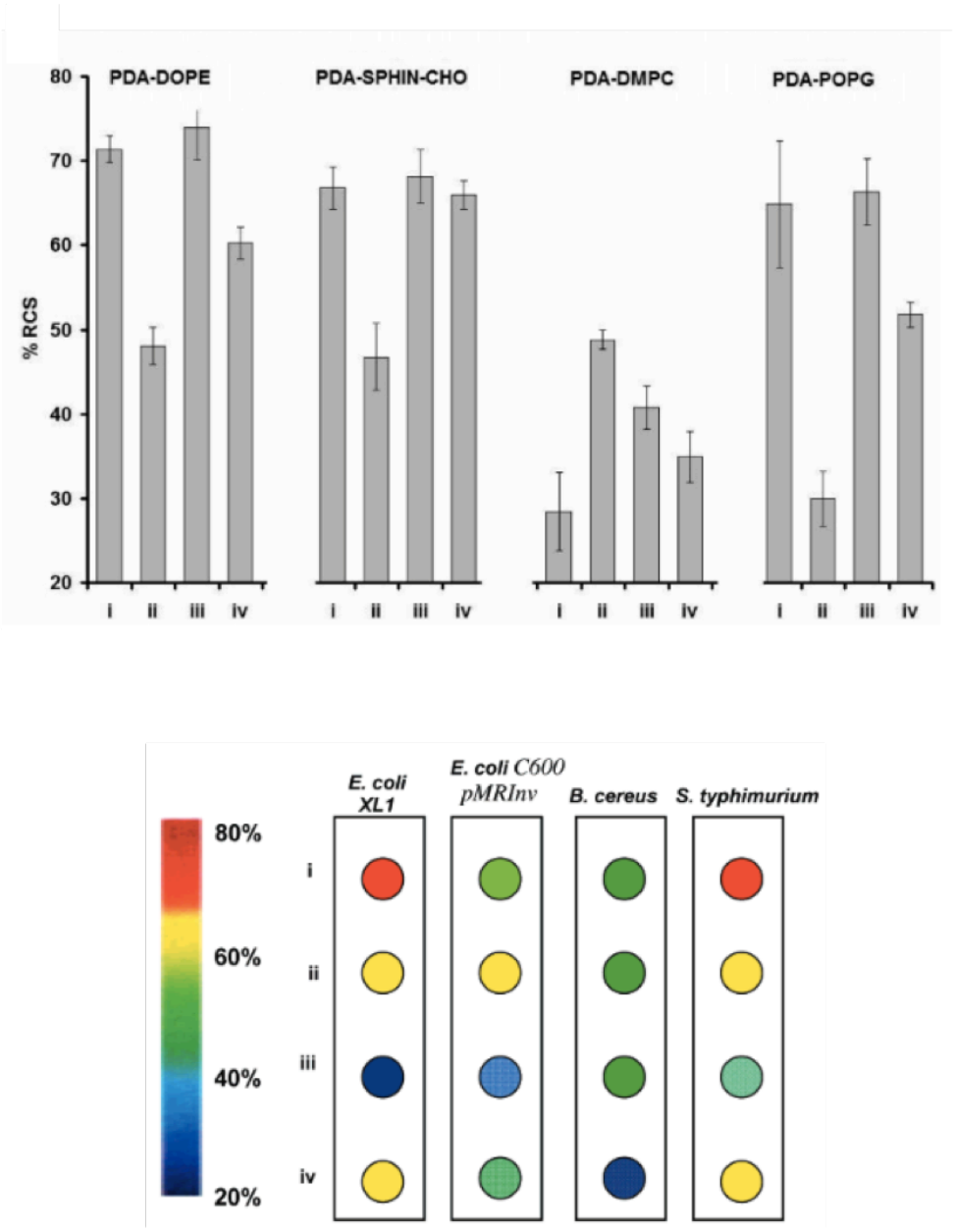

Figure 2.5. PDA fingerprinting of bacteria. Four types of PDA films created with varying lipid dopants exhibit unique chromatic transitions when exposed to different strains of bacteria. Adapted from ref. 72, Copyright 2007, *American Chemical Society*.

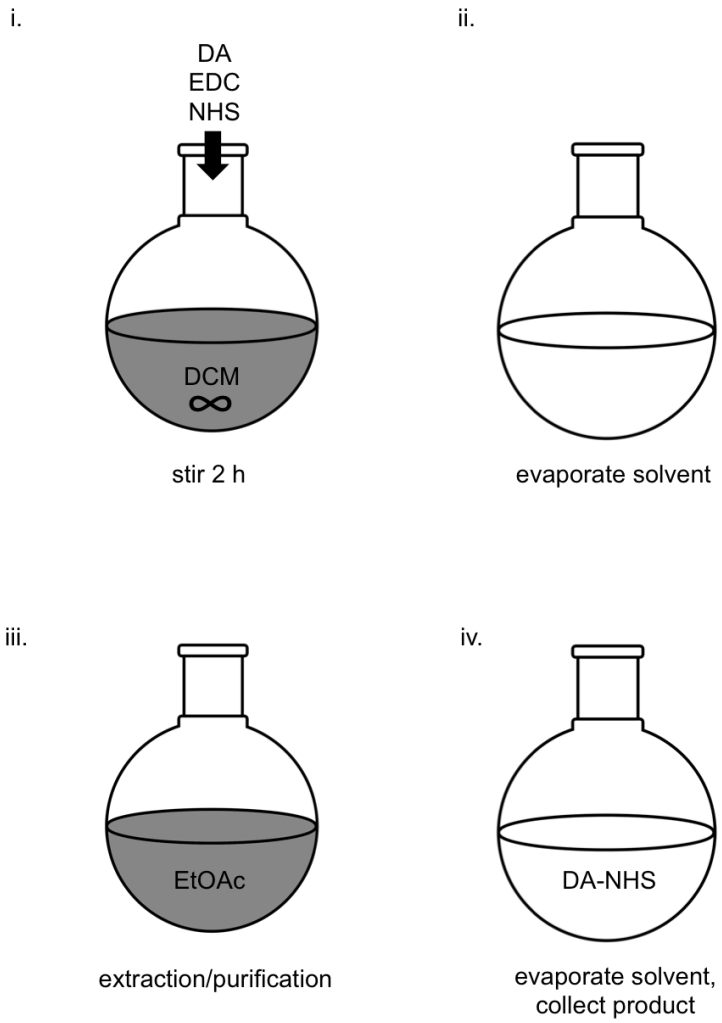

Figure 2.6. Protocol for conversion of diacetylenes (DA) to their succinimide ester. (i) Stir a mixture of DA, N-(3-dimethylaminopropyl)-N'-ethylcarbodiimide hydrochloride (EDC-HCl) and N-hydroxysuccinimide (NHS) in dichloromethane (DCM) for 2 h. (ii) Evaporate the solvent (dichloromethane) and (iii) purify the DA-NHS by resuspending in ethyl acetate (EtOAc). (iv) Evaporate the solvent (ethyl acetate) and collect the product.

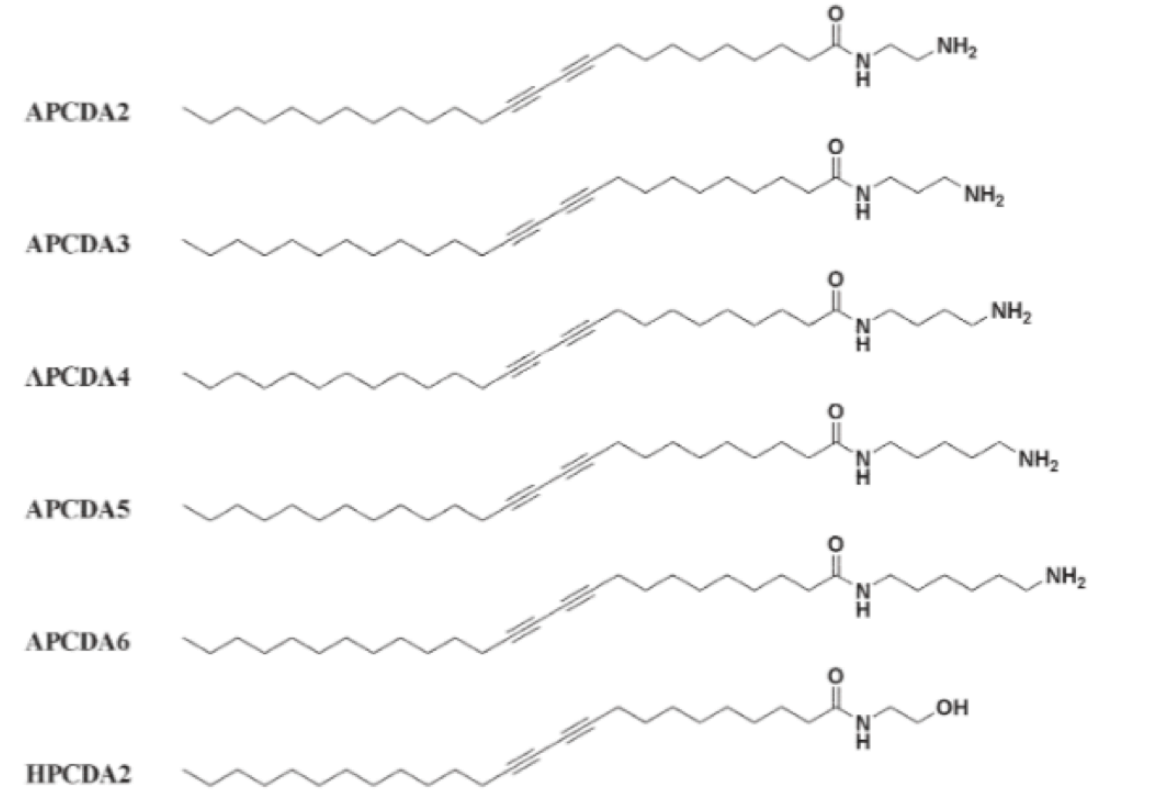

Figure 2.7. PCDA monomers modified with varying linker lengths from 2 to 6 carbons. Reproduced with permission from ref. 85, Copyright 2010, *John Wiley & Sons, Inc*.

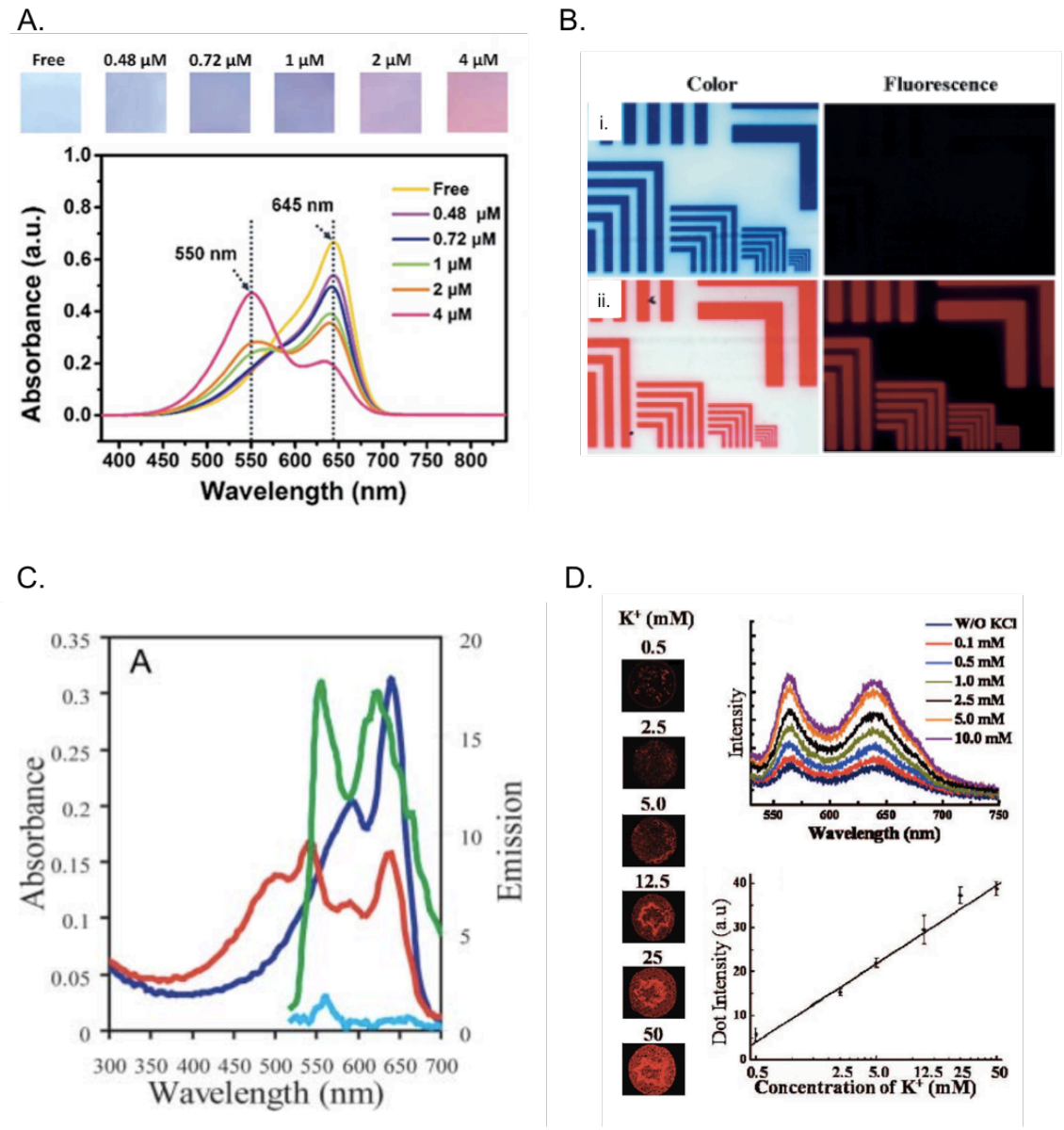

Figure 2.8. Color properties of PDA. (A) UV-Vis spectra of PDA strips exhibiting various colors from blue to red. Adapted from ref. 108, Copyright 2014, *Royal Society of Chemistry*. (B) Color and fluorescence images of blue phase and red phase PDA. Adapted from ref. 31, Copyright 2006, *John Wiley & Sons, Inc.* (C) Absorbance spectra of blue phase (blue) and red phase (red) PDA; and emission spectra of blue phase (light blue) and red phase (green) PDA. Adapted from ref. 41, Copyright 2007, *Royal Society of Chemistry*. (D) Fluorescence images (left), spectra (top right), and intensity (bottom right) of red to blue phase PDA (color not shown) exhibiting varying degrees of fluorescence. Adapted from ref. 16, Copyright 2008, *American Chemical Society.*

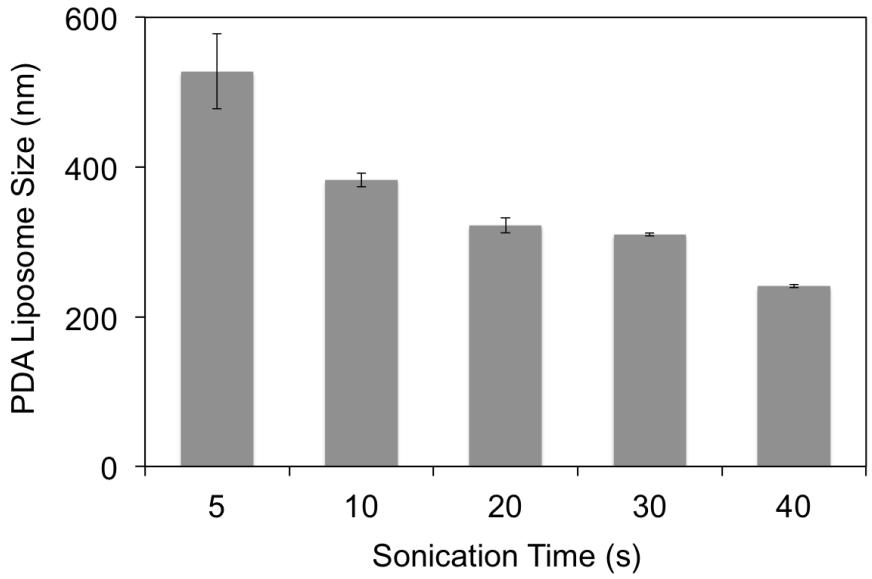

Figure 2.9. Size of PDA liposomes as a result of varying sonication times. Lipsomes were sonicated by a probe sonicator (Qsonica Q500) at 20% amplitude. Size of liposomes was determined by DLS. Data are represented as mean ± SD (n = 3).

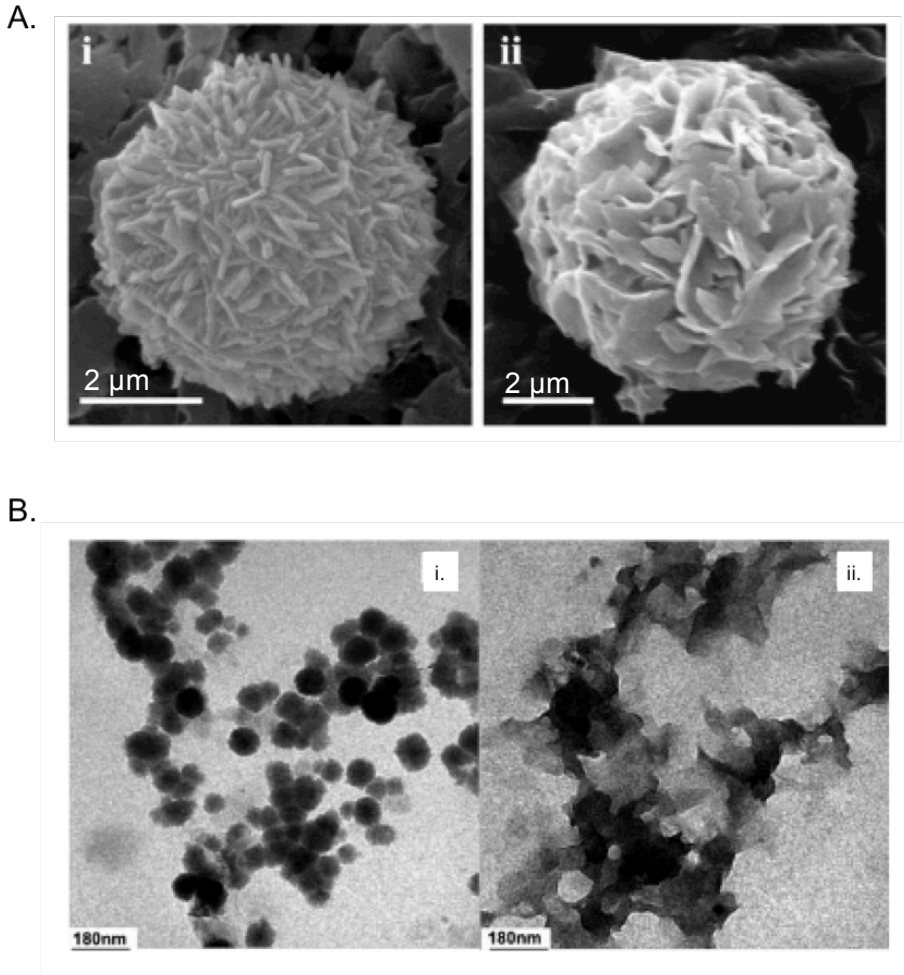

Figure 2.10. SEM images of giant biomimetic PDA liposomes (A), and TEM images of PB^{2+}-sensing liposomes before (i) and after (ii) the addition of 1 µM PB^{2+} (B). (A) Adapted from ref. 77, Copyright 2008, *John Wiley & Sons, Inc.* (B) Adapted from ref. 93, Copyright 2011, *Royal Society of Chemistry*.

A.

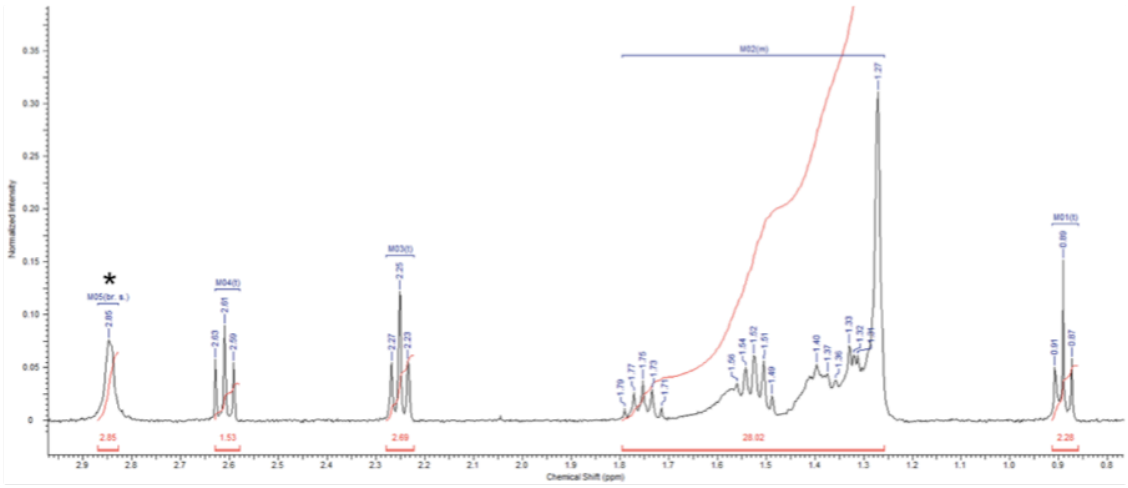

B.

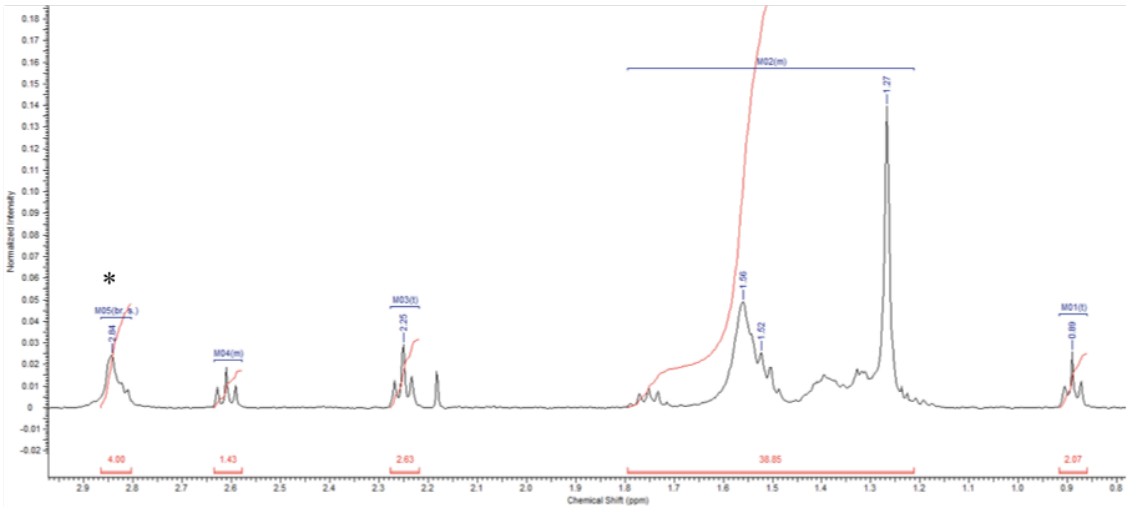

Figure 2.11. ^{1}H NMR spectra of TCDA-NHS (A) and PCDA-NHS (B), * indicates peak from N-hydroxysuccinimide.

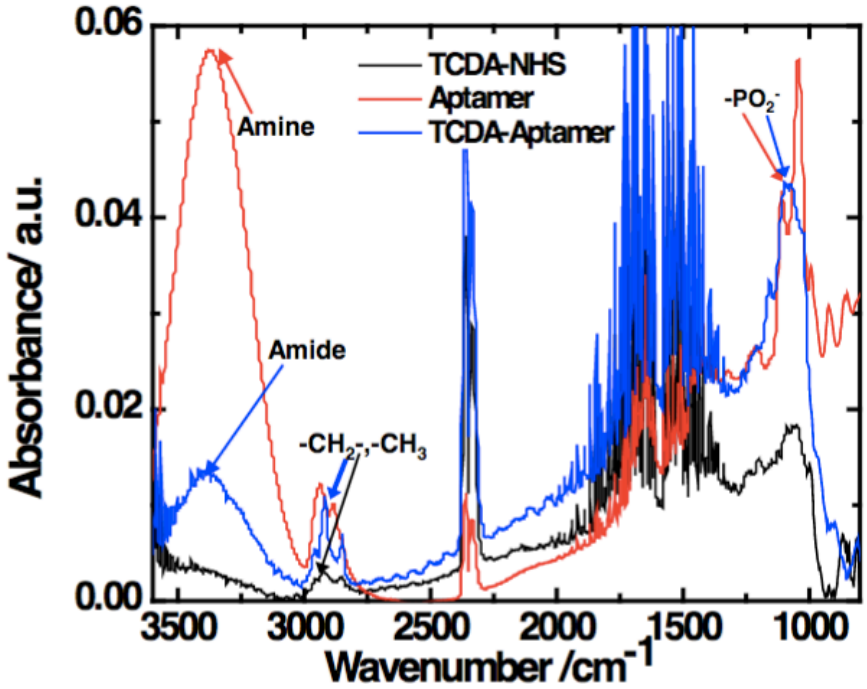

Figure 2.12. FTIR spectra of TCDA-NHS, aminated thrombin aptamer, and TCDA conjugated with thrombin aptamer. Reproduced with permission from ref. 14, Copyright 2010, *John Wiley & Sons, Inc*.

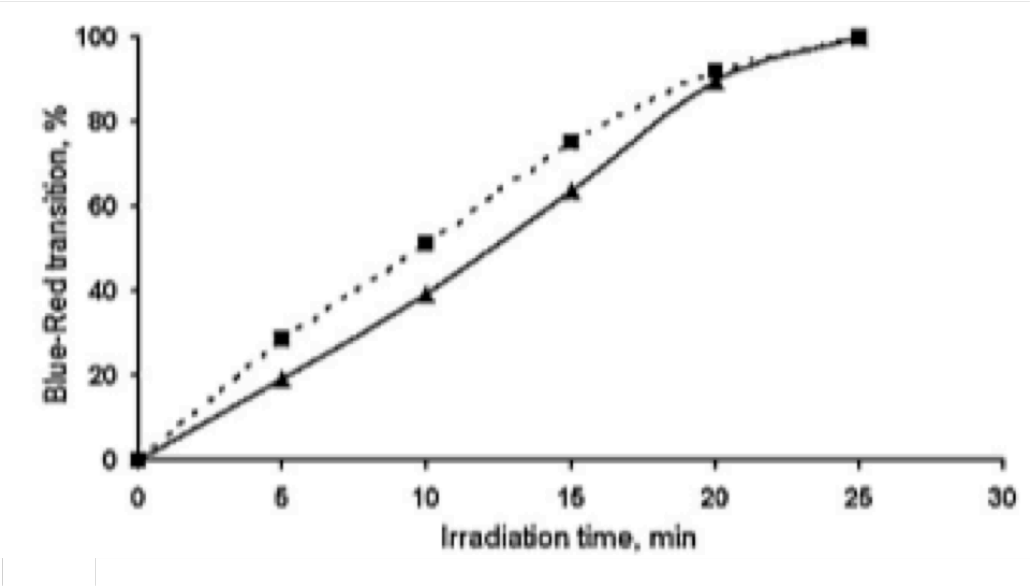

Figure 2.13. Blue to red transition of PDA films analyzed by digital colorimetric colorimetric analysis (%RCS curve, solid line) and UV-Vis spectrophotometry (%CR curve, dashed line). Reproduced with permission from ref. 100, Copyright 2002, *American Chemical Society*.

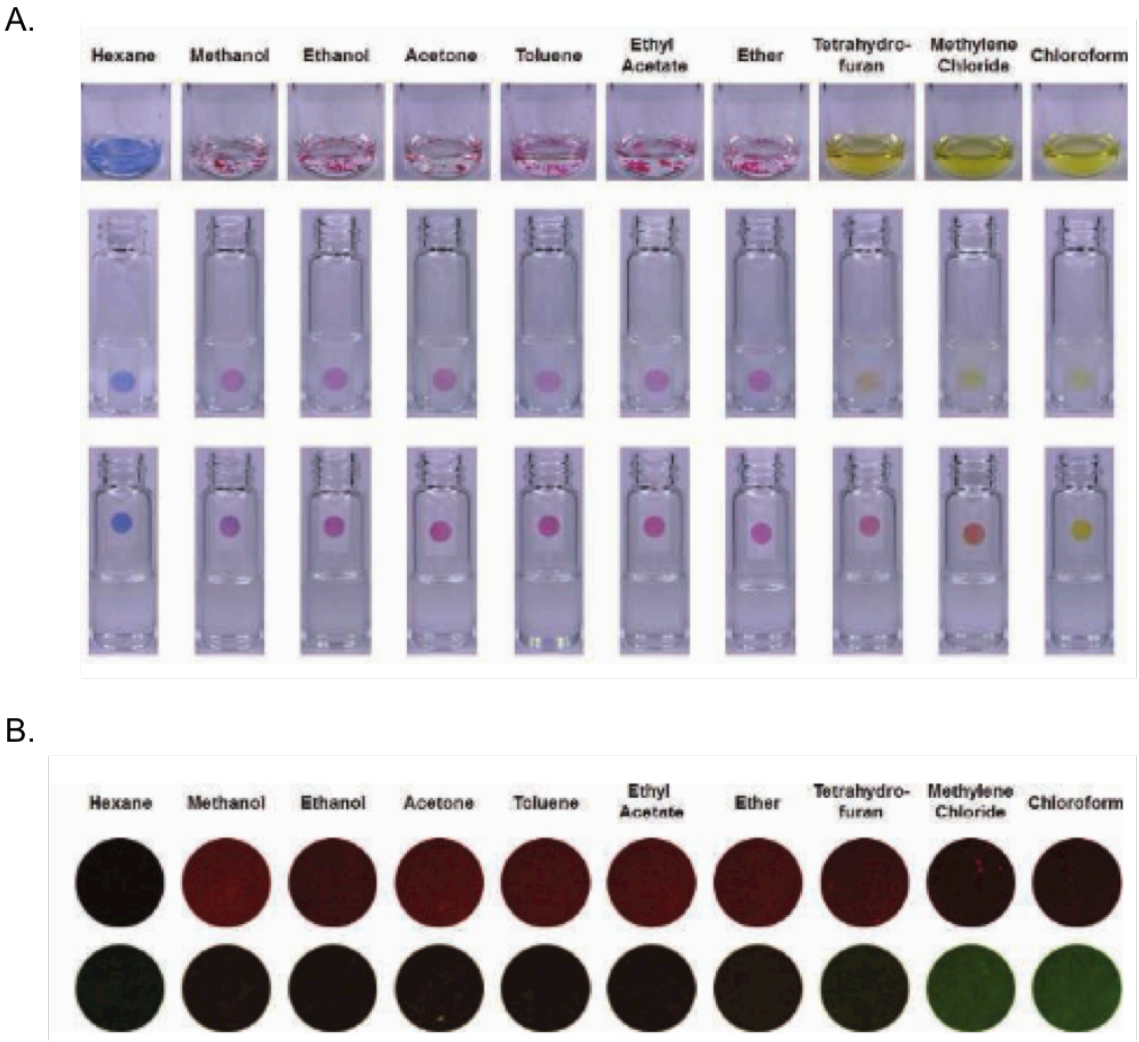

Figure 2.14. Chromatic and fluorescence transitions of inkjet printed PDA (poly-4BCMU) on paper strips. (A) Color of poly-4BCMU powder (top) and printed strips after reaction in various volatile organic compounds (middle) or to their vaporized form (bottom). (B) red (excitation 546 nm, top) and green (excitation 488 nm, bottom) fluorescence images of poly-4BCMU strips after exposure to volatile organic compounds. Adapted from ref. 105, Copyright 2013, *John Wiley & Sons, Inc.*

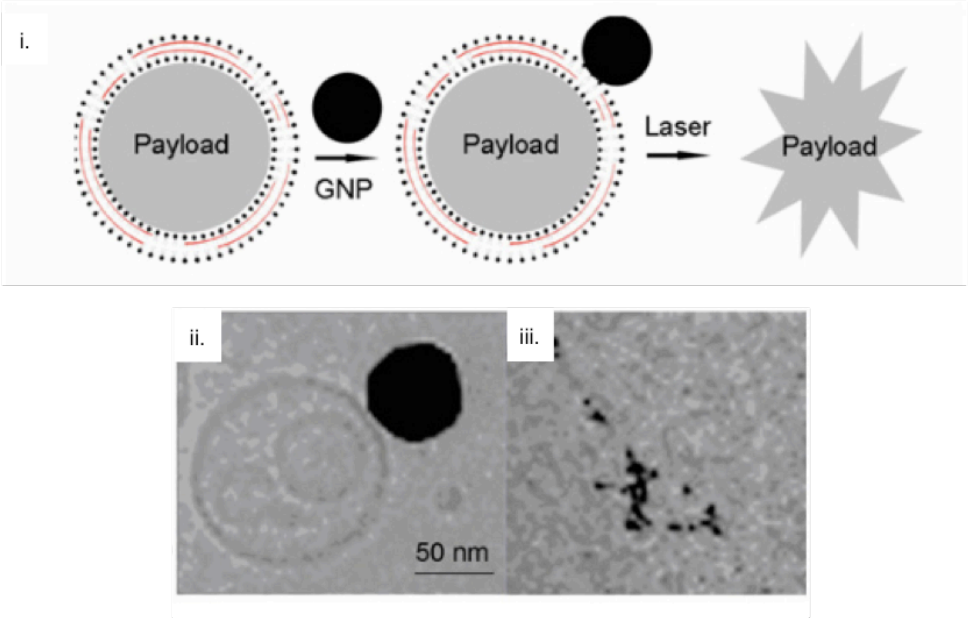

Figure 2.15. PDA liposomes for drug delivery. PDA bilayer liposomes carrying a "payload" (e.g., therapeutic drug) are conjugated with gold nanoparticles. When a laser excites the gold nanoparticles, the liposome is releases its payload to the surrounding environment (i). Electron cryo-microscopy images of the gold nanoparticle-tethered liposome before (ii) and after (iii) laser irradiation. Adapted from ref. 118, Copyright 2011, *IOP Publishing*.

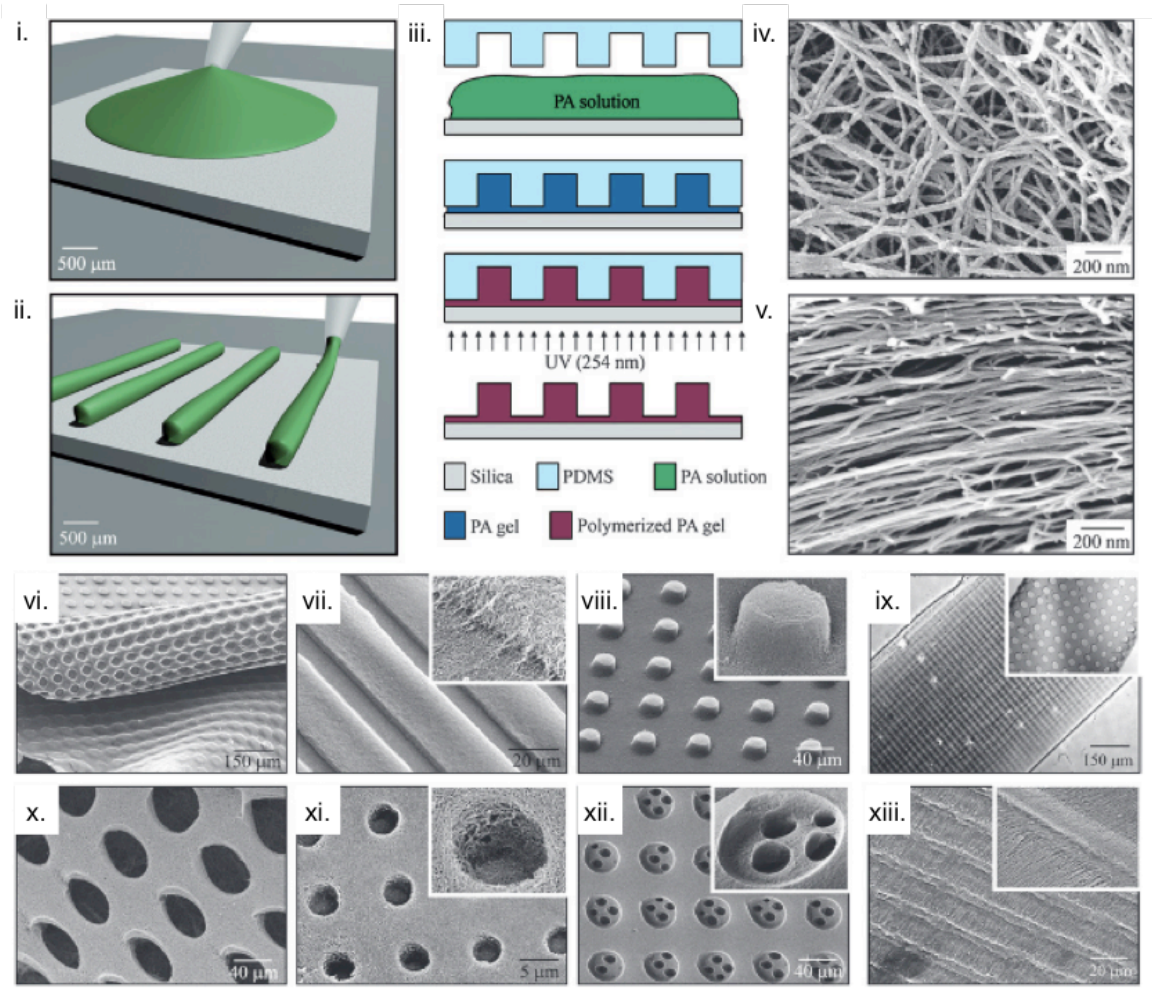

Figure 2.16. Micropatterned scaffolds for tissue engineering using peptide-conjugated PDA. Various techniques for scaffold fabrication (i-iii) create uniform or randomly oriented nanofibers (iv, v), removable layers (vi), microtextures (vii), pores (viii), channels (ix, xiii), holes (x), posts (xi), and two-level topographies (xii). This method produces PDA scaffold features down to 5 µm in size. Adapted from ref. 132, Copyright 2009, *Royal Society of Chemistry*.

Table 2.1 Modifications and methods to characterize/analyze PDA sensors

Reference	PDA Form	Detection Probe	Target	Functional Group(s)	Spacer	Additional Lipids	Characterization Methods	Analysis Methods	Detection Limit	Naked -Eye
Lee et al. (2007)	Liposomes	Anti-*Cryptospo-ridium parvum* antibody	*C. parvum*	Maleimide (MI)	N/A	N/A	1H NMR, spectrophotometry (UV-Vis), differential scanning calorimetry (DSC), transmission electron microscopy (TEM)	Color response (CR)	10^6 oocysts/mL	Yes
Jung et al. (2010)	Liposomes	Thrombin aptamers (BOCK and TASSET)	Thrombin	N/A	N/A	1,2-dimyristoyl-sn-glycero-3-phosphoethanol-amine (DMPE)	Scanning electron microscopy (SEM), fourier transfrom infrared spectroscopy (FTIR), dynamic light scattering (DLS), spectrophotometry (UV-Vis)	CR	0.5 mM thrombin	Yes
Wu et al. (2011)	Liposomes	Pentalysine-naphthalic acid (fluorophore) and Histidine	Bacterial lipopolysac-charide (LPS)	N/A	N/A	N/A	DLS, atomic force microscopy (AFM), spectrophotometry (UV-Vis, fluroescence)	photoluminscence /fluorescence microscopy and intensity, DLS (analysis of liposome size upon binding of target)	K (binding constant) = 1.5 x 10^6 M^{-1}, 4.91 x 10^8 cells/mL *E. coli*	No
Seo et al. (2010)	Liposomes	NH_2	diethyl phosphate (DEP, degraded nerve agent simulant)	N/A	Alkyl chains of different length (2-6 carbons)	N/A	Spectrophotometry (UV-Vis, photoluminscence)	CR	N/A (study compared CR based on size of targets, all targets were tested at 1mM)	N/A
Cho et al. (2013)	Liposomes	Amine-termianted diacetylenes	Heparin	N/A	2,26-(Ethylenedioxy)bis(ethylamine (EDEA)	N/A	DLS, Spectrophotometry (UV-Vis)	CR, Zeta Potential	2.5 μM in buffer, 5.6 uM in serum	No

Lee et al. (2008)	Liposomes immobilized on microarray	Potassium aptamer	Potassium	N/A	EDEA-succinic anhydride (EDEA-SA)	N/A	Spectrophotometry (UV-Vis, photoluminescence)	Fluorescence microscopy and intensity, circular dichroism (CD)	0.1 mM potassium	No
Kolusheva et al. (2012)	Liposomes embedded in sol-gel matrix	Various lipids (embedded) to create mulltiple vesicle types for fingerprinting	IBD, ALS and non-ALS disorders[1]	N/A	N/A	CAPPE, Chl, DCChl, DGS, DMPA, DMPC, DMPE, DMPG, DOPC, DTP, EA, PI, PTE, PS, SM, TM[1]	Confocal fluorescence microscopy, photo scanning (optical imaging)	Red chromatic shift	N/A	Yes
Jung et al. (2015)	Liposomes in hydrogel beads	Anti-phosphinothr-icin acetyltransfe-rase (PAT) antibody	PAT	N/A	N/A	1,2-dimyristoyl-sn-glycero-3-phosphocholi-ne (DMPC)	Spectrophotometry (UV-Vis)	RGB analysis (ImageJ module), Fluorescence intensity	20 nM PAT	Yes
Park et al. (2008)	Strips	Biotin; anti-microalbumi nruria monoclonal antibody	streptavidin (STA); microalbum-inaria (MAU)	TCDA-NH2/TCDA-OH; TCDA-OH	Diamine; N/A	N/A	FTIR, spectrophotometry (UV-Vis, photoluminescence)	Fluorescence microscopy and intensity; fluorescence microscopy	170 nM STA; 2 ug/mL MAU	No
Yoon et al. (2013)	Ink emulsion printed on paper	Bisurethane	Organic solvents	N/A	N/A	N/A	Spectrophotometry (UV-Vis), fluorescence imaging	Principal component analysis (PCA)	Discrimination between tetrahydrofuran (THF), methylene chloride and chloroform was achieved	Yes

[1] Abbreviations omitted due to space limitations, readers are refer article for full definitions

References

[1] Q. Cheng, R.C. Stevens, Charge-induced chromatic transition of amino acid-derivatized polydiacetylene liposomes, *Langmuir*, 14(1998) 1974-6.

[2] J. Song, Q. Cheng, S. Kopta, R.C. Stevens, Modulating artificial membrane morphology: pH-induced chromatic transition and nanostructural transformation of a bolaamphiphilic conjugated polymer from blue helical ribbons to red nanofibers, *J Am Chem Soc*, 123 (2001) 3205-13.

[3] H. Beckham, M. Rubner, On the origin of thermochromism in cross-polymerized diacetylene-functionalized polyamides, *Macromolecules*, 26(1993) 5198-201.

[4] R. Chance, G. Patel, J. Witt, Thermal effects on the optical properties of single crystals and solution-cast films of urethane substituted polydiacetylenes, *J Chem Phys*, 71(1979) 206-11.

[5] R.R. Chance, R.H. Baughman, H. Muller, C.J. Eckhardt, Thermochromism in a Polydiacetylene Crystal, *J Chem Phys*, 67(1977) 3616-8.

[6] R. Carpick, D. Sasaki, A. Burns, First observation of mechanochromism at the nanometer scale, *Langmuir*, 16(2000) 1270-8.

[7] I.K. Kwon, M.S. Song, S.H. Won, S.P. Choi, M. Kim, S.J. Sim, Signal amplification by magnetic force on polydiacetylene supramolecules for detection of prostate cancer, *Small*, 8(2012) 209-13.

[8] D.H. Charych, J.O. Nagy, W. Spevak, M.D. Bednarski, Direct colorimetric detection of a receptor-ligand interaction by a polymerized bilayer assembly, *Science*, 261(1993) 585-8.

[9] D.H. Charych, W. Spevak, J.O. Nagy, M.D. Bednarski, Specific interaction of influenza-virus with organized assemblies of polydiacetylenes, *Mater Res Soc Symp P*, 292(1993) 153-61.

[10] S.-H. Jung, H. Jang, M.-C. Lim, J.-H. Kim, K.-S. Shin, S.M. Kim, *et al.,* Chromatic biosensor for detection of phosphinothricin acetyltransferase (PAT) using polydiacetylene vesicles encapsulated within automatically generated immuno-hydrogel beads, *Anal Chem*, 87(2015) 2072-8.

[11] S.W. Lee, C.D. Kang, D.H. Yang, J.S. Lee, J.M. Kim, D.J. Ahn, *et al*., The development of a generic bioanalytical matrix using polydiacetylenes, *Adv Funct Mater*, 17(2007) 2038-44.

[12] H.K. Park, S.J. Chung, H.G. Park, J.-H. Cho, M. Kim, B.H. Chung, Mixed self-assembly of polydiacetylenes for highly specific and sensitive strip biosensors, *Biosens and Bioelectron*, 24(2008) 480-4.

[13] Y.-l. Su, J.-r. Li, L. Jiang, Chromatic immunoassay based on polydiacetylene vesicles, *Colloid Surface B*, 38(2004) 29-33.

[14] Y.K. Jung, T.W. Kim, H.G. Park, H.T. Soh, Specific colorimetric detection of proteins using bidentate aptamer-conjugated polydiacetylene (PDA) liposomes, *Adv Funct Mater*, 20(2010) 3092-7.

[15] J. Lee, H. Jun, J. Kim, Polydiacetylene–liposome microarrays for selective and sensitive mercury (II) detection, *Adv Mater*, 21(2009) 3674-7.

[16] J. Lee, H.-J. Kim, J. Kim, Polydiacetylene liposome arrays for selective potassium detection, *J Am Chem Soc*, 130(2008) 5010-1.

[17] J. Li, H.-E. Fu, L.-J. Wu, A.-X. Zheng, G.-N. Chen, H.-H. Yang, General colorimetric detection of proteins and small molecules based on cyclic enzymatic signal amplification and hairpin aptamer probe, *Anal Chem*, 84(2012) 5309-15.

[18] Y.K. Jung, T.W. Kim, C. Jung, D.Y. Cho, H.G. Park, A polydiacetylene microchip based on a biotin–streptavidin interaction for the diagnosis of pathogen infections, *Small*, 4(2008) 1778-84.

[19] J. Wu, A. Zawistowski, M. Ehrmann, T. Yi, C. Schmuck, Peptide functionalized polydiacetylene liposomes act as a fluorescent turn-on sensor for bacterial lipopolysaccharide, *J Am Chem Soc*, 133(2011) 9720-3.

[20] D.A. Jose, B. König, Polydiacetylene vesicles functionalized with N-heterocyclic ligands for metal cation binding, *Org Biomol Chem*, 8(2010) 655-62.

[21] W. Xue, D. Zhang, G. Zhang, D. Zhu, Colorimetric detection of glucose and an assay for acetylcholinesterase with amine-terminated polydiacetylene vesicles, *Chinese Sci Bull*, 56(2011) 1877-83.

[22] G. Wegner, Topochemische Reaktionen von Monomeren mit konjugierten Dreifachbindungen/Topochemical Reactions of Monomers with conjugated triple Bonds, *Makromol Chem B*, 24(1969) 824-32.

[23] S. Kolusheva, R. Zadmard, T. Schrader, R. Jelinek, Color fingerprinting of proteins by calixarenes embedded in lipid/polydiacetylene vesicles, *J Am Chem Soc*, 128(2006) 13592-8.

[24] R. Jelinek, S. Kolusheva, Polymerized lipid vesicles as colorimetric biosensors for biotechnological applications, *Biotechnol Adv*, 19(2001) 109-18.

[25] S.Y. Okada, R. Jelinek, D. Charych, Induced color change of conjugated polymeric vesicles by interfacial catalysis of phospholipase A2, *Angew Chem Int Ed*, 38(1999) 655-9.

[26] C. Wang, Z. Ma, Colorimetric detection of oligonucleotides using a polydiacetylene vesicle sensor, *Anal Bioanal Chem*, 382(2005) 1708-10.

[27] M.-C. Lim, Y.-J. Shin, T.-J. Jeon, H.-Y. Kim, Y.-R. Kim, Microbead-assisted PDA sensor for the detection of genetically modified organisms, *Anal Bioanal Chem*, 400 (2011) 777-85.

[28] T. Eaidkong, R. Mungkarndee, C. Phollookin, G. Tumcharern, M. Sukwattanasinitt, S. Wacharasindhu, Polydiacetylene paper-based colorimetric sensor array for vapor phase detection and identification of volatile organic compounds, *J Mater Chem*, 22(2012) 5970-7.

[29] S. Pumtang, W. Siripornnoppakhun, M. Sukwattanasinitt, A. Ajavakom, Solvent colorimetric paper-based polydiacetylene sensors from diacetylene lipids, *J Colloid Interf Sci*, 364(2011) 366-72.

[30] O.J. Dautel, M. Robitzer, J.P. Lere-Porte, F. Serein-Spirau, J.J.E. Moreau, Self-organized ureido substituted diacetylenic organogel. Photopolymerization of one-dimensional supramolecular assemblies to give conjugated nanofibers, *J Am Chem Soc*, 128(2006) 16213-23.

[31] J.-M. Kim, Y.B. Lee, S.K. Chae, D.J. Ahn, Patterned color and fluorescent images with polydiacetylene supramolecules embedded in poly(vinyl alcohol) films, *Adv Funct Mater*, 16(2006) 2103.

[32] N. Traiphol, N. Rungruangviriya, R. Potai, R. Traiphol, Stable polydiacetylene/ZnO nanocomposites with two-steps reversible and irreversible thermochromism: The influence of strong surface anchoring, *J Colloid Interf Sci*, 356(2011) 481-9.

[33] V. Haridas, S. Sadanandan, P.-Y. Collart-Dutilleul, S. Gronthos, N.H. Voelcker, Lysine-Appended Polydiacetylene Scaffolds for Human Mesenchymal Stem Cells, *Biomacromolecules*, 15(2014) 582-90.

[34] X. Wang, X. Sun, P.A. Hu, J. Zhang, L. Wang, W. Feng, *et al.*, Colorimetric Sensor Based on Self-Assembled Polydiacetylene/Graphene-Stacked Composite Film for Vapor-Phase Volatile Organic Compounds, *Adv Funct Mater*, 23(2013) 6044-50.

[35] J.T. Wen, K. Bohorquez, H. Tsutsui, Polydiacetylene-Coated Polyvinylidene Fluoride Strip Aptasensor for Colorimetric Detection of Zinc(II), *Sensor Actuat B-Chem*, (2016) doi:10.1016/j.snb.2016.03.118.

[36] D.J. Ahn, J.M. Kim, Fluorogenic polydiacetylene supramolecules: immobilization, micropatterning, and application to label-free chemosensors, *Acc Chem Res*, 41(2008) 805-16.

[37] R.W. Carpick, D.Y. Sasaki, M.S. Marcus, M.A. Eriksson, A.R. Burns, Polydiacetylene films: a review of recent investigations into chromogenic transitions and nanomechanical properties, *J Phys-Condens Mat*, 16 (2004) R679-R97.

[38] X. Chen, G. Zhou, X. Peng, J. Yoon, Biosensors and chemosensors based on the optical responses of polydiacetylenes, *Chem Soc Rev*, 41(2012) 4610-30.

[39] R. Jelinek, M. Ritenberg, Polydiacetylenes–recent molecular advances and applications, *RSC Adv*, 3(2013) 21192-201.

[40] S. Okada, S. Peng, W. Spevak, D. Charych, Color and chromism of polydiacetylene vesicles, *Accounts Chem Res*, 31(1998) 229-39.

[41] M.A. Reppy, B.A. Pindzola, Biosensing with polydiacetylene materials: structures, optical properties and applications, *Chem Commun*, 42(2007) 4317-38.

[42] X. Sun, T. Chen, S. Huang, L. Li, H. Peng, Chromatic polydiacetylene with novel sensitivity, *Chem Soc Rev*, 39(2010) 4244-57.

[43] B. Tieke, Polymerization of butadiene and butadiyne (diacetylene) derivatives in layer structures, *Adv Polym Sci*, 71(1985) 79-151.

[44] B. Yoon, S. Lee, J.M. Kim, Recent conceptual and technological advances in polydiacetylene-based supramolecular chemosensors, *Chem Soc Rev*, 38(2009) 1958-68.

[45] G. Wegner, Topochemical reactions of monomers with conjugated triple-bonds. IV. Polymerization of bis-(p-toluene sulfonate) of 2.4-hexadiin-1.6-diol, *Makromol Chem B*, 145(1971) 85-94.

[46] D. Charych, Q. Cheng, A. Reichert, G. Kuziemko, M. Stroh, J.O. Nagy, *et al.*, A 'litmus test' for molecular recognition using artificial membranes, *Chem Biol*, 3(1996) 113-20.

[47] R. Jelinek, S. Okada, S. Norvez, D. Charych, Interfacial catalysis by phospholipases at conjugated lipid vesicles: colorimetric detection and NMR spectroscopy, *Chem Biol*, 5(1998) 619-29.

[48] A. Reichert, D.J. Ahn, J. Nagy, D. Charych, Recognition and Detection at Tailored Polydiacetylene Molecular Assemblies, *Abstr Pap Am Chem S*, 209(1995) 163.

[49] W. Spevak, J.O. Nagy, D.H. Charych, Molecular Assemblies of Functionalized Polydiacetylenes, *Adv Mater*, 7(1995) 85-9.

[50] W. Spevak, J.O. Nagy, D.H. Charych, M.E. Schaefer, J.H. Gilbert, M.D. Bednarski, Polymerized Liposomes Containing C-Glycosides of Sialic-Acid - Potent Inhibitors of Influenza-Virus Invitro Infectivity, *J Am Chem Soc*, 115(1993) 1146-7.

[51] D.C. Lee, S.K. Sahoo, A.L. Cholli, D.J. Sandman, Structural aspects of the thermochromic transition in urethane-substituted polydiacetylenes, *Macromolecules*, 35(2002) 4347-55.

[52] G.G. Odian, Principles of polymerization: Wiley-Interscience New York; 2004.

[53] M.D. Mowery, C.E. Evans, Steric and substrate mediation of polymers formed within single molecular layers, *J Phys Chem B*, 101(1997) 8513-9.

[54] M.D. Mowery, H. Menzel, M. Cai, C.E. Evans, Fabrication of monolayers containing internal molecular scaffolding: effect of substrate preparation, *Langmuir*, 14(1998) 5594-602.

[55] D. Bloor, R. Chance, Polydiacetylenes: synthesis, structure and electronic properties: Springer; 1985.

[56] D.J. Ahn, E.H. Chae, G.S. Lee, H.Y. Shim, T.E. Chang, K.D. Ahn, *et al.*, Colorimetric reversibility of polydiacetylene supramolecules having enhanced hydrogen-bonding under thermal and pH stimuli, *J Am Chem Soc*, 125(2003) 8976-7.

[57] A. Lio, A. Reichert, D.J. Ahn, J.O. Nagy, M. Salmeron, D.H. Charych, Molecular imaging of thermochromic carbohydrate-modified polydiacetylene thin films, *Langmuir*, 13(1997) 6524-32.

[58] D.J. Sandman, J.M. Njus, B. Tran, Approaches to conjugated polymers via new solid state polymerizations, *Macromol Symp*, 216(2004) 77-85.

[59] J.-M. Kim, J.-S. Lee, H. Choi, D. Sohn, D.J. Ahn, Rational design and in-situ FTIR analyses of colorimetrically reversibe polydiacetylene supramolecules, *Macromolecules*, 38(2005) 9366-76.

[60] H. Shin, B. Yoon, I.S. Park, J.-M. Kim, An electrothermochromic paper display based on colorimetrically reversible polydiacetylenes, *Nanotechnology*, 25(2014) 094011.

[61] M.A. Reppy, Signal generation from switchable polydiacetylene fluorescence, *Mat Res Soc Symp Proc*, 723(2002) 147-52.

[62] Z.G. Soos, D.S. Galvao, S. Etemad, Fluorescence and Excited-State Structure of Conjugated Polymers, *Adv Mater*, 6(1994) 280-7.

[63] J. Olmsted, M. Strand, Fluorescence of polymerized diacetylene bilayer films, *J Phys Chem-Us*, 87(1983) 4790-2.

[64] S. Seo, J. Lee, E.J. Choi, E.J. Kim, J.Y. Song, J. Kim, Polydiacetylene Liposome Microarray Toward Influenza A Virus Detection: Effect of Target Size on Turn-On Signaling, *Macromol Rapid Comm*, 34(2013) 743-8.

[65] X. Li, S. Matthews, P. Kohli, Fluorescence resonance energy transfer in polydiacetylene liposomes, *J Phys Chem B*, 112(2008) 13263-72.

[66] X. Li, M. McCarroll, P. Kohli, Modulating fluorescence resonance energy transfer in conjugated liposomes, *Langmuir*, 22(2006) 8615-7.

[67] S. Kolusheva, L. Boyer, R. Jelinek, A colorimetric assay for rapid screening of antimicrobial peptides, *Nat Biotechnol*, 18(2000) 225-7.

[68] S. Kolusheva, R. Kafri, M. Katz, R. Jelinek, Rapid colorimetric detection of antibody-epitope recognition at a biomimetic membrane interface*, J Am Chem Soc*, 123(2001) 417-22.

[69] S. Kolusheva, T. Shahal, R. Jelinek, Cation-Selective Color Sensors Composed of Ionophore-Phospholipid-Polydiacetylene Mixed Vesicles*, J Am Chem Soc*, 122(2000) 776-80.

[70] S. Kolusheva, T. Shahal, R. Jelinek, Peptide−Membrane Interactions Studied by a New Phospholipid/Polydiacetylene Colorimetric Vesicle Assay, *Biochemistry-Us*, 39(2000) 15851-9.

[71] S. Kolusheva, E. Wachtel, R. Jelinek, Biomimetic lipid/polymer colorimetric membranes molecular and cooperative properties, *J Lipid Res*, 44(2003) 65-71.

[72] Y. Scindia, L. Silbert, R. Volinsky, S. Kolusheva, R. Jelinek, Colorimetric detection and fingerprinting of bacteria by glass-supported lipid/polydiacetylene films, *Langmuir*, 23(2007) 4682-7.

[73] L. Silbert, I. Ben Shlush, E. Israel, A. Porgador, S. Kolusheva, R. Jelinek, Rapid chromatic detection of bacteria by use of a new biomimetic polymer sensor, *Appl Environ Microb*, 72(2006) 7339-44.

[74] K.W. Kim, H. Choi, G.S. Lee, D.J. Ahn, M.K. Oh, Effect of phospholipid insertion on arrayed polydiacetylene biosensors, *Colloid Surface B*, 66(2008) 213-7.

[75] D. Evrard, E. Touitou, S. Kolusheva, Y. Fishov, R. Jelinek, A new colorimetric assay for studying and rapid screening of membrane penetration enhancers, *Pharm Res*, 18(2001) 943-9.

[76] R. Halevy, A. Rozek, S. Kolusheva, R.E. Hancock, R. Jelinek, Membrane binding and permeation by indolicidin analogs studied by a biomimetic lipid/polydiacetylene vesicle assay, *Peptides*, 24(2003) 1753-61.

[77] A. Pevzner, S. Kolusheva, Z. Orynbayeva, R. Jelinek, Giant chromatic lipid/polydiacetylene vesicles for detection and visualization of membrane interactions, *Adv Funct Mater*, 18(2008) 242-7.

[78] T.J. Deming, Synthetic polypeptides for biomedical applications, *Prog Polym Sci*, 32(2007) 858-75.

[79] Z. Orynbayeva, S. Kolusheva, N. Groysman, N. Gavrielov, L. Lobel, R. Jelinek, Vaccinia virus interactions with the cell membrane studied by new chromatic vesicle and cell sensor assays, *J Virol*, 81(2007) 1140-7.

[80] M.D. Wyrsta, A.L. Cogen, T.J. Deming, A parallel synthetic approach for the analysis of membrane interactive copolypeptides*, J Am Chem Soc*, 123(2001) 12919-20.

[81] A. Siano, M.V. Humpola, M.C. Rey, A. Simonetta, G.G. Tonarelli, Interaction of Acylated and Substituted Antimicrobial Peptide Analogs with Phospholipid-Polydiacetylene Vesicles. Correlation with their Biological Properties, *Chem Biol Drug Des*, 78(2011) 85-93.

[82] M. Sokolovski, T. Sheynis, S. Kolusheva, R. Jelinek, Membrane interactions and lipid binding of casein oligomers and early aggregates, *Biochimica et Biophysica Acta*, 1778(2008) 2341-9.

[83] G.T. Hermanson, Bioconjugate techniques: Academic press; 2013.

[84] J. Lee, J. Kim, Multiphasic sensory alginate particle having polydiacetylene liposome for selective and more sensitive multitargeting detection, *Chem Mater*, 24(2012) 2817-22.

[85] D. Seo, J. Kim, Effect of the molecular size of analytes on polydiacetylene chromism, *Adv Funct Mater*, 20(2010) 1397-403.

[86] Y.-S. Cho, K.H. Ahn, Molecular interactions between charged macromolecules: colorimetric detection and quantification of heparin with a polydiacetylene liposome, *J Phys Chem B*, 1(2013) 1182-9.

[87] Y.K. Jung, T.W. Kim, J. Kim, J.M. Kim, H.G. Park, Universal colorimetric detection of nucleic acids based on polydiacetylene (PDA) liposomes, *Adv Funct Mater*, 18(2008) 701-8.

[88] H.-C. Lee, S. Jeon, J.-M. Kim, C.-W. Chung, Colorimetric polydiacetylene for plasma diagnostics, *Sensor Actuat B-Chem*, 203(2014) 130-4.

[89] M. Nieuwland, N. van Gijzel, J.C. van Hest, D.W. Löwik, The influence of amino acid sequence on structure and morphology of polydiacetylene containing peptide fibres, *Soft Matter*, 11(2015) 1335-44.

[90] R.W. Carpick, T.M. Mayer, D.Y. Sasaki, A.R. Burns, Spectroscopic ellipsometry and fluorescence study of thermochromism in an ultrathin poly(diacetylene) film: Reversibility and transition kinetics, *Langmuir*, 16(2000) 4639-47.

[91] A.A. Deckert, L. Fallon, L. Kiernan, C. Cashin, A. Perrone, T. Encalarde, Kinetics of the reversible thermochromism in langmuir-blodgett-films of $Cd2^{+}$ salts of polydiacetylenes studied using UV-Vis spectroscopy, *Langmuir*, 10(1994) 1948-54.

[92] Q. Huo, K.C. Russell, R.M. Leblanc, Chromatic studies of a polymerizable diacetylene hydrogen bonding self-assembly: A "self-folding" process to explain the chromatic changes of polydiacetylenes, *Langmuir*, 15(1999) 3972-80.

[93] X. Pan, Y. Wang, H. Jiang, G. Zou, Q. Zhang, Benzo-15-crown-5 functionalized polydiacetylene-based colorimetric self-assembled vesicular receptors for lead ion recognition, *J Mater Chem*, 21(2011) 3604-10.

[94] B. Chu, R.L. Xu, Chromatic Transition of Polydiacetylene in Solution, Accounts *Chem Res*, 24(1991) 384-9.

[95] D.N. Batchelder, S.D. Evans, T.L. Freeman, L. Haussling, H. Ringsdorf, H. Wolf, Self-Assembled Monolayers Containing Polydiacetylenes, *J Am Chem Soc*, 116(1994) 1050-3.

[96] H. Menzel, S. Horstmann, M.D. Mowery, M. Cai, C.E. Evans, Diacetylene polymerization in self-assembled monolayers: influence of the odd/even nature of the methylene spacer, *Polymer*, 41(2000) 8113-9.

[97] N. Mino, H. Tamura, K. Ogawa, Analysis of Color Transitions and Changes on Langmuir-Blodgett-Films of a Polydiacetylene Derivative, *Langmuir*, 7(1991) 2336-41.

[98] R. Volinsky, F. Gaboriaud, A. Berman, R. Jelinek, Morphology and organization of phospholipid/diacetylene Langmuir films studied by Brewster angle microscopy and fluorescence microscopy, *J Phys Chem B*, 106(2002) 9231-6.

[99] T.S. Kim, R.M. Crooks, M. Tsen, L. Sun, Polymeric Self-Assembled Monolayers. 2. Synthesis and Characterization of Self-Assembled Polydiacetylene Monolayers and Multilayers, *J Am Chem Soc*, 117(1995) 3963-7.

[100] R. Volinsky, M. Kliger, T. Sheynis, S. Kolusheva, R. Jelinek, Glass-supported lipid/polydiacetylene films for colour sensing of membrane-active compounds, *Biosens Bioelectron*, 22(2007) 3247-51.

[101] S. Friedman, S. Kolusheva, R. Volinsky, L. Zeiri, T. Schrader, R. Jelinek, Lipid/polydiacetylene films for colorimetric protein surface-charge analysis, *Anal Chem*, 80(2008) 7804-11.

[102] R. Jelinek, S. Kolusheva, E. Mann, M. Aviram, Chromatic polymer assays for the analysis of lipid and lipoprotein peroxidation, *Lipid Technology*, 27(2015) 86-9.

[103] S. Kolusheva, R. Yossef, A. Kugel, M. Katz, R. Volinsky, M. Welt, *et al*., Array-based disease diagnostics using lipid/polydiacetylene vesicles encapsulated in a sol-gel matrix, *Anal Chem*, 84(2012) 5925-31.

[104] W.K. Pratt, Digital Image Processing, 3rd ed., John Wiley & Sons, Inc. 2001, pp. 643-72.

[105] B. Yoon, I.S. Park, H. Shin, H.J. Park, C.W. Lee, J.M. Kim, A Litmus-Type Colorimetric and Fluorometric Volatile Organic Compound Sensor Based on Inkjet‐Printed Polydiacetylenes on Paper Substrates, *Macromol Rapid Comm*, 34(2013) 731-5.

[106] B. Yoon, H. Shin, E.-M. Kang, D.W. Cho, K. Shin, H. Chung, *et al.*, Inkjet-Compatible Single-Component Polydiacetylene Precursors for Thermochromic Paper Sensors, *ACS Appl Mater Interfaces*, 5(2013) 4527-35.

[107] T. Soga, Y. Jimbo, K. Suzuki, D. Citterio, Inkjet-printed paper-based colorimetric sensor array for the discrimination of volatile primary amines, *Anal Chem*, 85(2013) 8973-8.

[108] Y. Li, L. Wang, X. Yin, B. Ding, G. Sun, T. Ke, *et al*., Colorimetric Strips for Visual Lead Ion Recognition Utilizing Polydiacetylenes Embedded Nanofibers, *J Mater Chem A*, 2(2014) 18304-12.

[109] Y. Li, L. Wang, Y. Wen, B. Ding, G. Sun, T. Ke, *et al*., Constituting Visually Detection System for Lead (II) on Polydiacetylene-Glycine Embedded Nanofibrous Membranes, *J Mater Chem A*, 3(2015) 9722-30.

[110] J.M. Collins, Pharmacologic rationale for regional drug delivery, *J Clin Oncol*, 2(1984) 498-504.

[111] L.D. Mayer, L.C. Tai, D.S. Ko, D. Masin, R.S. Ginsberg, P.R. Cullis*, et al*., Influence of vesicle size, lipid composition, and drug-to-lipid ratio on the biological activity of liposomal doxorubicin in mice, *Cancer Res*, 49(1989) 5922-30.

[112] C. Guo, S. Liu, C. Jiang, W. Li, Z. Dai, H. Fritz*, et al.,* A promising drug controlled-release system based on diacetylene/phospholipid polymerized vesicles, *Langmuir*, 25(2009) 13114-9.

[113] A. Gabizon, D. Papahadjopoulos, Liposome formulations with prolonged circulation time in blood and enhanced uptake by tumors, *Proc Natl Acad Sci USA*, 85(1988) 6949-53.

[114] J. Okada, S. Cohen, R. Langer, In vitro evaluation of polymerized liposomes as an oral drug delivery system, *Pharm Res*, 12(1995) 576-82.

[115] J.M. Jeong, Y.C. Chung, J.H. Hwang, Enhanced adjuvantic property of polymerized liposome as compared to a phospholipid liposome, *J Biotechnol*, 94(2002) 255-63.

[116] H. Chen, V. Torchilin, R. Langer, Lectin-bearing polymerized liposomes as potential oral vaccine carriers, *Pharm Res*, 13(1996) 1378-83.

[117] N. Khan, C.A. Wyres, Multi-colour printing, Google Patents, 2005.

[118] G. Qin, Z. Li, R. Xia, F. Li, B.E. O'Neill, J.T. Goodwin, *et al.*, Partially polymerized liposomes: stable against leakage yet capable of instantaneous release for remote controlled drug delivery, *Nanotechnology*, 22(2011) 155605.

[119] G. Wu, A. Mikhailovsky, H.A. Khant, C. Fu, W. Chiu, J.A. Zasadzinski, Remotely triggered liposome release by near-infrared light absorption via hollow gold nanoshells, *J Am Chem Soc*, 130(2008) 8175-7.

[120] C. Guo, S. Liu, Z. Dai, C. Jiang, W. Li, Polydiacetylene vesicles as a novel drug sustained-release system, *Colloid Surface B*, 76(2010) 362-5.

[121] X. Yan, X. An, Multifunctional polydiacetylene-liposome with controlled release and fluorescence tracing, *RSC Adv*, 4(2014) 18604-7.

[122] N. Mackiewicz, E. Gravel, A. Garofalakis, J. Ogier, J. John, D.M. Dupont, *et al.*, Tumor‐Targeted polydiacetylene micelles for *in vivo* imaging and drug delivery, *Small*, 7(2011) 2786-92.

[123] J.T. Wen, C. Castro, H. Tsutsui, *In planta* microsphere-based lateral flow leaf biosensor in maize, *J Lab Autom*, 20(2015)500-505.

[124] J.D. Hartgerink, E. Beniash, S.I. Stupp, Peptide-amphiphile nanofibers: a versatile scaffold for the preparation of self-assembling materials, *Proc Natl Acad Sci USA*, 99(2002) 5133-8.

[125] J.B. Matson, S.I. Stupp, Self-assembling peptide scaffolds for regenerative medicine, *Chem Commun*, 48(2012) 26-33.

[126] J.B. Matson, R.H. Zha, S.I. Stupp, Peptide Self-Assembly for Crafting Functional Biological Materials, *Curr Opin Solid State Mater Sci*, 15(2011) 225-35.

[127] L.A. Smith, P.X. Ma, Nano-fibrous scaffolds for tissue engineering, *Colloid Surface B*, 39(2004) 125-31.

[128] M.A. Biesalski, A. Knaebel, R. Tu, M. Tirrell, Cell adhesion on a polymerized peptide-amphiphile monolayer, *Biomaterials*, 27(2006) 1259-69.

[129] E. Jahnke, I. Lieberwirth, N. Severin, J.P. Rabe, H. Frauenrath, Topochemical polymerization in supramolecular polymers of oligopeptide-functionalized diacetylenes, *Angew Chem Int Ed*, 45(2006) 5383-6.

[130] S.K. Chae, H. Park, J. Yoon, C.H. Lee, D.J. Ahn, J.M. Kim, Polydiacetylene supramolecules in electrospun microfibers: Fabrication, micropatterning, and sensor applications, *Adv Mater*, 19(2007) 521-4.

[131] H.S. Peng, X.M. Sun, F.J. Cai, X.L. Chen, Y.C. Zhu, G.P. Liao, *et al.*, Electrochromatic carbon nanotube/polydiacetylene nanocomposite fibres, *Nat Nanotechnol*, 4(2009) 738-41.

[132] A. Mata, L. Hsu, R. Capito, C. Aparicio, K. Henrikson, S.I. Stupp, Micropatterning of bioactive self-assembling gels, *Soft Matter*, 5(2009) 1228-36.

CHAPTER 3:

METHODOLOGY

Abstract

This chapter provides a detailed description of the general protocols followed in the studies from this research. These include the preparation and analysis of polydiacetylene liposomes and coated strips. Procedures for the bacterial cultures used in this work and the method for corn growth is additionally delineated. For details regarding the materials used for individual studies, readers are referred to Materials and Methods section of the corresponding chapter for that study.

1. PREPARATION OF DIACETYLENE-N-HYDROXYSUCCINIMIDE (DA-NHS)

Conversion of diacetylene (DA) to its succinimide ester (DA-NHS) was carried out as previously described in literature [1, 2]. Briefly, 0.72 mmol DA, 1.35 mmol of N-(3-dimethylaminopropyl)-N'-ethylcarbodiimide hydrochloride (EDC-HCl) and 1.07 mmol of N-hydroxysuccinimide (NHS) were dissolved in 4 mL of dichloromethane. The solution was stirred with a magnetic stirrer for 2 h at room temperature. The solvent was evaporated by a stream of nitrogen and the residue was purified by extraction with ethyl acetate to yield DA-NHS monomers as a white solid. ^{1}H NMR (400 MHz, CHLOROFORM-*d*) d ppm: TCDA-NHS - 0.89 (t, 3 H) 1.26 - 1.79 (m, 28 H) 2.25 (t, 4 H) 2.61 (t, 2 H) 2.85 (br. s., 4 H); PCDA-NHS - 0.89 (t, 3 H) 1.21 - 1.79 (m, 36 H) 2.25 (t, 4 H) 2.61 (t, 2 H) 2.84 (br. s., 4 H) (Figure 2.11).

2. LIPOSOME SYNTHESIS[1] (Chapters 4 and 7)

DA-NHS, DA and phospholipid were mixed in chloroform, and the solvent was evaporated by a stream of nitrogen air. The mixture was resuspended in deionized water and sonicated (Qsonica Q500, 20% amplitude) at 80 ºC for 15 m. The aptamer (Chapter 4) or antibody (Chapter 7) was then added to the solution and gently agitated for 4 h to allow for conjugation (Figure 3.1). Unreacted NHS was quenched by the addition of ethanolamine (Chapter 4) or bovine serum albumin (BSA) (Chapter 7). The solution was stored at 4 ºC overnight. Photopolymerization of the solution under 254 nm UV light

yielded a blue PDA liposome solution. Liposome size was determined by dynamic light scattering (DLS, Malvern Zetasizer Nano ZS90)

3. STRIP FABRICATION (Chapters 4 and 5)

3.1 Aptamer Conjugation (Chapter 4)

850 nmol of TCDA-NHS was incubated with 200 nmol of aptamer **1** in 300 μL dichloromethane for 4 h at room temperature in the dark. Unreacted compounds were removed by dialysis.

3.2 Strip Preparation[1]

A DA solution containing DA-aptamer (Chapter 4) or DA-NHS (Chapter 5), DA, and phospholipid was prepared in 500 μL chloroform. Polyvinylidene fluoride (PVDF) strips were prepared using a guillotine paper cutter and scissors. The strips were dipped into and immediately removed from the DA solution and allowed to dry under ambient conditions in a fume hood (< 10 s).

3.3 Antibody Conjugation (Chapter 5)

Prepared strips were incubated in a solution containing 0.04 mg/mL of anti-*Xylella fastidiosa* antibody for 4 h in room temperature or overnight at 4 ºC. Following

[1]Exact amounts of compounds and reagents used are not given in this subsection due to variation among the studies. Readers are referred to individual chapters for this information.

conjugation, the strips were incubated in 18.3 nM BSA for 1 h to inactivate remaining NHS sites and remove any unconjugated antibody, rinsed in deionized water, and allowed to dry in the dark.

3.4 Polymerization

Photopolymerization of the strips under a mask with 254 nm UV light (Spectroline E-series, 6 W) for 60 s yielded blue-colored polydiacetylene (PDA) tips.

4. ANALYSIS

4.1 Color Response of Liposomes (Chapters 4 and 7)

Absorption measurements of liposomes were recorded by a spectrophotometer (Thermo Scientific NanoDrop 2000c). All experiments were performed in triplicates and three measurements were recorded for each sample. Color Response (CR) was calculated as previously described [3] (Chapter 2, Section 4.2.1). Briefly, the percent blue, PB, was first defined as:

$$PB = \frac{A_{blue}}{A_{blue} + A_{red}} \times 100\%$$

where A_{blue} is the absorbance peak at 647 nm (PDA blue form) and A_{red} is the absorbance peak at 521 nm (PDA red form). Then, the CR was defined as:

$$CR = \frac{\left(PB_0 - PB_f\right)}{PB_0} \times 100\%$$

where PB_0 is the initial precent blue of untested liposomes and PB_f is the final percent blue of liposomes incubated with test samples.

4.2 Red Chromatic Shift of Strips (Chapters 4 and 5)

Color images of PDA strips were recorded using a Nikon D5100 digital camera. Data from collected images were extracted using ImageJ software as 8-bit red-green-blue (RGB) values. Red chromatic shift (RCS) was calculated using digital colorimetric analysis as previously described [4] (Chapter 2, Section 4.2.2). In short, the red chromaticity level (r), calculated as

$$r = \frac{R}{R + G + B}$$

depicts the relative intensity of the red component of the image. The RCS, which then defines the extent of the blue-to-red transition, was determined by:

$$\%\ RCS = \frac{r_{sample} - r_0}{r_{max} - r_0} \times 100\%$$

where r_{sample} is the average red chromaticity level of the sample image, r_0 is the average red chromaticity level of strips dipped in deionized water (Chapter 4) or media (Chapter 7) (negative control), and r_{max} is the average red chromaticity level of strips in 1 M NaOH (positive control). PDA materials in 1 M NaOH are commonly used as a positive control because its high pH (=14) readily induces clear red transitions [4]. All experiments were performed in triplicates.

4.3 Principle Component Analysis of Strips (Chapters 4 and 5)

To extract further information from RGB data sets, principal component analysis (PCA) of three variables (red, green, blue) was employed using the Microsoft Excel add-in Multibase package (Numerical Dynamic, Japan). PCA is a mathematical transformation of multivariate data that is often used to statistically visualize RGB data sets due to their high dimensionality, where each image is represented by three RGB values [5-7]. The transformation reduces dimensionality of the RGB data, converting the data set to a new PCA score plot, on which the axes are determined by orthogonal factors drawn from the data that maximize the variance of the data set [8, 9].

5. BACTERIAL CULTURES (Chapters 5 and 7)

Xylella fastidiosa subsp. *fastidiosa* (Temecula-1) was streaked from a stock stored at -80 ºC onto six PD3 agar plates and incubated at 28 ºC for six days. Subsequently, 1 mL of PD3 media was added to each plate and the cells were harvested by scraping them into the liquid. The liquid cell culture was then transferred from each plate into a conical tube and vortexed gently to resuspend cell clumps. The final volume of the culture was adjusted to 10 mL by addition of PD3 media with an OD_{600} of 0.68. The concentration of the culture was determined by cell counting using a hemocytometer to be 4.1×10^8 cells/mL. The culture was stored at 4 ºC until use to prevent additional growing of cells.

Pantoea stewartii subsp. *stewartii* (DC283) was grown on solid Luria Agar at 28 ºC and was used to inoculate an overnight culture of Luria Broth shaken at the same

temperature at 180 rpm. OD_{600} was measured at 3.37. The concentration of the culture was determined by cell counting using a hemocytometer to be 4.7 x 10^8 cells/mL. The culture was stored at 4 ºC until use to prevent additional growing of cells.

Escherichia coli BL21 (DE3) was grown on solid Luria Agar at 37 ºC and was used to inoculate an overnight culture of LB media shaken at the same temperature at 200 rpm. OD_{600} was measured at 1.70. The concentration of the culture was determined by cell counting using a hemocytometer to be 1.36 x 10^9 cells/mL. The culture was stored at 4 ºC until use to prevent additional growing of cells.

6. MAIZE GROWTH (Chapters 6 and 7)

Maize seeds were germinated in coarse vermiculite in a greenhouse maintained within a temperature range of 16-27 ºC (61-81 ºF). Seeds and plants were immersed once a day in fertilizer solution (125 ppm N).

7. FIGURES

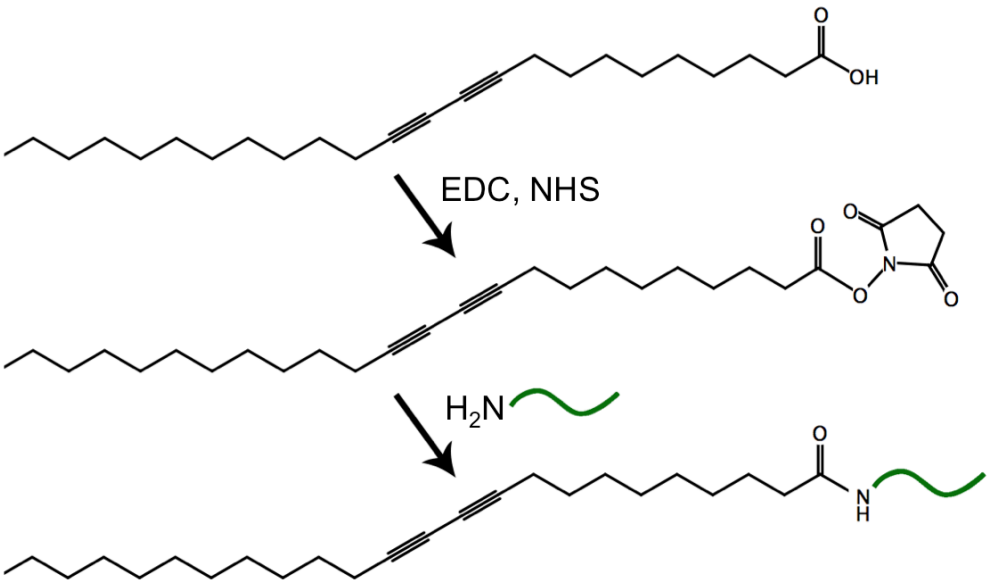

Figure 3.1. Conjugation of detection probe (green) to diacetylenes through activation with N-(3-dimethylaminopropyl)-N'-ethylcarbodiimide (EDC) and N-hydroxysuccinimide (NHS).

References

[1] J. Lee, H. Jun, J. Kim, Polydiacetylene–liposome microarrays for selective and sensitive mercury(II) detection, *Adv Mater*, 21(2009) 3674-7.

[2] J. Lee, H.-J. Kim, J. Kim, Polydiacetylene liposome arrays for selective potassium detection, *J Am Chem Soc*, 130(2008) 5010-1.

[3] S. Okada, S. Peng, W. Spevak, D. Charych, Color and chromism of polydiacetylene vesicles, *Accounts Chem Res*, 31(1998) 229-39.

[4] R. Volinsky, M. Kliger, T. Sheynis, S. Kolusheva, R. Jelinek, Glass-supported lipid/polydiacetylene films for colour sensing of membrane-active compounds, *Biosens Bioelectron*, 22(2007) 3247-51.

[5] Y. Li, L. Wang, X. Yin, B. Ding, G. Sun, T. Ke, *et al.,* Colorimetric strips for visual lead ion recognition utilizing polydiacetylenes embedded nanofibers, *J Mater Chem A*, 2(2014) 18304-12.

[6] T. Soga, Y. Jimbo, K. Suzuki, D. Citterio, Inkjet-printed paper-based colorimetric sensor array for the discrimination of volatile primary amines, *Anal Chem*, 85(2013) 8973-8.

[7] B. Yoon, I.S. Park, H. Shin, H.J. Park, C.W. Lee, J.M. Kim, A litmus-type colorimetric and fluorometric volatile organic compound sensor based on inkjet-printed polydiacetylenes on paper substrates, *Macromol Rapid Comm*, 34(2013) 731-5.

[8] S. Wold, K. Esbensen, P. Geladi, Principal component analysis, *Chemom Intell Lab Syst*, 2(1987) 37-52.

[9] M. Ringnér, What is principal component analysis?, *Nat Biotechnol*, 26(2008) 303-4.

PREFACE: CHAPTERS 4 & 5

Chapters 4 and 5 of this dissertation describe the development of polydiacetylene-based strip sensors. These devices are aimed for *in vitro* in-field diagnostics of processed plant materials. The studies reported in Chapter 4 have been previously published all or in part by *Elsevier B.V.* (Copyright, 2016, doi: 10.1016/j.snb.2016.03.118).

CHAPTER 4:

STRIP APTASENSOR FOR CHROMATIC DETECTION OF ZINC(II)

Abstract

This chapter reports a polydiacetylene sensor strip for simple visual detection of zinc ions in aqueous solution. The specificity of this sensor comes from Zn^{2+} DNA aptamer probes conjugated onto the polydiacetylene layer. Effects of aptamer length and structure on the sensitivity of polydiacetylene color transitions were first investigated. Diacetylenes conjugated with the optimal aptamer sequence were then coated onto a strip of polyvinylidene fluoride membrane and photopolymerized by UV exposure. The newly developed sensor exhibited a blue to red chromatic change in a semi-quantitative manner in response to zinc ions. No discernable change was observed in solutions containing other common ions. Advantages of this sensor include its ease of fabrication, high specificity, and equipment-free detection, all of which are desirable for in-field applications and use in resource-limited settings.

1. INTRODUCTION

Polydiacetylene (PDA) materials have become popular in biosensing applications due to their unique optical property that is readily discernable by the naked eye. PDA undergoes chromatic changes from blue to red in response to temperature [1-3], pH [4, 5], and molecular binding events [6, 7]. Furthermore, the chromatic changes can be made specific to the binding of a target analyte by conjugating detection probes onto PDA head groups. In such systems, the detection probes can be antibodies [8-11], proteins [10, 12, 13], or DNA aptamers [14-16]. Among them, DNA aptamers have several advantages, including but not limited to, ease of design, economical production, and chemical stability, all without compromising high specificity and affinity [17].

To date, analyte-specific PDA sensors are mostly developed in the form of liposomes in colloidal suspension [11, 18, 19] or a deposited layer on rigid substrate surfaces [20-23]. However, due to complex sample handling requirements (e.g., multiple pipetting) and high costs of fabrication, these forms are not always ideal for biosensing applications in remote areas or resource-limited settings, which would most benefit from PDA's instrument-free and naked-eye detection. Therefore, the development of PDA sensors in the form of a membrane strip, which are light, low cost, and easy to use, will be of significant benefit. Nevertheless, only a few PDA sensor strips have been reported and most are limited to the detection of volatile organic compounds and solvents [24-28].

In this study, we present a new PDA sensor strip that is conjugated with DNA aptamers for the detection of Zn^{2+} in aqueous solution. Other optical cationic sensors, such as traditional optodes, rely on spectrophotometric measurements of indicator dyes

after their reaction with the target cation for detection analysis [29, 30]. The PDA sensor platform used in this study foregoes the need for bulky external analytical instruments and utilizes DNA aptamers for highly specific detection of Zn^{2+}. First, using PDA liposomes, four candidate Zn^{2+} aptamers were compared to investigate effects of the aptamers' hairpin structure, base length, and linker length. The aptamer design that induced chromatic changes most rapidly was then selected for the fabrication of a PDA sensor strip on polyvinylidene fluoride (PVDF) membrane. The sensor strip successfully undergoes a chromatic change discernable to the naked eye when dipped into Zn^{2+} solution, but not in solutions containing other non-zinc ions.

2. MATERIALS AND METHODS

2.1 Materials

The diacetylene (DA) monomer, 10,12-tricosadiynoic acid (TCDA) was purchased from GFS Chemicals (Powell, OH, USA) and 1,2-dimyristoyl-sn-glycero-3-phosphoethanolamine (DMPE) was obtained from VWR International (Radnor, PA, USA). Organic solvents, PVDF transfer membranes (EMD Millipore, 0.45 μm), and Slide-A-Lyzer MINI Dialysis Devices with molecular weight cut off of 3.5 kDa were purchased from Fisher Scientific (Pittsburgh, PA, USA). Amine-modified Zn^{2+} aptamers were purchased from Integrated DNA Technologies (Coralville, IA, USA). All other

compounds used are research grade and were obtained from Sigma Aldrich (St. Louis, MO, USA).

2.2 Preparation of PDA liposomes for Aptamer Study

PDA liposome solution (25.5 nmol TCDA-N-hydroxysuccinimide (NHS), 237 nmol TCDA and 487.5 nmol DMPE) was prepared and incubated with 7.5 nmol of one of four amine-modified Zn^{2+} aptamers (Table 4.1: **1-4**) before photopolymerization (Chapter 3, Section 2). Dynamic light scattering (DLS, Malvern Zetasizer Nano ZS90) analysis indicated the mean diameter of the liposomes was approximately 120 nm (Figure 4.S1).

2.3 Analysis of PDA liposomes

PDA liposomes were incubated with 5 mM Zn^{2+} for 30 m and absorpance measurements were recorded by a spectrophotometer (Figure 4.S2). Color Response (CR) was calculated as previously described [31] (Chapter 3, Section 4.1).

2.4 Preparation of PDA Strips for Zinc Detection

Prepared strips were dipped in a 500 μL chloroform solution containing TCDA-**1** (200 nmol), TCDA (700 nmol), and DMPE (600 nmol) before photopolymerization (Chapter 3, Section 3). The total lipid concentration of the resulting solution was 3 mM with 13.3% TCDA-**1**.

2.5 Colorimetric Zinc Detection and Analysis of PDA Strip Sensor

Strips were dipped into solutions containing various concentrations of Zn^{2+} (as $ZnCl_2$) from 0 to 1 mM in deionized water at room temperature. Color images of PDA strips were recorded at incubation times from 30 m to 4 h. Red chromatic shift (RCS) was calculated using digital colorimetric analysis as previously described [32] (Chapter 3, Section 4.2).

Principal component analysis (PCA) was additionally employed (Table 4.S1, Figure 4.S5) (Chapter 3, Section 4.3). The first principal component (PC1) is expressed as PC1 = 0.71 x R + 0.00 x G – 0.71 x B, and the second principal component (PC2) as PC2 = – 0.19 x R – 0.96 x G – 0.19 x B. The 2D PCA score plot indicates that PC1 accounts for 63.8% of the total data variance and PC2 accounts for 35.9%.

3. RESULTS AND DISCUSSION

2.1 Effect of Aptamer Length, Linker Length and Structure on PDA Liposome Color Transitions

Four variations, **1-4** (Table 4.1, Figure 4.S3), of a previously screened Zn^{2+} aptamer [33], were investigated for the effects of aptamer length and structure on the sensitivity of PDA color transitions. Aptamers **1** and **2** are hairpin aptamers composed of 65 nucleobases and differ by 6 carbons in the 5’ carbon linker (between the first base and

the liposome membrane surface). Aptamers **3** and **4** are non-hairpin aptamers composed of 65 and 54 bases respectively. PDA liposomes composed of 1% (by total moles of lipids) of each Zn^{2+} aptamer were prepared and incubated in 500 μM Zn^{2+} solution for 30 m.

Color Response (CR) analysis [31] of liposomes conjugated with **1-4,** after 30 m in Zn^{2+} solutions indicates that liposomes conjugated with **1** demonstrated the most significant color change (39.6% CR), followed by **2** (37.8% CR)**, 3** (31.4% CR) and **4** (24.2% CR) (Figure 4.1). This suggests that an increasing aptamer length increases the sensitivity of color transitions. In particular, the difference in length by 11 bases between **3** (65 bases, non-hairpin) and **4** (54 bases, non-hairpin) resulted in an average 7.2% CR difference. Contrastingly, **1** and **2** differ only by a length of 6 carbons in the carbon linker from the 5' base to the original PDA side chain. This small change in the linker length had an insignificant effect on color transitions (Figure 4.1B).

While the mechanism behind PDA transitions remains to be fully understood, it is suggested that perturbations in the alternating –ene –yne backbone cause slight rotational changes that shift the optical absorption of the backbone from low (blue phase) to high energy (red phase) [34-36]. Accordingly, the folding of aptamers conjugated to the surface of PDA liposomes around target biomolecules results in the formation of bulky aptamer-target groups at the liposome surface, which repulse one another. This steric repulsion at the liposome surface disrupts the stabilizing hydrogen bonds between the PDA head groups and translates into perturbations at the PDA backbone, which cause the liposome to change from blue to red [15, 16, 34]. Consequently, an increasing aptamer

length results in even bulkier aptamer-target complexes and increased steric repulsion. This likely results in more sensitive color transitions (Figure 4.2A).

Additionally, liposomes conjugated with **1** and **2** (hairpin aptamers), demonstrated a higher CR as compared to liposomes conjugated with **3** and **4** (non-hairpin aptamers). As hairpin aptamers, the structural conformation of **1** and **2** changes from a closed loop to an open loop upon binding with Zn^{2+} [33, 37]. As the aptamer unfolds to form the aptamer-target complex, the large conformational switch results in additional repulsion at the liposome surface (Figure 4.2B).

2.2 Testing of Zn^{2+} Sensor Strips

For the fabrication of our PDA sensor strip, **1** was selected as the detection probe due to the greatest CR reported by liposomes conjugated with it. To fabricate the sensor, PVDF strips were immersed in a chloroform solution containing 13.3% **1**-conjugated DA monomers, 46.7% unmodified DA monomers and 40% DMPE phospholipid. PVDF has been previously employed in a fluorescence PDA sensor [38] and was selected as our sensor substrate due to its robust and inert properties that allow it to withstand harsh chemical environments and intense UV exposure [38, 39]. Photopolymerization of the PDA layer with 254 nm UV light yielded a blue-colored area on the strip (Figure 4.3).

The PDA-coated PVDF strips (PDA strips) were dipped into solutions containing 0, 62.5, 125, 250, 500, and 1000 μM Zn^{2+} ions. The strips were imaged after incubation for 30 m, 1 h, 2 h and 4 h in the solutions. After 4 h in solution, they yielded a range of colors from blue to pink/red with increasing Zn^{2+} concentration (Figure 4.4A). For

quantification of the chromatic transitions, color images were analyzed using ImageJ, an image processing software, to extract image-averaged red-green-blue (RGB) values. The RGB data was analyzed using digital colorimetric analysis [32], to generate a red chromatic shift (RCS) curve for each of the incubation periods indicated above (Figure 4.4B). Previous studies have shown that a color shift of approximately 10-15% or greater is readily detectable by the naked eye [11, 40]. Accordingly, the limits of detection were determined to be 1000 μM (19% RCS) at 30 m, 500 μM (23% RCS) at 1 h, 250 μM (25% RCS) at 2 h, and 125 μM (29% RCS) at 4 h.

The RCS analysis of the PDA strips at 4 h indicates that two color transitions occurred. The first was at the detection limit of the sensor, 125 μM (8.16 ppm) Zn^{2+}, at which a blue to purple color transition occurred. The second was at 500 μM (32.65 ppm) Zn^{2+} and above, at which the sensor exhibited a purple to pink/red color transition. This second transition corresponds to a 45% RCS, which is 16% higher than that of the purple transition at 125 μM (29% RCS), and is therefore readily discernable by the naked eye.

The strips were further evaluated by PCA (Figure 4.5). Distinctly, the PCA plot can be divided into three clusters. The first cluster contains RGB values from 0 and 62.5 μM Zn^{2+}, the second cluster contains values from 125 and 250 μM Zn^{2+}, and the third cluster contains values from 500 μM and 1000 μM Zn^{2+}. This further confirms three colors exhibited by the sensor, blue, purple, and pink/red, which were also indicated by the RCS analysis (Figure 4.4).

Zn^{2+} is an important nutrient found in staple food crops such as maize, rice, soybean, peanut, and cassava. Significantly, critical Zn^{2+} concentrations in these crops

are in the range of 122-489 μM (8-30 ppm) (Table 4.S2) [41], which align well with this sensor's transitions. From an application standpoint, having more than one color transition is advantageous because each color can indicate a certain level of detection. Specifically, for the sensor described in this study, blue may serve to indicate Zn^{2+} deficiency (Zn^{2+} administration is needed), purple indicates Zn^{2+} levels in the critical range (no corrective action required), and pink/red indicates Zn^{2+} levels above the critical range (no more Zn^{2+} administration needed).

To test the sensor's specificity, PDA strips were incubated in solutions containing 1000 μM of one of six nutrients Cu^{2+}, Mn^{2+} and Fe^{2+}, Na^{+}, Mg^{2+} or K^{+} (as their chloride salts). RCS analysis of the strips after 4 h indicate that significant color transitions did not occur in any solutions containing ions other than Zn^{2+} (Figure 4.6). Specifically, the RCS of the strips dipped in solutions containing Zn^{2+} is 13 times higher than that of strips dipped in solutions containing Mn^{2+}, which displayed the highest chromatic shift from all of the control conditions. Notably, aptamer sequence **1** was previously reported to bind non-specifically to Cd^{2+} [33]. However, another biosensor employing **1** reported insignificant non-specific interactions with Cd^{2+} in control studies [42]. Because Cd is both highly toxic and carcinogenic, and is not one of the nutrients in food crops, this specific control was not included in the present study.

Finally, the stability of the PDA strips was evaluated over a 28-day period, during which strips were stored under four different conditions and tested every 7 days (Figure 4.7). The storage conditions included (1) under normal air, at room temperature, in the dark, (2) under normal air, at 4 ºC, in the dark, (3) under N_2 gas, at room temperature, in

the dark, and (4) under normal air, at room temperature, under constant light. RCS analysis shows that all strips stored in the dark demonstrated successful Zn^{2+} detection after 28 days (Figures 4.7B, 4.7C). Strips stored under constant light exhibited non-specific color transition that progressed over time and were not sensitive to Zn^{2+} solutions at the end of the 28-day period. A successful strip was determined as one that demonstrated a blue to pink/red transition that is readily discernable by the naked eye after 4 h incubation in 1000 μM Zn^{2+} solution.

4. CONCLUSIONS

We observed that aptamer lengths and structural switches (such as those displayed by hairpin aptamers) significantly increase the sensitivity of color transitions in PDA liposomes. This provides insight into methods by which the color transitions of aptamer-conjugated PDA sensors can be optimized through changing the characteristics of conjugated aptamers. Subsequently, we demonstrated a PDA sensor strip for the discrimination of Zn^{2+} levels. Our sensor has a detection limit of 125 μM (8.16 ppm), which aligns well with the lower limit of critical concentrations in many food crops. Additionally, two distinct color transitions of the sensor enable three-stage, semi-quantitative detection. This technology can be easily adapted, by changing the detection probe (i.e., aptamer), to target a wide range of analytes from ions to pathogen biomarkers. Consequently, this sensor platform has a great potential for applications in many areas, including agriculture, environmental management and biomedicine.

5. FIGURES

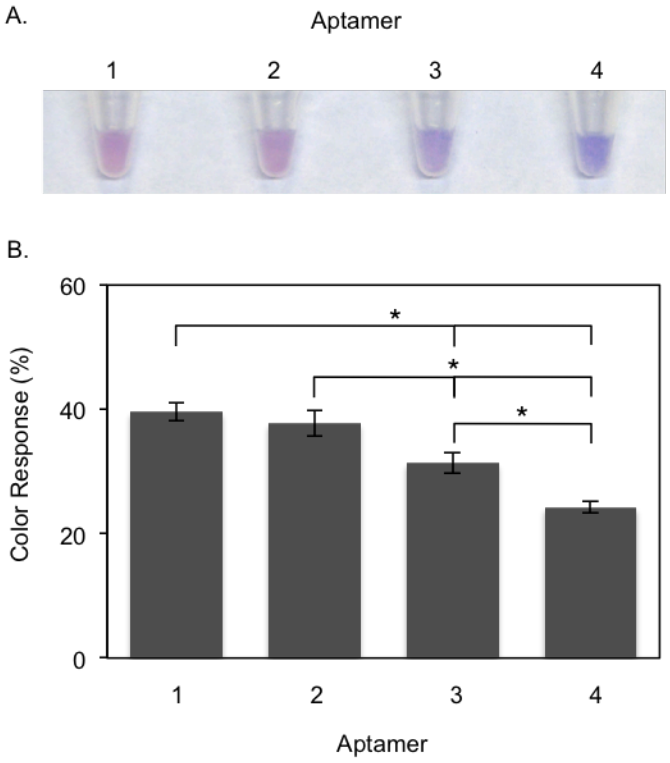

Figure 4.1 Color transitions of liposomes conjugated with four different aptamers (**1**-**4** in Table 1). (A) Images of liposome solutions after 30 m incubation in 500 μM Zn^{2+} solution. (B) Color response of liposomes after 30 m incubation in 500 μM Zn^{2+} solution. Color response data are represented as mean ± SD (n = 9). *$p < 0.05$. Reprinted with permission from *Elsevier B.V.*, Copyright 2016, doi: 10.1016/j.snb.2016.03.118.

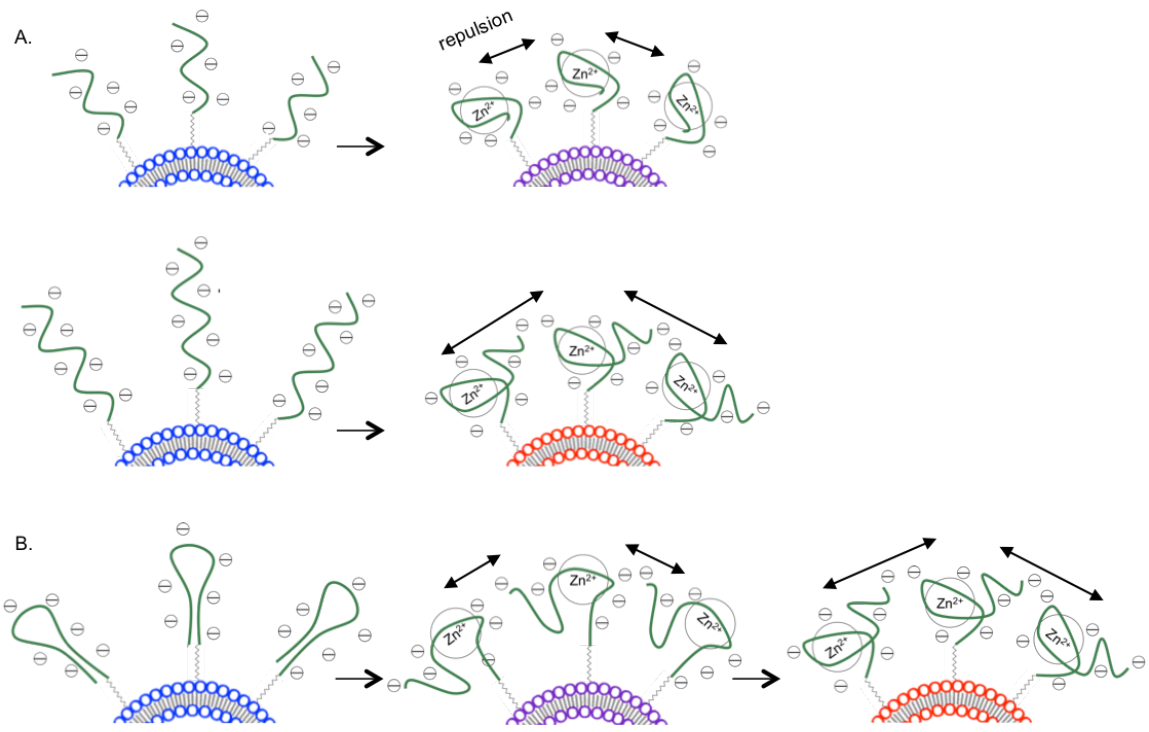

Figure 4.2 Schematic representation of Zn^{2+} detection by aptamers. (A) Aptamers of increasing length cause greater steric repulsion and lead to more sensitive color changes. (B) The un-folding of hairpin aptamers causes additional steric repulsion. Reprinted with permission from *Elsevier B.V.*, Copyright 2016, doi: 10.1016/j.snb.2016.03.118.

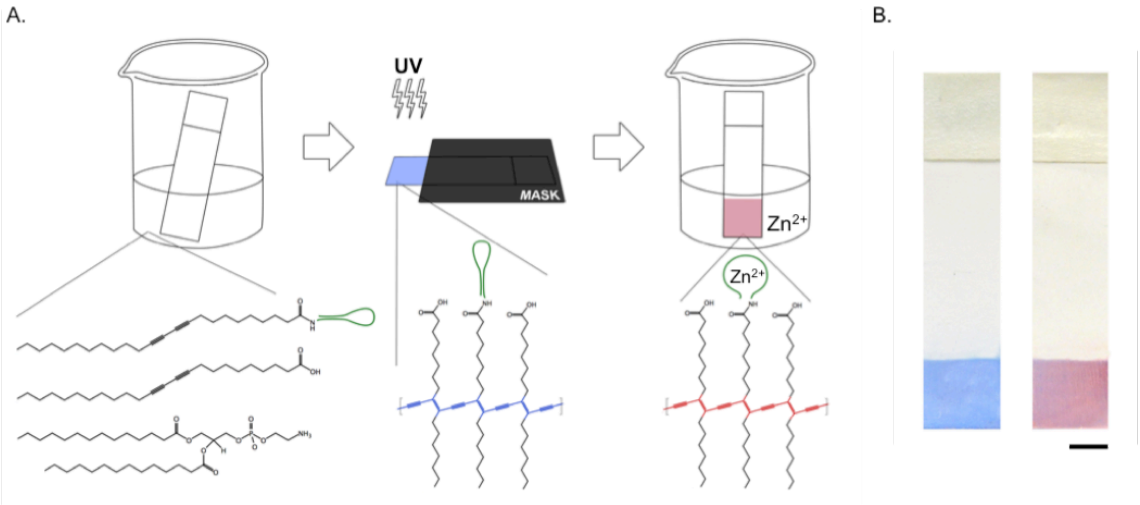

Figure 4.3 Preparation of PDA-coated PVDF strips. (A) PVDF strips are dipped into chloroform solution containing DA monomers conjugated with Zn^{2+} aptamer, unmodified DA monomers and DMPE (left), and subsequently photopolymerized by 254 nm UV irradiation under a mask to yield a blue-colored device (middle). Dipping the device in Zn^{2+} solution causes a blue to pink/red color transition as a result of direct interaction between Zn^{2+} ions in solution and Zn^{2+} aptamers (right). (B) Prepared devices before (left) and after (right) color transition. Scale bar = 2.5 mm. Reprinted with permission from *Elsevier B.V.*, Copyright 2016, doi: 10.1016/j.snb.2016.03.118.

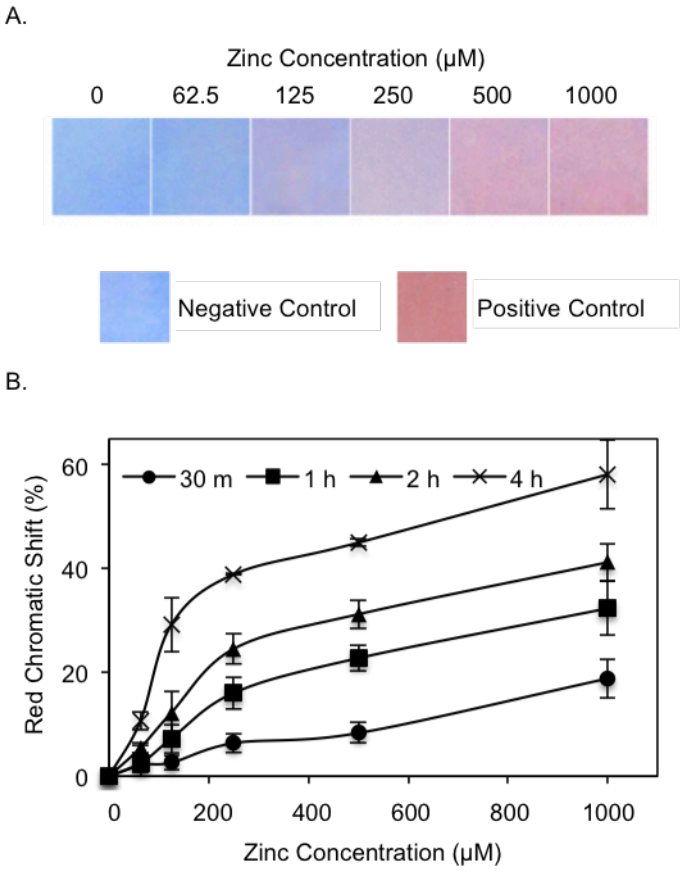

Figure 4.4 Zn^{2+} detection by PDA strips. (A) Images of the strips after 4 h incubation in Zn^{2+} solutions. The negative and positive control images are from strips dipped in deionized water and 1 M NaOH, respectively. (B) Red chromatic shift of the strips after 30 m, 1 h, 2 h and 4 h incubation in Zn^{2+} solutions. Red chromatic shift data are represented as mean ± SD (n = 3). Reprinted with permission from *Elsevier B.V.*, Copyright 2016, doi: 10.1016/j.snb.2016.03.118.

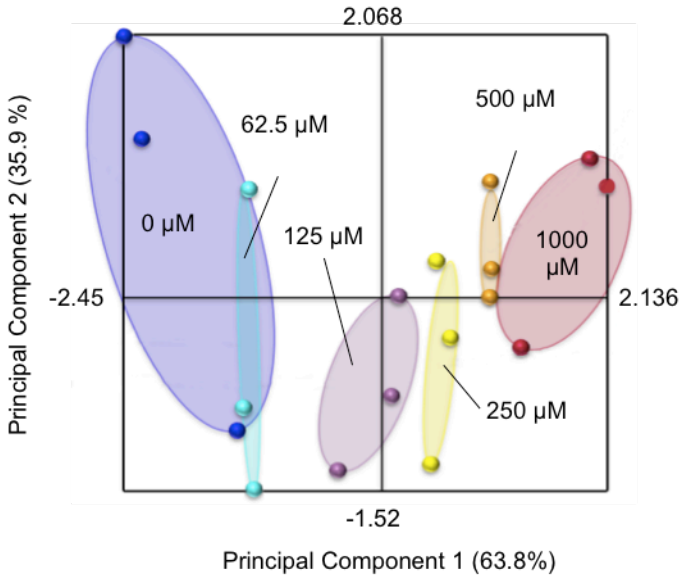

Figure 4.5. PCA transformation of RGB values (Table 4.S1). Reprinted with permission from *Elsevier B.V.*, Copyright 2016, doi: 10.1016/j.snb.2016.03.118.

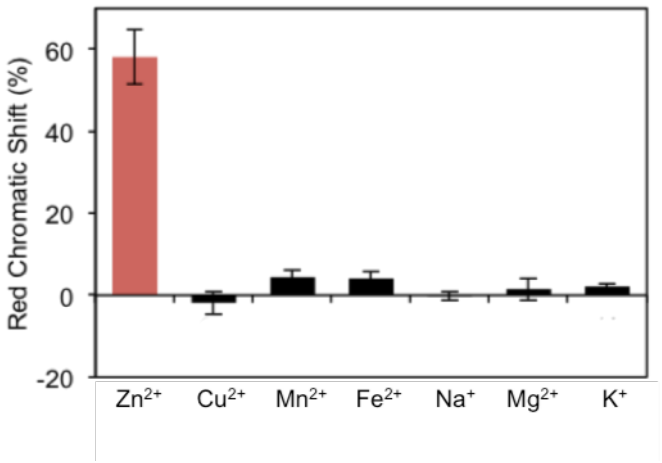

Figure 4.6 Red chromatic shift of the strips after 4 h incubation in solutions containing 1000 μM of various nutrients. All data are represented as mean ± SD (n = 3). Reprinted with permission from *Elsevier B.V.*, Copyright 2016, doi: 10.1016/j.snb.2016.03.118.

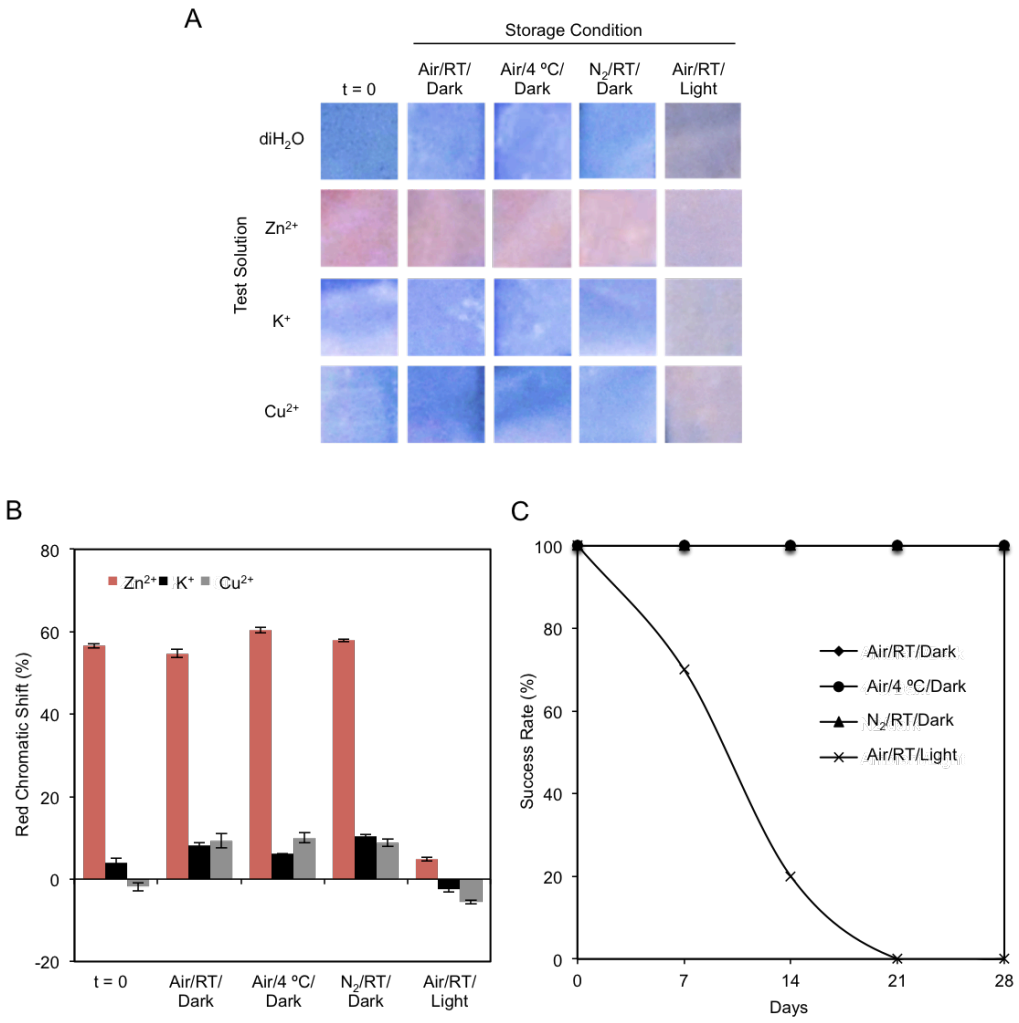

Figure 4.7 Stability test of PDA strips over 28 days. (A) Images of tested strips immediately after production (t = 0) and after storage under various conditions for 28 days. Strips were imaged after 4 h incubation in deionized water or 1000 µM solutions containing Zn^{2+}, K^{+} or Cu^{2+}. (B) Red chromatic shift of tested strips after 28 days of storage under various conditions. Data are represented as mean ± SD (n = 10 for strips tested in Zn^{2+} solutions, n = 3 for strips tested in control solutions). (C) Success rate of strips under various conditions over a 28-day period. Success rates were calculated as a percentage of successful strips out of 10 for each storage condition. RT = room temperature. Reprinted with permission from *Elsevier B.V.*, Copyright 2016, doi: 10.1016/j.snb.2016.03.118.

Table 4.1. Aptamer variations used in the study[1]

Aptamer	Sequence	5' Carbon Linker Length	Number of Bases	Hairpin
1	5'-GCATCAGTTAGTCATTACGCT TACGGCGGCTCTATCCTAACTGA TATATTGTGAAGTCGTGTCCC-3' *	12	65	Yes
2	5'-GCATCAGTTAGTCATTACGCT TACGGCGGCTCTATCCTAACTGA TATATTGTGAAGTCGTGTCCC-3'	6	65	Yes
3	5'-ATGCTGACCGATCATTACGCT TACGGCGGCTCTATCCTAACTGA TATATTGTGAAGTCGTGTCCC-3'	12	65	No
4	5'-TCATTACGCTTACGGCGGCTC TATCCTAACTGATATATTGTGAAG TCGTGTCCC-3'	12	54	No

* sequence from [31]

[1] Reprinted with permission from *Elsevier B.V.*, Copyright 2016, doi: 10.1016/j.snb.2016.03.118.

References

[1] H. Beckham, M. Rubner, On the origin of thermochromism in cross-polymerized diacetylene-functionalized polyamides, *Macromolecules*, 26 (1993) 5198-201.

[2] R.R. Chance, R.H. Baughman, H. Muller, C.J. Eckhardt, Thermochromism in a polydiacetylene crystal, *J Chem Phys*, 67(1977) 3616-8.

[3] R.R. Chance, G.N. Patel, J.D. Witt, Thermal effects on the optical properties of single crystals and solution-cast films of urethane substituted polydiacetylenes, *J Chem Phys*, 71(1979) 206-11.

[4] Q. Cheng, R.C. Stevens, Charge-induced chromatic transition of amino acid-derivatized polydiacetylene liposomes, *Langmuir*, 14(1998) 1974-6.

[5] J. Song, Q. Cheng, S. Kopta, R.C. Stevens, Modulating artificial membrane morphology: pH-induced chromatic transition and nanostructural transformation of a bolaamphiphilic conjugated polymer from blue helical ribbons to red nanofibers*, J Am Chem Soc*, 123(2001) 3205-13.

[6] D.H. Charych, J.O. Nagy, W. Spevak, M.D. Bednarski, Direct colorimetric detection of a receptor-ligand interaction by a polymerized bilayer assembly, *Science*, 261(1993) 585-8.

[7] D.H. Charych, W. Spevak, J.O. Nagy, M.D. Bednarski, Specific interaction of influenza-virus with organized assemblies of polydiacetylenes, *Mater Res Soc Symp P*, 292(1993) 153-61.

[8] S.-H. Jung, H. Jang, M.-C. Lim, J.-H. Kim, K.-S. Shin, S.M. Kim, *et al.*, Chromatic biosensor for detection of phosphinothricin acetyltransferase (PAT) using polydiacetylene vesicles encapsulated within automatically generated immuno-hydrogel beads, *Anal Chem*, 87(2015) 2072-8.

[9] S.W. Lee, C.D. Kang, D.H. Yang, J.S. Lee, J.M. Kim, D.J. Ahn, *et al.*, The development of a generic bioanalytical matrix using polydiacetylenes, *Adv Funct Mater*, 17(2007) 2038-44.

[10] H.K. Park, S.J. Chung, H.G. Park, J.-H. Cho, M. Kim, B.H. Chung, Mixed self-assembly of polydiacetylenes for highly specific and sensitive strip biosensors, *Biosens and Bioelectron*, 24(2008) 480-4.

[11] Y.-l. Su, J.-r. Li, L. Jiang, Chromatic immunoassay based on polydiacetylene vesicles, *Colloid Surface B*, 38(2004) 29-33.

[12] Y.K. Jung, T.W. Kim, C. Jung, D.Y. Cho, H.G. Park, A polydiacetylene microchip based on a biotin–streptavidin interaction for the diagnosis of pathogen infections, *Small*, 4(2008) 1778-84.

[13] J. Wu, A. Zawistowski, M. Ehrmann, T. Yi, C. Schmuck, Peptide functionalized polydiacetylene liposomes act as a fluorescent turn-on sensor for bacterial lipopolysaccharide, *J Am Chem Soc*, 133(2011) 9720-3.

[14] Y.K. Jung, T.W. Kim, H.G. Park, H.T. Soh, Specific colorimetric detection of proteins using bidentate aptamer□conjugated polydiacetylene (PDA) liposomes, *Adv Funct Mater*, 20(2010) 3092-7.

[15] J. Lee, H. Jun, J. Kim, Polydiacetylene-liposome microarrays for selective and sensitive mercury (II) detection, *Adv Mater*, 21(2009) 3674-7.

[16] J. Lee, H.-J. Kim, J. Kim, Polydiacetylene liposome arrays for selective potassium detection, J Am Chem Soc, 130 (2008) 5010-1.

[17] S.D. Jayasena, Aptamers: an emerging class of molecules that rival antibodies in diagnostics, *Clin Chem*, 45(1999) 1628-50.

[18] A. Reichert, J.O. Nagy, W. Spevak, D. Charych, Polydiacetylene liposomes functionalized with sialic acid bind and colorimetrically detect influenza virus, *J Am Chem Soc*, 117(1995) 829-30.

[19] S. Rozner, S. Kolusheva, Z. Cohen, W. Dowhan, J. Eichler, R. Jelinek, Detection and analysis of membrane interactions by a biomimetic colorimetric lipid/polydiacetylene assay, *Anal Biochem*, 319(2003) 96-104.

[20] E. Geiger, P. Hug, B.A. Keller, Chromatic transitions in polydiacetylene langmuir-blodgett films due to molecular recognition at the film surface studied by spectroscopic methods and surface analysis, *Macromol Chem Phys*, 203(2002) 2422-31.

[21] B. Ma, Y. Fan, L. Zhang, X. Kong, Y. Li, J. Li, Direct colorimetric study on the interaction of Escherichia coli with mannose in polydiacetylene Langmuir-Blodgett films, *Colloid Surface B*, 27 (2003) 209-13.

[22] M.-C. Lim, Y.-J. Shin, T.-J. Jeon, H.-Y. Kim, Y.-R. Kim, Microbead-assisted PDA sensor for the detection of genetically modified organisms, *Anal Bioanal Chem*, 400(2011) 777-85.

[23] J. Olmsted III, M. Strand, Fluorescence of polymerized diacetylene bilayer films, *J Phys Chem-Us*, 87(1983) 4790-2.

[24] T. Eaidkong, R. Mungkarndee, C. Phollookin, G. Tumcharern, M. Sukwattanasinitt, S. Wacharasindhu, Polydiacetylene paper-based colorimetric sensor array for vapor phase detection and identification of volatile organic compounds, *J Mater Chem*, 22(2012) 5970-7.

[25] S. Pumtang, W. Siripornnoppakhun, M. Sukwattanasinitt, A. Ajavakom, Solvent colorimetric paper-based polydiacetylene sensors from diacetylene lipids, *J Colloid Interf Sci*, 364(2011) 366-72.

[26] T. Soga, Y. Jimbo, K. Suzuki, D. Citterio, Inkjet-printed paper-based colorimetric sensor array for the discrimination of volatile primary amines, *Anal Chem*, 85(2013) 8973-8.

[27] X. Wang, X. Sun, P.A. Hu, J. Zhang, L. Wang, W. Feng, *et al.*, Colorimetric sensor based on self□assembled polydiacetylene/graphene-stacked composite film for vapor-phase volatile organic compounds, *Adv Funct Mater*, 23(2013) 6044-50.

[28] B. Yoon, I.S. Park, H. Shin, H.J. Park, C.W. Lee, J.M. Kim, A litmus-type colorimetric and fluorometric volatile organic compound sensor based on inkjet-printed polydiacetylenes on paper substrates, *Macromol Rapid Comm*, 34(2013) 731-5.

[29] B.R. Eggins, Chemical sensors and biosensors: John Wiley & Sons; 2008.

[30] P. Bühlmann, E. Pretsch, E. Bakker, Carrier-based ion-selective electrodes and bulk optodes. 2. Ionophores for potentiometric and optical sensors, *Chem Rev*, 98(1998) 1593-688.

[31] S. Okada, S. Peng, W. Spevak, D. Charych, Color and chromism of polydiacetylene vesicles, Accounts Chem Res, 31 (1998) 229-39.

[32] R. Volinsky, M. Kliger, T. Sheynis, S. Kolusheva, R. Jelinek, Glass-supported lipid/polydiacetylene films for colour sensing of membrane-active compounds, *Biosens Bioelectron*, 22(2007) 3247-51.

[33] M. Rajendran, A.D. Ellington, Selection of fluorescent aptamer beacons that light up in the presence of zinc, *Anal Bioanal Chem*, 390(2008) 1067-75.

[34] R.W. Carpick, D.Y. Sasaki, M.S. Marcus, M.A. Eriksson, A.R. Burns, Polydiacetylene films: a review of recent investigations into chromogenic transitions and nanomechanical properties, *J Phys-Condens Mat*, 16(2004) R679-R97.

[35] R. Jelinek, M. Ritenberg, Polydiacetylenes-recent molecular advances and applications, *RSC Adv*, 3(2013) 21192-201.

[36] M.A. Reppy, B.A. Pindzola, Biosensing with polydiacetylene materials: structures, optical properties and applications, *Chem Commun*, (2007) 4317-38.

[37] E.J. Cho, J.-W. Lee, A.D. Ellington, Applications of aptamers as sensors, *Annu Rev Anal Chem*, 2(2009) 241-64.

[38] H.K. Park, S.J. Chung, H.G. Park, J.-H. Cho, M. Kim, B.H. Chung, Mixed self-assembly of polydiacetylenes for highly specific and sensitive strip biosensors, *Biosens Bioelectron*, 2 (2008) 480-4.

[39] G.J. Ross, J.F. Watts, M.P. Hill, P. Morrissey, Surface modification of poly (vinylidene fluoride) by alkaline treatment 1. The degradation mechanism, *Polymer*, 41(2000) 1685-96.

[40] S. Kolusheva, L. Boyer, R. Jelinek, A colorimetric assay for rapid screening of antimicrobial peptides, *Nat Biotechnol*, 18(2000) 225-7.

[41] B.J. Alloway, Zinc in soils and crop nutrition, Brussels, Belgium: International Zinc Association 2004.

[42] Z. Li, M. Liu, L. Fan, H. Ke, C. Luo, G. Zhao, A highly sensitive and wide-ranged electrochemical zinc(II) aptasensor fabricated on core–shell SiO 2-Pt@ meso-SiO 2, *Biosens Bioelectron*, 52(2014) 293-7.

6. SUPPLEMENTARY DATA

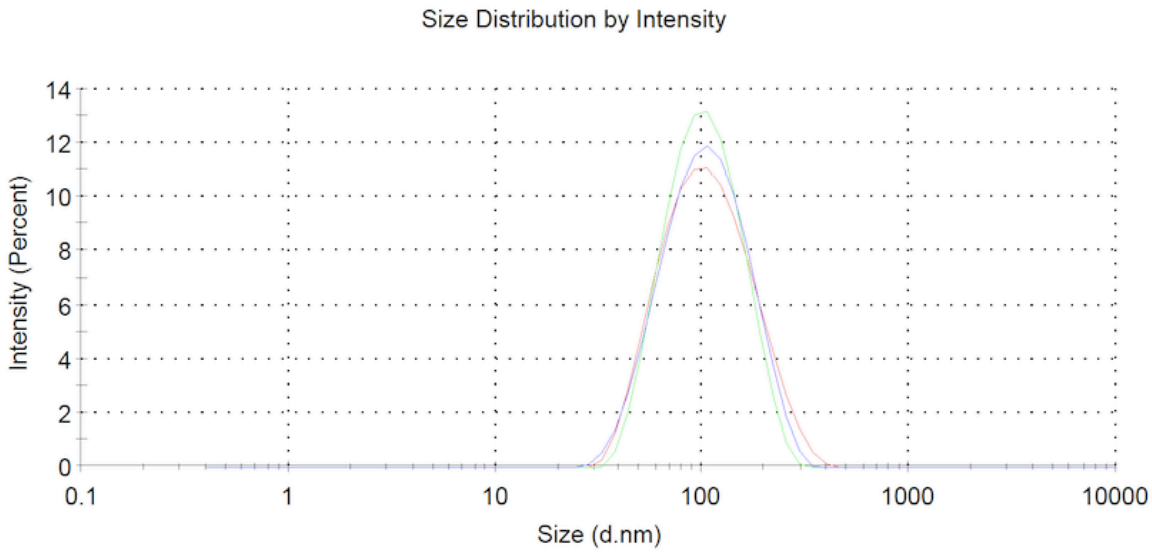

Figure 4.S1. DLS graph of PDA liposome size. All lines represent data recorded from a single sample. Reprinted with permission from *Elsevier B.V.*, Copyright 2016, doi: 10.1016/j.snb.2016.03.118.

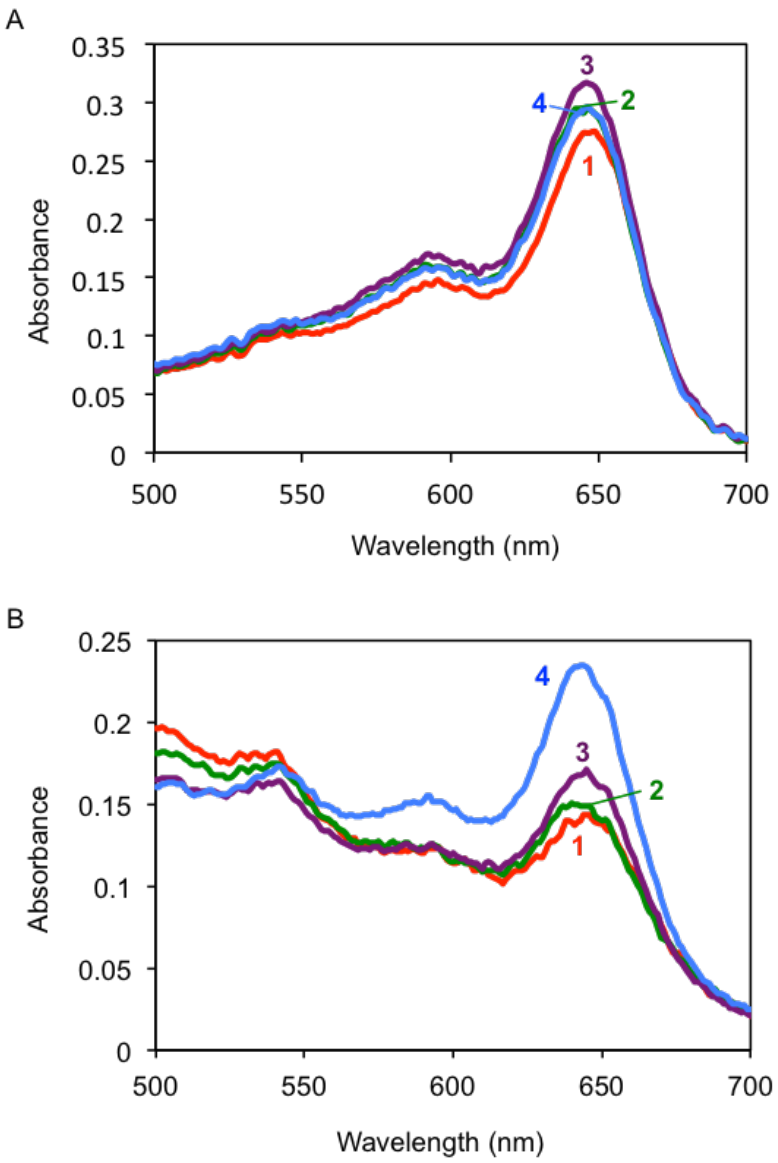

Figure 4.S2. Absorbance spectra of PDA liposomes conjugated with aptamers **1-4** before (A) and after (B) incubation with 5 mM Zn^{2+}. Reprinted with permission from *Elsevier B.V.*, Copyright 2016, doi: 10.1016/j.snb.2016.03.118.

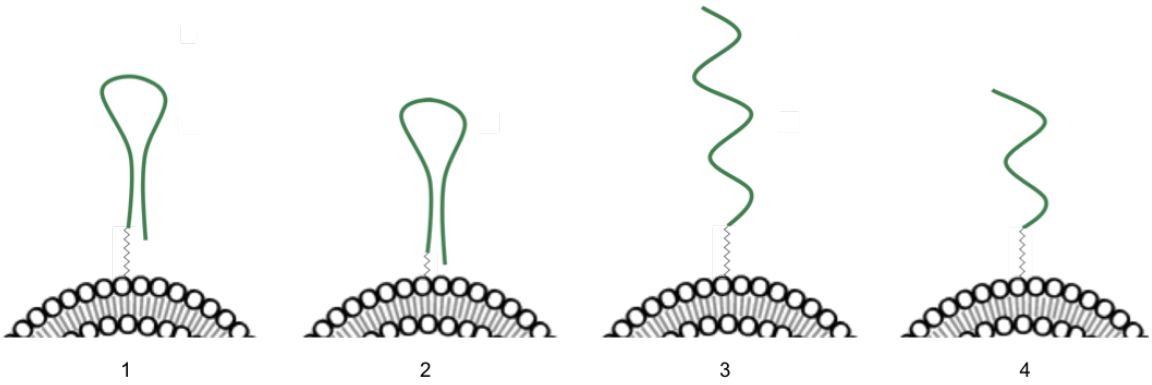

Figure 4.S3. Schematic depiction of aptamers **1-4** conjugated to the surface of liposomes. Image is not drawn to scale to exaggerate the differences between the aptamers. Reprinted with permission from *Elsevier B.V.*, Copyright 2016, doi: 10.1016/j.snb.2016.03.118.

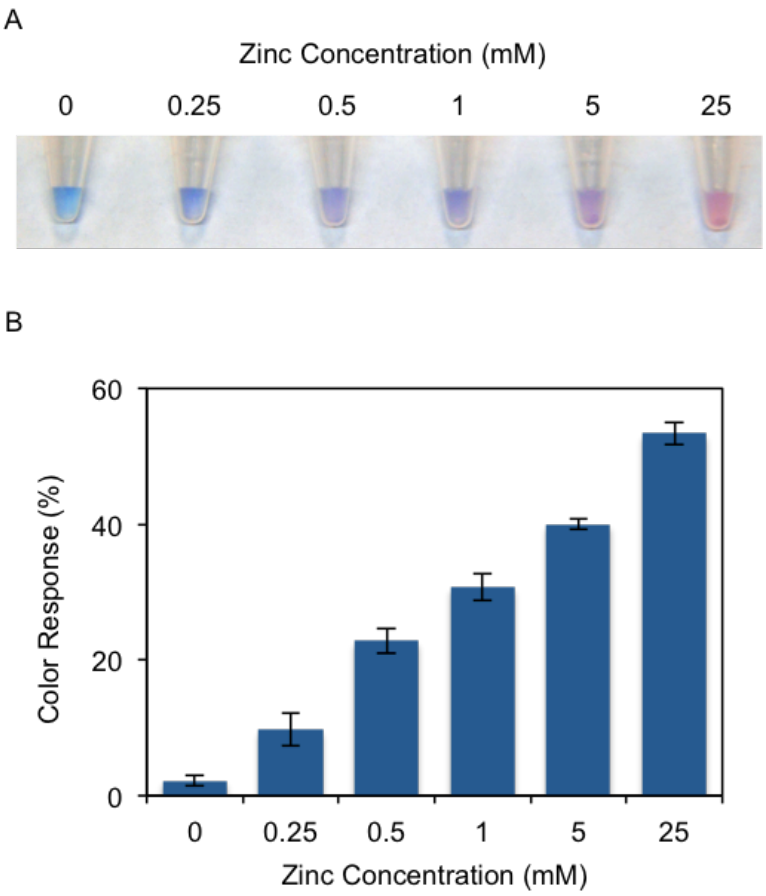

Figure 4.S4. Color transitions of liposomes with 1% of aptamer **1** after 1 h incubation in solutions containing 0 to 25 mM Zn^{2+}. Color response data are represented as mean ± SD (n = 9). Reprinted with permission from *Elsevier B.V.*, Copyright 2016, doi: 10.1016/j.snb.2016.03.118.

Table 4.S1. RGB values extracted from strips after 4 h in Zn^{2+} solution[1]

Sample	Red	Green	Blue
0 μM - 1	143.8	182.2	240.4
0 μM - 2	104.3	154.0	243.1
0 μM - 3	113.5	161.1	244.3
62.5 μM - 1	143.2	180.6	238.8
62.5 μM - 2	150.4	186.3	240.4
62.5 μM - 3	135.9	164.9	233.7
125 μM - 1	173.3	179.6	223.7
125 μM - 2	169.4	172.6	220.1
125 μM - 3	163.1	185.4	229.6
250 μM - 1	177.1	169.9	216.2
250 μM - 2	187.2	184.2	222.9
250 μM - 3	179.2	175.9	214.4
500 μM - 1	179.5	164.8	206.2
500 μM - 2	187.8	172.6	210.8
500 μM - 3	184.4	170.9	208.7
1000 μM - 1	197.5	176.1	209.4
1000 μM - 2	204.0	162.4	198.4
1000 μM - 3	205.6	164.7	195.6

[1]Reprinted with permission from *Elsevier B.V.*, Copyright 2016, doi: 10.1016/j.snb.2016.03.118.

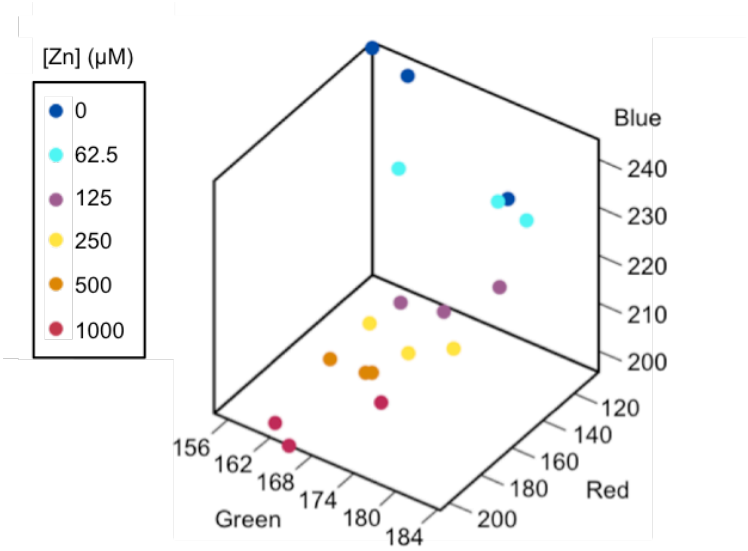

Figure 4.S5. 3D plot of RGB values. Reprinted with permission from *Elsevier B.V.*, Copyright 2016, doi: 10.1016/j.snb.2016.03.118.

Table 4.S2. Critical Zn^{2+} concentrations*[1]

Crop	Tissue	Critical [Zn] (ppm)
maize	upper third leaves	15-16
rice	whole shoot	10-20
soybean	upper recently matured leaves, early bloom	20
peanut	youngest fully emerged leaf early pegging	8-10
wheat	shoot	32
canola	shoot	23
sorghum	youngest fully emerged leaf	8-10
cassava	youngest mature blade	30

* as reported by [1]

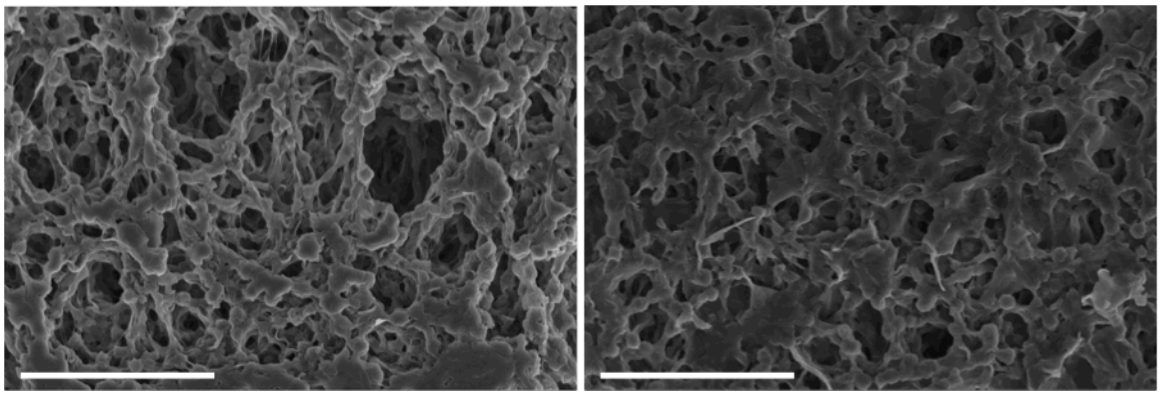

Figure 4.S6 SEM images of strips before (left, blue) and after (right, pink/red) incubation in Zn^{2+} solution. Scale bar = 10 μm.

References

[1] B.J. Alloway, Zinc in soils and crop nutrition, Brussels, Belgium: International Zinc Association 2004.

CHAPTER 5:

STRIP SENSOR FOR IMMUNOCHROMATIC DETECTION OF *X. FASTIDIOSA*

Abstract

This study presents a sensor strip for user-friendly, naked-eye detection of *Xylella fasitdiosa*, the causal agent of Pierce's disease in grapevine. This sensor utilizes anti-*X. fastidiosa* antibodies conjugated to a polydiacetylene layer on a polyvinylidene fluoride strip to generate specific color transitions and discriminate levels of the pathogen. The detection limit of the sensor is 0.8 x 10^8 cells/mL, which is similar to bacterial load in grapevine 18 days following bacterial inoculation. The advantages of this sensor include equipment-free detection and high specificity, characteristics desirable for in-field diagnostic tools in resource-limited settings.

1. INTRODUCTION

Xylella fastidiosa is a gram-negative, xylem-limited bacterium that was listed as a top 10 scientifically and economically important plant pathogenic bacterium in 2012 [1]. It is the causal agent of Pierce's disease in grapevine and is additionally responsible for a number of other economically devastating agricultural diseases including phony peach disease, plum leaf scald, almond leaf scorch, and citrus variegated chlorosis [2, 3]. Particularly, widespread Pierce's disease epidemics have resulted in severe vineyard losses across the United States and parts of Mexico and Central America [4]. In California, where the primary vector for transmission is the glassy-winged sharpshooter, *Homalodisca coagulata*, up to 50% of the vines in some vineyards have been reported with PDirece's disease-related symptoms in a given year [3, 5, 6]. Symptoms of Pierce's disease include marginal leaf necrosis, leaf scorching, and wilted, shriveled fruit [4, 7].

Current methods to diagnose Pierce's disease include detection of *X. fastidiosa* in plant tissue samples through optical or fluorescence microscopy, bacterial culture, or enzyme-linked immunosorbent assay (ELISA) [8-10]. However, bacterial culture and microscopy are time-consuming and inefficient [10]. ELISA is currently the favored method for high through-put and rapid *X. fastidiosa* detection, nevertheless this procedure still requires a laboratory environment and trained operators to complete [8, 11, 12]. More recently, polymerase chain reaction (PCR) has been suggested as a highly sensitive detection method as compared to ELISA, but has not been widely adopted due to costly and complicated protocols for DNA extraction and amplification [11, 13]. With the high incidence of the Pierce's disease in the United States and particularly California, a user-

friendly, in-field device for *X. fastidiosa* detection would be an advantageous tool to prevent grapevine loss from the pathogen.

This study reports the development of a polydiacetylene (PDA)-coated "dipstick" sensor strip for quick and easy detection of *X. fastidiosa.* PDA is a class of amphiphilic lipid polymers known for their unique blue to red color transitions in response to stimuli such as high pH [14, 15], high temperature [16-18] and molecular binding events [19, 20]. These chromatic properties have resulted in the popular use of PDA in a range of colorimetric biosensing applications in the form of liposomes [21-23], Langmuir-Blodgett films [24, 25], strips [26-28] and others [29, 30]. The additional fluorescence "turn-on" characteristic of red-phase PDA is attributable to its use in the development of fluorescence-based sensors [31-33]. Even more, recent investigations have taken advantage of the biocompatibility of PDA liposomes and employed them in biomedical drug delivery systems [34, 35]. Its application as an injectable *in planta* sensor to monitor pathogenic infection of plants has also been recently suggested [36]. In this study, highly specific anti-*X. fastidiosa* antibodies were conjugated to surface of PDA-coated strips of polyvinylidene fluoride (PVDF). When incubated in liquid cultures containing *X. fastidiosa*, the strips exhibited blue to pink transitions that were readily discernable by the naked eye. Recently, we reported a PDA strip sensor conjugated with DNA aptamer probes to selectively detect zinc ions in test samples [26]. The current study extends the capacity of this platform by using antibodies to demonstrate the detection of live bacterium, which is particularly relevant to agricultural disease diagnostics.

2. MATERIALS AND METHODS

2.1 Materials

Diacetylene monomer, 10,12-pentacosadiynoic acid (PCDA) was purchased from Spectrum Chemicals (Gardena, CA, USA), and 1,2-dimyristoyl-*sn*-glycero-3-phosphocholine (DMPC) was obtained from Avanti Polar Lipids, Inc. (Alabaster, AL, USA). Organic solvents and PVDF transfer membranes (EMD Millipore, 0.45 μm) were purchased from Fisher Scientific (Pittsburgh, PA, USA). Anti-*X. fastidiosa* antibody was purchased from Agdia, Inc. (Elkhart, IN, USA). PD3 media, Luria-Bertani (LB) media and LB agar were obtained from Difco Laboratories (Detroit, MI, USA). All other compounds are research grade and were purchased from Sigma Aldrich (St. Louis, MO, USA).

2.2 Preparation of Sensor Strips for X. fastidiosa Detection

A solution 6 mM DA solution (300 nmol PCDA-N-hydroxysuccinimide (NHS), 3300 nmol PCDA, and 2400 nmol DMPC) was prepared in chloroform. The strips were then incubated in a solution containing 0.04 mg/mL of anti-*X. fastidiosa* antibody for 4 h in room temperature or overnight at 4 ºC before photopolymerization (Chapter 3, Section 3).

2.3 Bacterial Cultures

X. fastidiosa subsp. *fastidiosa* (Temecula-1), *Pantoea stewartii* subsp. *stewartii* (DC283), and *Escherichia coli* BL21(DE3) were used in this study (Chapter 3, Section 5).

2.4 X. fastidiosa Detection and Sensor Analysis

Prepared strips were dipped into solutions containing various concentrations of *X. fastidiosa* from 0 to 4.1 x 10^8 cells/mL in LB media at room temperature. Color images of strips were recorded at incubation times from 1 h to 4 h. Red chromatic shift (RCS) was calculated using digital colorimetric analysis as previously described [37] (Chapter 3, Section 4.2).

Principal component analysis (PCA) was additionally employed (Table 5.S1, Figure 5.S1) (Chapter 3, Section 4.3). The first principal component (PC1) is expressed as PC1 = 0.76 x R + 0.44 x G – 0.47 x B, and the second principal component (PC2) as PC2 = –0.01 x R – 0.72 x G – 0.69 x B. The 2D PCA score plot indicates that PC1 accounts for 53.8% of the total data variance and PC2 accounts for 41.3%.

3. RESULTS AND DISCUSSION

The prepared strips (Figure 5.1) were incubated in liquid cultures of *X. fastidiosa* of varying concentrations from 0 to 4.1 x 10^8 cells/mL. The strips were imaged after each hour over a 4-hour period. After 4 h, they displayed a range of colors from blue to pink corresponding to increasing concentrations of *X. fastidiosa* culture (Figure 5.2). The detection limit of the sensor was determined as the lowest concentration of bacterial cells

that resulted in a color transition discernable by the naked eye. Accordingly, the detection limits at each hour were 1.2 x 10^8 cells/mL after both 1 h (12.3% RCS) and 2 h (17.6% RCS), and 0.8 x 10^8 cells/mL after 3 h (16.0% RCS) and 4 h (17.1% RCS). This indicates that an RCS of approximately 10-15% or greater is readily discernable by the naked eye, which has also been reflected in previous studies [23, 42].

After 4 h incubation in *X. fastidiosa* solution, the strips displayed four distinct colors and three color transitions. The first transition was at 0.8 x 10^8 cells/mL, the detection limit of the sensor, at which a blue to indigo transition occurred. This is reflected by a 17.1% RCS between strips incubated in 0 cells/mL (LB media) and 0.8 x 10^8 cells/mL. The second transition occurred at 1.8 x 10^8 cells/mL, at which an indigo to purple transition is denoted by a 9.6% RCS between strips in 0.8 x 10^8 cells/mL and strips in 1.8 x 10^8 cells/mL. The final purple to pink transition was at 2.7 x 10^8 cells/mL at which a 12.1% RCS is observed between strips in 1.8 x 10^8 cells/mL and those in 2.7 x 10^8 cells/mL. The multi-colored spectrum displayed by the strips allows for semi-quantitative naked-eye detection of *X. fastidiosa,* in which each color may indicate a certain degree of bacterial load within the plant.

The detection limit of the strips at 0.8 x 10^8 cells/mL after 4 h is comparable to the bacterial load found in *X. fastiodiosa*-infected grapevine tissue approximately 18 days after inoculation [6, 43]. While the detection limit of the current ELISA methods is in the range of 10^5 cells/mL (bacterial load approximately 6 days after inoculation) [6, 8], this threshold remains significant since symptoms of the disease appear in a broad range from 30 days up to 1 year after transmission [3]. Moreover, approximately 24 days after

inoculation, the rate of disease transmission of infected grapevine increases considerably [6]. Notably, this 24-day transmission threshold aligns well with the second color transition (indigo to purple) of our sensor. Accordingly, this sensor's color transitions are advantageous for disease management in that indigo may indicate that transmission rates are low (surrounding vines are likely healthy), purple may indicate that an increase in transmission rate is imminent (surrounding vines are at risk), and pink may indicate that disease transmission is high (surrounding vines are likely infected). As a result, both the detection limit of the sensor and the sensor's color transitions are relevant for early disease detection and disease management.

PCA was additionally employed to distinguish the color transitions between successive *X. fastidiosa* concentrations (Figure 5.3). For this analysis, the first principal component (PC1) is expressed as PC1 = 0.76 x R + 0.44 x G – 0.47 x B, and the second principal component (PC2) as PC2 = –0.01 x R – 0.72 x G – 0.69 x B. The 2D PCA score plot indicates that PC1 accounts for 53.8% of the total data variance and PC2 accounts for 41.3%. Notably, the PCA plot displays six distinct groups. This suggests that six distinct colors can be distinguished after 4 h by PCA quantification. In particular, the PCA plot confirms an additional distinction between strips incubated in 0.8 x 10^8 cells/mL and 1.2 x 10^8 cells/mL and strips in 2.7 x 10^8 cells/mL and 4.1 x 10^8 cells/mL, which are not discernable by the naked eye. PCA can be applied in future investigations of this sensing platform to provide further discrimination of *X. fastidiosa* levels by the strips that is indistinguishable with the unaided eye. Specifically, a smartphone

application to provide user-friendly PCA of smartphone image inputs of the strips would facilitate aided in-field analysis.

Finally, to test the specificity of the sensor, strips were incubated in bacterial cultures containing 4.1 x 10^8 cells/mL of *P. stewartii* (causal agent for Stewart's Wilt in maize [44]) and *E. coli*. RCS analysis of the strips after 4 h incubation indicates that significant color transitions did not occur in cultures containing bacterium other than *X. fastidiosa* (Figure 5.4). Specifically, RCS of strips incubated 4.1 x 10^8 cells/mL *X. fastidiosa* are 7 times higher than those incubated in 4.1 x 10^8 cells/mL *P. stewartii* and 42 times higher than those in 4.1 x 10^8 cells/mL *E. coli*.

4. CONCLUSIONS

We report a new sensor strip for naked-eye detection of *X. fastidiosa*. The detection limit of our sensor after 4 h incubation is 0.8 x 10^8 cells/mL, which is comparable to bacterial load 18 days after vector transmission of the disease [6]. Even more, the color transitions exhibited by the strip is expected to provide critical information regarding disease transmission of infected grapevine. Additionally, PCA suggests the potential to further discriminate *X. fastidiosa* levels through quantification of an image input. By foregoing the need for expensive detection instruments and reagents outside of leaf sample processing, this sensor platform has great potential for in-field use.

5. FIGURES

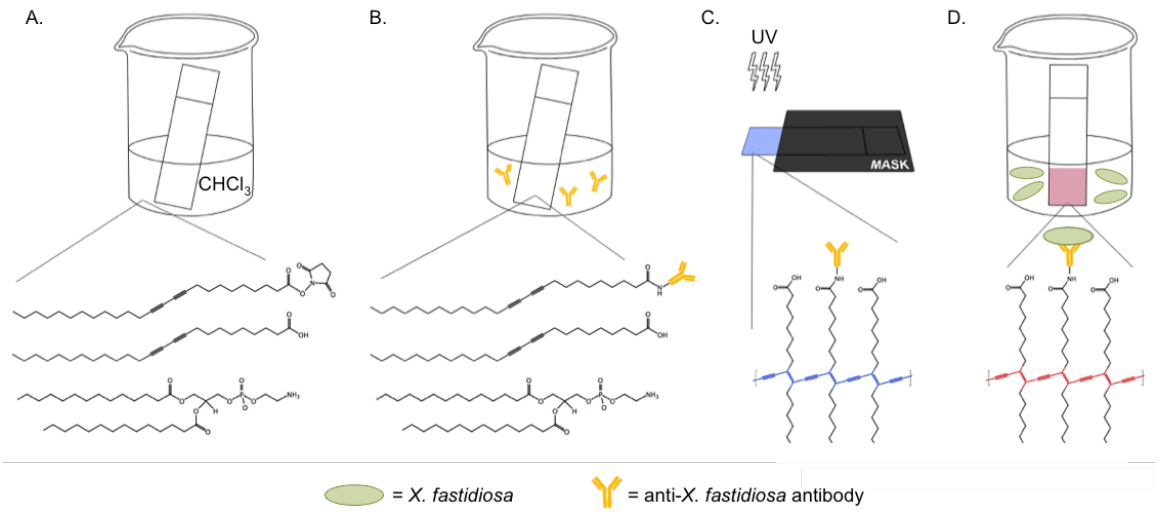

Figure 5.1. Preparation of *X. fastidiosa*-sensing strips. (A) PVDF strips are dipped into chloroform solution containing PCDA-NHS, PCDA, and DMPC and (B) subsequently incubated in a solution containing 1 mg/mL anti-*X. fastidiosa* antibody. (C) The PDA coat is then photopolymerized by 254 nm UV irradiation under a mask to yield a blue-colored device. (D) Dipping the device in solution containing *X. fastidiosa* causes a blue to pink color transition as a result of direct interaction between *X. fastidiosa* in solution and anti-*X. fastidiosa* antibody.

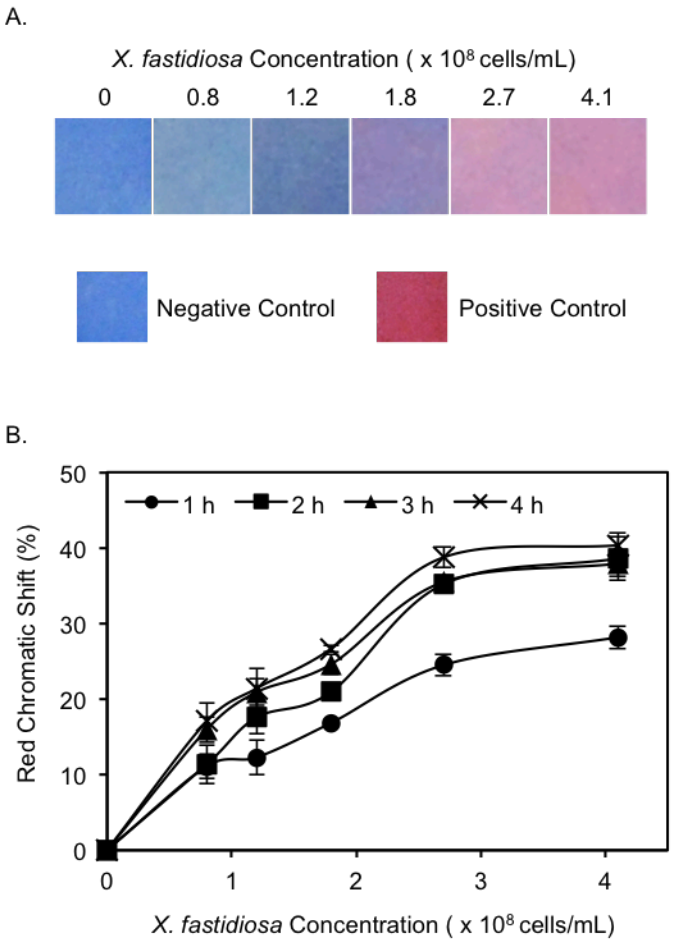

Figure 5.2. *X. fastidiosa* detection by strips. (A) Images of the strips after 4 h incubation in *X. fastidiosa* solutions. The negative and positive control images are from strips dipped in LB media and 1 M NaOH, respectively. (B) Red chromatic shift of the strips after 1 h, 2 h, 3 h and 4 h incubation in *X fastidiosa* solutions. Red chromatic shift data are represented as mean ± SD (n = 3).

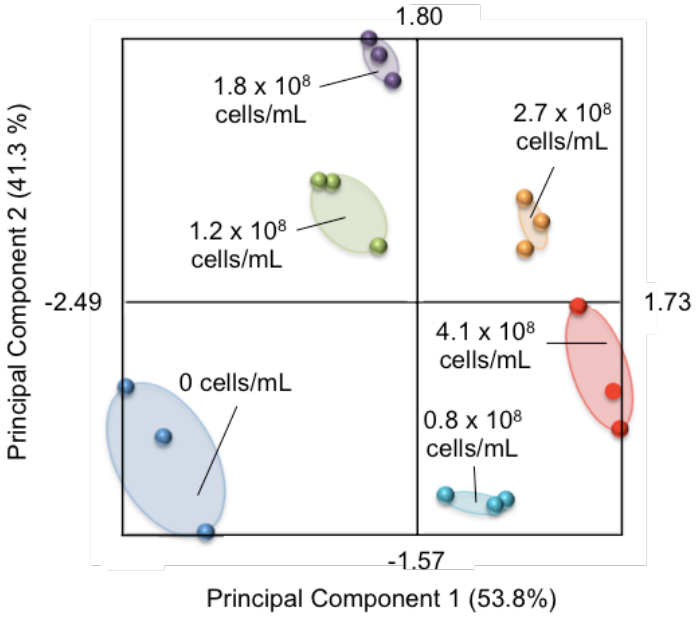

Figure 5.3. PCA transformation of RGB values (Table 5.S1). PCA facilitates additional discrimination of the sensor's colors that is not discernable by the naked eye.

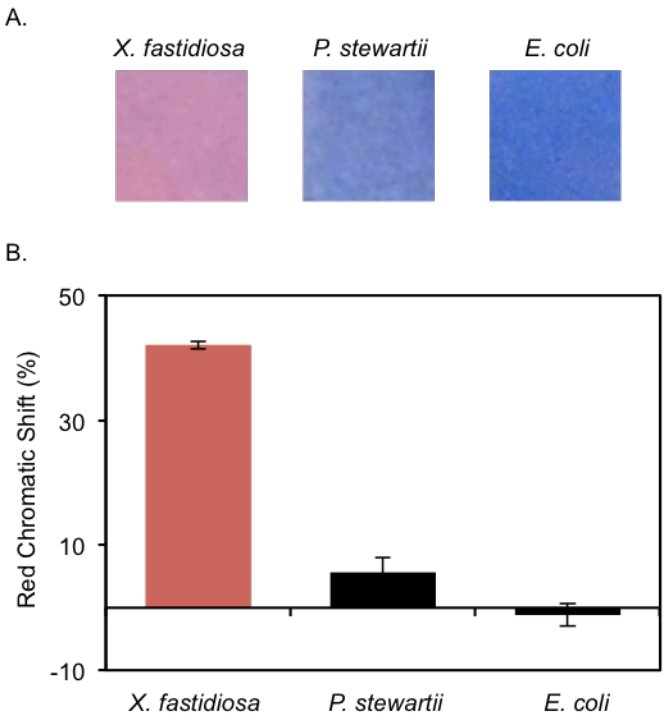

Figure 5.4. Specificity of the strips. Images (A) and red chromatic shift (B) of the strips after 4 h incubation in solutions containing 4.1 x 10^8 cells/mL of *X. fastidiosa, P. stewartii,* and *E. coli*. All data are represented as mean ± SD (n = 3).

References

[1] J. Mansfield, S. Genin, S. Magori, V. Citovsky, M. Sriariyanum, P. Ronald, *et al.*, Top 10 plant pathogenic bacteria in molecular plant pathology, *Mol Plant Pathol*, 13(2012) 614-29.

[2] D. Hopkins, Xylella fastidiosa: xylem-limited bacterial pathogen of plants, *Annu Rev Phytopathol*, 27(1989) 271-90.

[3] D. Hopkins, A. Purcell, Xylella fastidiosa: cause of Pierce's disease of grapevine and other emergent diseases, *Plant Dis*, 86(2002) 1056-66.

[4] J. Janse, A. Obradovic, Xylella fastidiosa: its biology, diagnosis, control and risks, *J Plant Pathol*, (2010) S35-S48.

[5] R.P. Almeida, A.H. Purcell, Transmission of Xylella fastidiosa to grapevines by Homalodisca coagulata (Hemiptera: Cicadellidae), *J Econ Entomol*, 96(2003) 264-71.

[6] B. Hill, A. Purcell, Populations of Xylella fastidiosa in plants required for transmission by an efficient vector, *Phytopathology*, 87(1997) 1197-201.

[7] M. Van Sluys, M. De Oliveira, C. Monteiro-Vitorello, C. Miyaki, L. Furlan, L. Camargo, *et al.*, Comparative analyses of the complete genome sequences of Pierce's disease and citrus variegated chlorosis strains of Xylella fastidiosa, *J Bacteriol*, 185(2003) 1018-26.

[8] D. Carbajal, K.A. Morano, L.D. Morano, Indirect immunofluorescence microscopy for direct detection of Xylella fastidiosa in xylem sap, *Curr Microbiol*, 49(2004) 372-5.

[9] G. Loconsole, O. Potere, D. Boscia, G. Altamura, K. Djelouah, T. Elbeaino, *et al.*, Detection of Xylella fastidiosa in olive trees by molecular and serological methods, *J Plant Pathol*, 96(2014) 1-8.

[10] G. Minsavage, C. Thompson, D. Hopkins, R. Leite, R. Stall, Development of a polymerase chain reaction protocol for detection of Xylella fastidiosa in plant tissue, *Phytopathology*, 84(1994) 456-61.

[11] N. Schaad, D. Opgenorth, P. Gaush, Real-time polymerase chain reaction for one-hour on-site diagnosis of Pierce's disease of grape in early season asymptomatic vines, *Phytopathology*, 92(2002) 721-8.

[12] S.N.B. Raju, A. Goheen, G. Nyland, D. Docampo, Enzyme-linked Immunosorbent Assay for Pierce's Disease Bacteria in Plant Tissues, *Phytopathology*, 70(1980) 746-9.

[13] Q. Huang, J. Bentz, J. Sherald, Fast, easy and efficient DNA extraction and one-step polymerase chain reaction for the detection of Xylella fastidiosa in potential insect vectors, *J Plant Pathol*, 88(2006) 77-81.

[14] Q. Cheng, R.C. Stevens, Charge-induced chromatic transition of amino acid-derivatized polydiacetylene liposomes, *Langmuir*, 14(1998) 1974-6.

[15] J. Song, Q. Cheng, S. Kopta, R.C. Stevens, Modulating artificial membrane morphology: pH-induced chromatic transition and nanostructural transformation of a bolaamphiphilic conjugated polymer from blue helical ribbons to red nanofibers, *J Am Chem Soc*, 123(2001) 3205-13.

[16] H. Beckham, M. Rubner, On the origin of thermochromism in cross-polymerized diacetylene-functionalized polyamides, *Macromolecules*, 26(1993) 5198-201.

[17] R. Chance, G. Patel, J. Witt, Thermal effects on the optical properties of single crystals and solution-cast films of urethane substituted polydiacetylenes, *J Chem Phys*, 71(1979) 206-11.

[18] R.R. Chance, R.H. Baughman, H. Muller, C.J. Eckhardt, Thermochromism in a Polydiacetylene Crystal, *J Chem Phys*, 67(1977) 3616-8.

[19] D.H. Charych, J.O. Nagy, W. Spevak, M.D. Bednarski, Direct colorimetric detection of a receptor-ligand interaction by a polymerized bilayer assembly, *Science*, 261(1993) 585-8.

[20] D.H. Charych, W. Spevak, J.O. Nagy, M.D. Bednarski, Specific interaction of influenza-virus with organized assemblies of polydiacetylenes, *Mater Res Soc Symp Proc*, 292(1993) 153-61.

[21] Y.K. Jung, T.W. Kim, H.G. Park, H.T. Soh, Specific colorimetric detection of proteins using bidentate aptamer-conjugated polydiacetylene (PDA) liposomes, *Adv Funct Mater*, 20 (2010) 3092-7.

[22] R. Jelinek, S. Kolusheva, Polymerized lipid vesicles as colorimetric biosensors for biotechnological applications, *Biotechnol Adv*, 19(2001) 109-18.

[23] Y.-l. Su, J.-r. Li, L. Jiang, Chromatic immunoassay based on polydiacetylene vesicles, *Colloid Surface B*, 38(2004) 29-33.

[24] E. Geiger, P. Hug, B.A. Keller, Chromatic transitions in polydiacetylene langmuir-blodgett films due to molecular recognition at the film surface studied by spectroscopic methods and surface analysis, *Macromol Chem and Physic*, 203(2002) 2422-31.

[25] B. Ma, Y. Fan, L. Zhang, X. Kong, Y. Li, J. Li, Direct colorimetric study on the interaction of Escherichia coli with mannose in polydiacetylene Langmuir–Blodgett films, *Colloid Surface B*, 27(2003) 209-13.

[26] J.T. Wen, K. Bohorquez, H. Tsutsui, Polydiacetylene-Coated Polyvinylidene Fluoride Strip Aptasensor for Colorimetric Detection of Zinc(II), *Sensor Actuat B-Chem*, (2016) doi:10.1016/j.snb.2016.03.118.

[27] T. Eaidkong, R. Mungkarndee, C. Phollookin, G. Tumcharern, M. Sukwattanasinitt, S. Wacharasindhu, Polydiacetylene paper-based colorimetric sensor array for vapor phase detection and identification of volatile organic compounds, *J Mater Chem*, 22(2012) 5970-7.

[28] B. Yoon, I.S. Park, H. Shin, H.J. Park, C.W. Lee, J.M. Kim, A litmus-type colorimetric and fluorometric volatile organic compound sensor based on inkjet-printed polydiacetylenes on paper substrates, *Macromol Rapid Comm*, 34(2013) 731-5.

[29] M.-C. Lim, Y.-J. Shin, T.-J. Jeon, H.-Y. Kim, Y.-R. Kim, Microbead-assisted PDA sensor for the detection of genetically modified organisms, *Anal Bioanal Chem*, 400(2011) 777-85.

[30] S.-H. Jung, H. Jang, M.-C. Lim, J.-H. Kim, K.-S. Shin, S.M. Kim, *et al.,* Chromatic biosensor for detection of phosphinothricin acetyltransferase (PAT) using polydiacetylene vesicles encapsulated within automatically generated immuno-hydrogel beads, *Anal Chem*, 87(2015) 2072-8.

[31] J. Lee, H. Jun, J. Kim, Polydiacetylene-liposome microarrays for selective and sensitive mercury (II) detection, *Adv Mater*, 21(2009) 3674-7.

[32] S. Seo, J. Lee, E.J. Choi, E.J. Kim, J.Y. Song, J. Kim, Polydiacetylene Liposome Microarray Toward Influenza A Virus Detection: Effect of Target Size on Turn-On Signaling, *Macromol Rapid Comm*, 34(2013) 743-8.

[33] D.J. Ahn, J.M. Kim, Fluorogenic polydiacetylene supramolecules: immobilization, micropatterning, and application to label-free chemosensors, *Acc Chem Res*, 41(2008) 805-16.

[34] E. Gravel, J. Ogier, T. Arnauld, N. Mackiewicz, F. Ducongé, E. Doris, Drug delivery and imaging with polydiacetylene micelles, *Chemistry*, 18(2012) 400-8.

[35] G. Qin, Z. Li, R. Xia, F. Li, B.E. O'Neill, J.T. Goodwin, *et al.*, Partially polymerized liposomes: stable against leakage yet capable of instantaneous release for remote controlled drug delivery, *Nanotechnology*, 22(2011) 155605.

[36] J.T. Wen, C. Castro, H. Tsutsui, *In planta* microsphere-based lateral flow leaf biosensor in maize, *J Lab Autom*, 20(2015)500-505.

[37] R. Volinsky, M. Kliger, T. Sheynis, S. Kolusheva, R. Jelinek, Glass-supported lipid/polydiacetylene films for colour sensing of membrane-active compounds, *Biosens Bioelectron*, 22(2007) 3247-51.

[38] Y. Li, L. Wang, X. Yin, B. Ding, G. Sun, T. Ke, *et al.,* Colorimetric strips for visual lead ion recognition utilizing polydiacetylenes embedded nanofibers, *J Mater Chem A*, 2(2014) 18304-12.

[39] T. Soga, Y. Jimbo, K. Suzuki, D. Citterio, Inkjet-printed paper-based colorimetric sensor array for the discrimination of volatile primary amines, *Anal Chem*, 85(2013) 8973-8.

[40] S. Wold, K. Esbensen, P. Geladi, Principal component analysis, *Chemom Intell Lab Syst*, 2(1987) 37-52.

[41] M. Ringnér, What is principal component analysis?, *Nat Biotechnol*, 26(2008) 303-4.

[42] S. Kolusheva, L. Boyer, R. Jelinek, A colorimetric assay for rapid screening of antimicrobial peptides, *Nat Biotechnol*, 18(2000) 225-7.

[43] B. Hill, A. Purcell, Multiplication and movement of Xylella fastidiosa within grapevine and four other plants, *Phytopathology*, 85(1995) 1368-72.

[44] M.C. Roper, Pantoea stewartii subsp. stewartii: lessons learned from a xylem-dwelling pathogen of sweet corn, *Mol Plant Pathol*, 12(2011) 628-37.

6. SUPPLEMENTARY DATA

Table 5.S1. RGB values extracted from strips after 4 h in *X. fastidiosa* culture.

Sample (x 10^8 cells/mL)	Red	Green	Blue
0 - 1	96.3	143.1	224.6
0 - 2	87.5	134.4	219.3
0 - 3	80.4	128.8	218.4
0.8 - 1	144.9	162.0	185.5
0.8 - 2	142.8	161.7	187.1
0.8 - 3	131.5	158.6	190.3
1.2 - 1	120.4	137.6	173.7
1.2 - 2	109.6	131.0	171.3
1.2 - 3	106.1	130.5	172.0
1.8 - 1	127.5	126.1	158.0
1.8 - 2	124.8	123.6	157.0
1.8 - 3	122.5	122.0	156.3
2.7 - 1	171.0	136.1	165.3
2.7 - 2	167.1	140.8	168.2
2.7 - 3	170.4	140.0	163.8
4.1 - 1	186.4	158.1	176.6
4.1 - 2	180.6	146.8	169.9
4.1 - 3	195.1	152.1	178.7

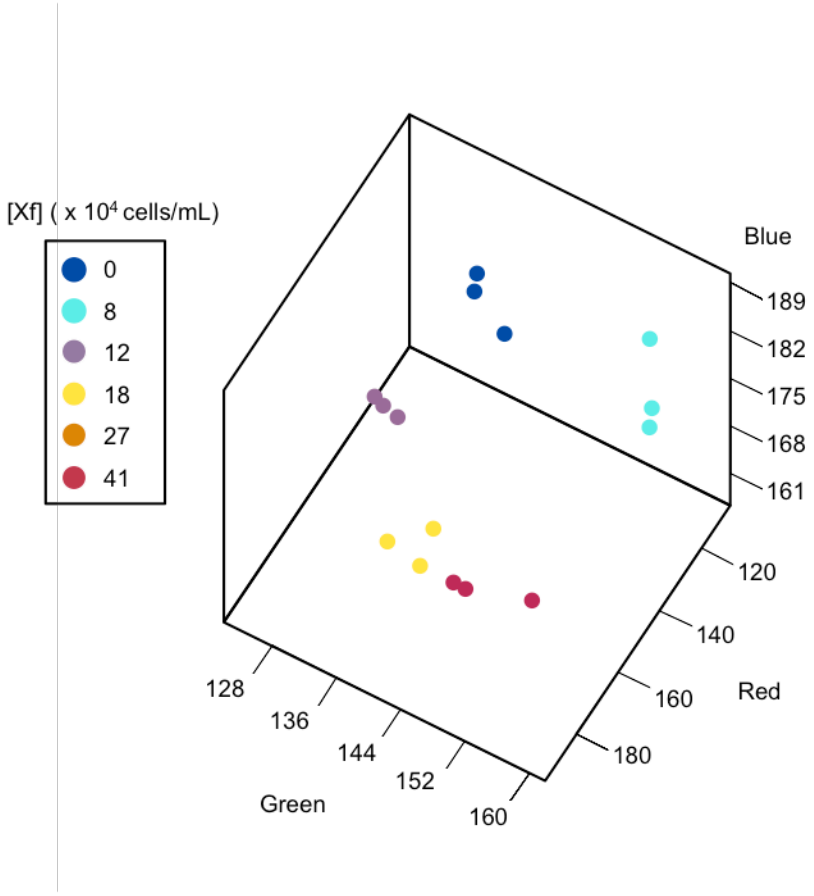

Figure 5.S1. 3D plot of RGB values.

PREFACE: CHAPTERS 6 & 7

Chapters 6 and 7 of this dissertation report the ongoing development of a proposed *in vivo* detection system for the in-field diagnostics of exogenous plant pathogenic bacteria. Specifically, a proof-of-concept study of the proposed platform is described in Chapter 6, and the fabrication of injectable polydiacetylene liposome sensors for detection of exogenous bacterium, *P. stewartii* is subsequently reported in Chapter 7. The studies described in Chapter 6 have been previously published all or in part by *Society for Laboratory Automation and Screening* (Copyright 2015, doi: 10.1177/2211068214551826).

CHAPTER 6:

IN VIVO MICROSPHERE-BASED LATERAL FLOW BIOSENSOR IN MAIZE LEAVES

Abstract

Low-cost and quick detection of biotic stresses is critically important for protection of staple food crops, such as maize, in smallholder farms. This is particularly critical in developing countries, where access to improved seed varieties, fertilizers, and pesticides is restricted due to financial and geographical limitations. This chapter reports the development of an *in vivo* lateral flow detection technology. Specifically, this platform is directly integrated in a maize leaf, where microspheres conjugated with analyte-specific capture antibodies are non-invasively injected. In this study, we optimized microsphere size for effective infiltration and immobilization in the leaf, and further demonstrated the detection of a fluorescent mock biomarker, fluorescein, in a live maize plant. Results of the study indicate that antibody-conjugated microspheres captured and detected analyte in a concentration-specific manner. This *in vivo* lateral flow biosensor is the first of its kind and is expected to provide a low-cost and user-friendly detection method for biotic stresses in the field.

1. INTRODUCTION

Maize is one of the most widely grown staple crops globally, and is especially critical in developing regions of sub-Saharan Africa and Mesoamerica, where maize alone comprises over 20% of food calories and up to 73% of total production is used as a food source [1]. Despite high demand, maize growth suffers from significant losses at both pre- and post-harvest stages due to biotic stresses such as viruses, fungi, bacteria, and other pests and pathogens. Numerous methods to improve maize growth and yield, including adoption of improved seed varieties, use of fertilizers, and application of pesticides, have been suggested to alleviate recurrent food shortages; however, these have not been widely employed by smallholder farmers due to their high cost and lack of accessibility [2, 3].

Quick and efficient detection of plant pathogens is desirable for the timely intervention of plant diseases. Standard methodologies in plant diagnostics range from physical examination of symptoms to the use of molecular diagnostics such as enzyme-linked immunosorbent assay (ELISA) or polymerase chain reaction (PCR) [4-6]. Although ELISA and PCR offer high sensitivity and specificity, both of these approaches require expensive laboratory facilities and trained operators. On the other hand, physical examination can only offer a diagnosis well past the onset of pathogenic infection.

Recently, lateral flow devices have gained much attention as inexpensive, user-friendly, in-field diagnostic tools [7]. Lateral flow devices typically incorporate the use of a nitrocellulose test strip and capture antibodies to detect the presence of analyte in a two-step sandwich assay. Wicking of analyte-containing sample solution onto the

nitrocellulose substrate results in capture of analyte by the first antibody, conjugated to a colored particle. The analyte-antibody pair then flow downstream to a second analyte-specific antibody that is immobilized on the surface of the test strip (the detection zone). The accumulation of the initial analyte-antibody pair at the detection zone results in a positive test indicated by the aggregation of colored particles visible to the naked eye [7]. While lateral flow devices have recently been developed to detect plant pathogens [5], these external devices require the user to initiate testing and are likely used for rapid confirmation of pathogenic infection already suspected from physical examination. An ideal detection platform would provide notification at the first onset of pathogenic infection. Such a platform would require a biodetection strategy that is integrated directly within the host plant itself.

Syringe agroinfiltration is a method of gene introduction into plant hosts via delivery of genes through *Agrobacterium* [8, 9]. First, a needleless syringe is filled with *Agrobacterium*-containing media. The tip of the needless syringe is then placed against the abaxial (back) side of an intact plant leaf, and the media is manually injected into the leaf interstitium. A temporary color change from light to dark green indicates successful infiltration of *Agrobacterium* into the leaf [10, 11]. Syringe agroinfiltration has been demonstrated successfully in several plant species [11, 12]. While there are other methods of transient gene expression in live plant hosts, including biolistics (microprojectile bombardment) [13] and microneedle injection [14], the need for minimal equipment and simplicity of procedure has made syringe agroinfiltration a popular choice in recent years.

This study reports the first development of a lateral flow biosensor that utilizes the maize leaf itself as the substrate for the lateral flow "test strip". By modifying the established agroinfiltration procedure, we introduced and immobilized antibody-conjugated microspheres in the leaf interstitium. Our one-step lateral flow detection platform aims to target fluorescent biomarkers (e.g., aflatoxins) or to incorporate the use of detection-sensitive, colorimetric polydiacetylene (PDA) vesicles [15, 16] to simplify the procedure and eliminate the need for two-step sandwich assays. In this study, we successfully detect a mock pathogen, fluorescein, using infiltrated microspheres conjugated with anti-fluorescein antibody (Figure 6.1A).

2. MATERIALS AND METHODS

2.1 Materials

Maize seeds were obtained from Carolina Biological Supply Company (Burlington, NC, USA). 1 mL needleless syringes were from Fisher Scientific (Waltham, MA, USA). Fluorescent microspheres were obtained from Spherotech (Lake Forest, IL, USA), and biotinylated anti-fluorescein antibody was from eBiosciences (San Diego, CA, USA). All other chemicals used are research grade and were obtained from Sigma Aldrich (St. Louis, MO, USA).

2.2 Maize Growth

Readers are referred to Chapter 3 (Section 6) for a detailed protocol for maize growth.

2.3 Infiltration of Microspheres

Fluorescent microspheres were washed in 1X phosphate buffered saline (PBS) solution and resuspended in infiltration buffer (10 mM $MgCl_2$, 10 mM MES-potassium, pH 5.6). Microsphere solutions (0.5% v/v solids) were infiltrated into the abaxial side of intact maize leaves. Immediately after infiltration, the abaxial epidermis of leaves were gently wiped with deionized water to remove residual uninfiltrated microspheres. Infiltrated leaves were examined from the adaxial (front) surface under a Leica DM2000 fluorescence microscope following infiltration and every 24 h for 72 h. Fluorescence intensities were determined as a ratio of the signal intensity of the target region to the leaf background. Retention rate was calculated as a ratio of fluorescence intensity at 72 h after infiltration and immediately following infiltration.

2.4 Lateral Flow Detection

Anti-fluorescein antibody-coated red fluorescent microspheres (AF microspheres) were first prepared. 0.5 μm streptavidin-coated red fluorescent microspheres were mixed with biotinylated anti-fluorescein antibodies, washed, and resuspended in infiltration buffer. AF microsphere solutions (0.5% v/v solids) were injected into the second leaf from the bottom of 15- to 20-day-old maize plants, examined for initial microsphere content and transferred to fluorescein solutions containing 0, 3.2, 8, 20 or 50 μM fluorescein in PBS

(pH adjusted to 6.8). The plants were grown in fluorescein solution for 72 h to allow for sufficient fluorescein uptake by the plants, and the solution was changed every 12 h. The plants were examined again at the end of the 72 h experiment. For the duration of the experiment, plant roots were fully immersed in fluorescein solution and the solution was protected from light. Fluorescence intensities were determined as a ratio of the mean signal intensity in a region of interest (ROI) to the leaf background. The ROI is defined per plant as a fixed rectangular space that encompasses the region where red fluorescent microspheres have been infiltrated. The leaf background is defined as a corresponding region on the same leaf lateral to the ROI. Normalized fluorescence intensities for test plants were calculated as the ratio of fluorescence intensity to the mean intensity of control plants grown in 0 μM fluorescein solution.

3. RESULTS AND DISCUSSION

3.1 Infiltration of Microspheres in Leaf Tissue

A pressure-driven infiltration technique, inspired by agroinfiltration, was developed to non-invasively introduce microspheres into the leaf. Specifically, a pressure gradient, introduced by the syringe on the leaf surface, propelled bioreagents through pores in the leaf abaxial epidermis and into the leaf apoplast (intercellular space) (Figure 6.1B). Infiltration in maize leaves was successfully demonstrated without damaging the leaf epidermis (Figure 6.1C). In this platform, microspheres were used to provide stationary surfaces through which

antibodies were immobilized within the leaf tissue. Without such surfaces, antibodies cannot be retained at a fixed spot inside the leaf.

Microsphere sizes were characterized for both high infiltration efficiency and retention rate post-infiltration. Spheres too large cannot pass through the leaf epidermis, whereas spheres too small are easily removed from the infiltrated spot. Fluorescent microspheres, ranging from 0.1 to 1 μm in diameter, were infiltrated into intact maize leaves. Fluorescence microscopy analysis of the microspheres injected and retained at the injection site over the 72 h period indicated that the 0.5 μm diameter microspheres produced initial signal intensities 2.5, 3, and 4 times higher than 0.3, 0.1, and 1.0 μm infiltrated microspheres, respectively (Figure 6.2A, 6.2B). Additionally, 0.5 μm infiltrated microspheres yielded a nearly 100% retention rate over 72 h (Figure 6.2C). These results suggest that a 0.5 μm diameter particle size is desirable for high infiltration and retention efficiency, and is appropriate for the immobilization of foreign biomolecules (e.g., antibodies) in the maize leaf tissue.

3.2 Lateral Flow Detection of Fluorescein by AF Microspheres In Vivo

Detection of fluorescein by AF microspheres was performed as a proof-of-concept demonstration of the proposed *in vivo* biosensing technology. AF microspheres were prepared (Figure 6.3A) and injected into leaves of live maize plants. Infiltrated plants were grown in fluorescein solution for 72 h before optical analysis. It was demonstrated that AF microspheres themselves did not emit green fluorescence (Figure 6.3B, 0 μM fluorescein concentration), but effectively captured trace amounts of fluorescein

molecules taken up by the maize plant. This was exhibited by the localized accumulation of green fluorescence signals (Figure 6.3B, 3.2-50 μM). Specifically, quantitative analysis of fluorescein detection by AF microspheres indicate a 22%, 34%, 51%, and 71% increase in normalized fluorescence intensity by plants infiltrated with AF microspheres grown in 3.2 μM, 8 μM, 20 μM, and 50 μM fluorescein solution respectively, as compared to control plants grown in 0 μM fluorescein solution (Figure 6.3C). In addition, plants infiltrated with control (non-conjugated) microspheres did not show increased fluorescence intensity with increasing fluorescein concentration, further confirming specific detection by test plants infiltrated with AF microspheres. The limit of detection (LoD) [17], defined as two standard deviations above the arithmetic mean of normalized fluorescence intensity of control plants grown in 0 μM fluorescein, was 19 μM. Collectively, these data indicate the feasibility of *in vivo* detection of biomolecules in maize based on the proposed technology.

The anticipated use of this technology is for the early detection of disease onset over a plant's lifetime. The microsphere sensors would therefore be injected into plant leaves at a young and healthy age. While capture antibodies are likely to degrade and become inactive over time in plant leaves, especially in the field (e.g., in high temperatures and sun light), more stable and economical capture probes such as DNA aptamers are a desirable alternative for long-term applications [18]. In addition, DNA aptamers are more economical to produce than monoclonal antibodies, thereby allowing for further cost reduction of the proposed low-cost diagnostic method.

4. CONCLUSIONS

We have developed a minimally invasive *in vivo* biomolecular detection platform for maize. The design of our detection system incorporates the immobilization of antibody-conjugated microspheres in the leaf to capture analyte and produce a detection signal. Unlike conventional lateral flow assays, which require sample processing (e.g., grinding of plant and extraction of analyte solution) and are single-use, the proposed, directly integrated technology does not require processing of plants post-infiltration and is intended for continuous monitoring of biomarker levels over time, potentially enabling early notification of disease onset. This not only eliminates the need for multiple tests per plant but also an external substrate for the lateral flow test strip, thereby reducing the costs and resources needed for disease detection. This simple method is minimally invasive, cost-effective, and is, to our best knowledge, the first report of a lateral flow biodetection technology that is integrated directly within living plant hosts. Because syringe infiltration is easily translatable [10, 11], this proposed technology is expected to be applicable to a variety of plants, monocots and dicots alike. Although this initial report focuses on the demonstration of *in vivo* detection of a fluorescent mock pathogen (i.e., fluorescein) only, with further development, particularly with the incorporation of colorimetric, stimuli-responsive PDA vesicles (Figure 6.4) [15, 16], this technology is likely to yield an equipment-free and colorimetric *in vivo* diagnosis. We anticipate that such an innovative tool will make a significant impact on improving the yield of healthy food crops by smallholder farmers across developing countries worldwide.

5. FIGURES

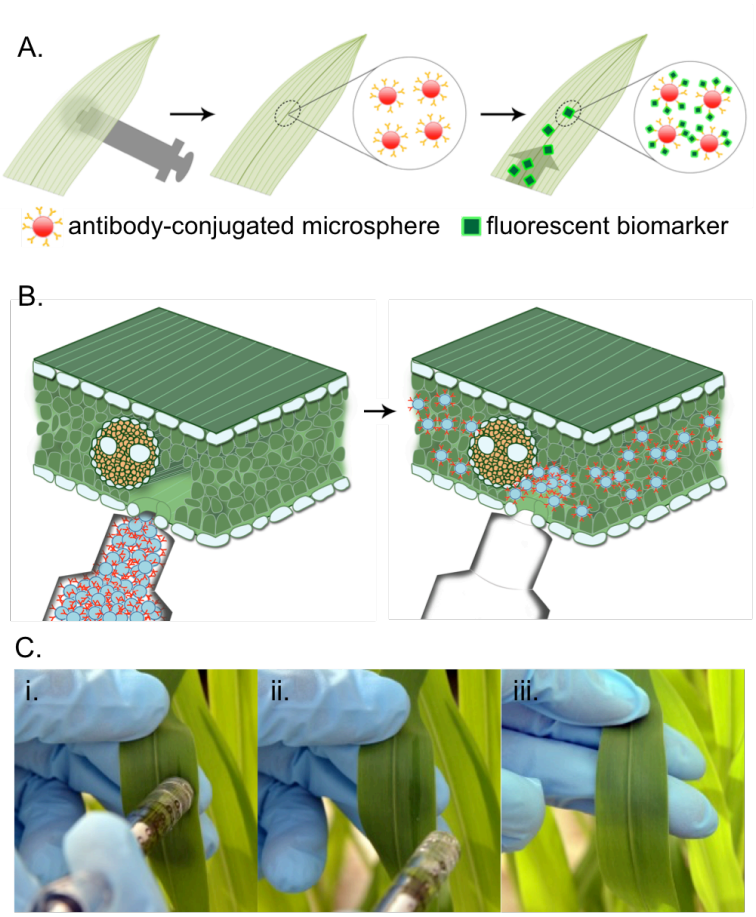

Figure 6.1. Method of one-step lateral flow detection of pathogen markers in live maize leaves. This study focuses on the detection of a fluorescent biomarker using antibody-conjugated microspheres (A), which serves as the basis for future developments to detect non-fluorescent biomarkers by incorporating stimuli-sensitive colorimetric liposomes (Figure 6.4). (B) Schematic of infiltration of microspheres into leaf tissue before infiltration (left) and after infiltration (right). (C) Infiltration in a maize leaf: (i) infiltration with a needleless syringe, (ii) immediately after injection, where injected buffer solution is visible, and (iii) 10 min after injection, where injected buffer evaporates without leaving visible marks. Reprinted with permission from *Society for Laboratory Automation and Screening*, Copyright 2015, doi: 10.1177/2211068214551826.

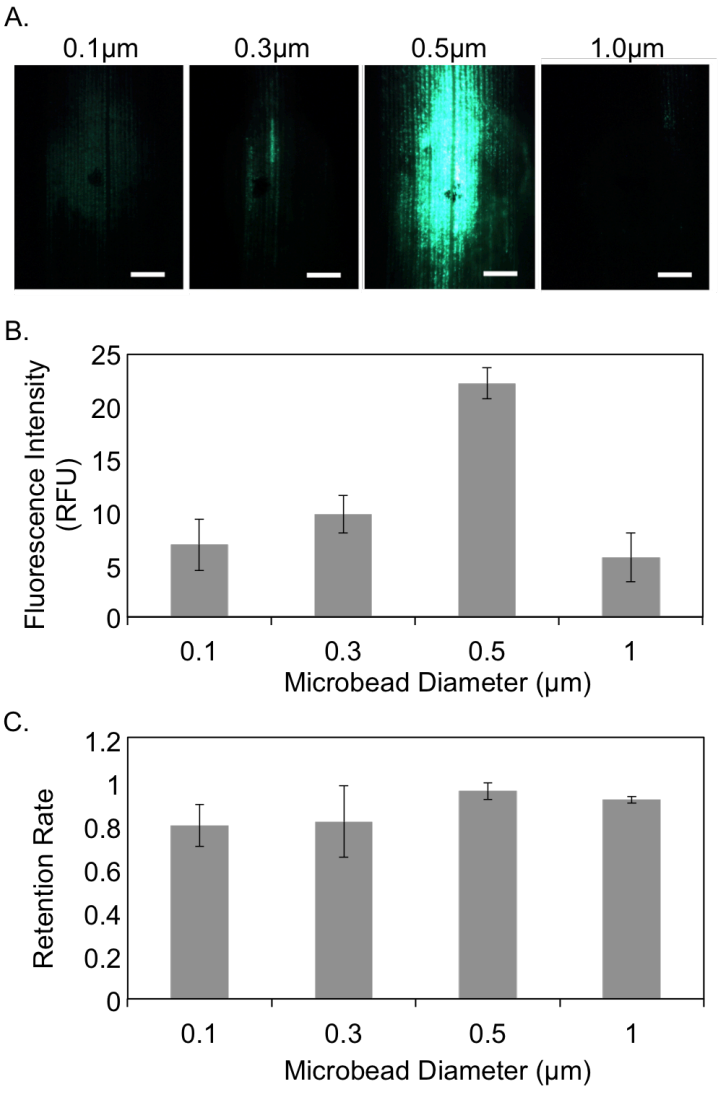

Figure 6.2. Infiltration of microspheres in leaf. (A) Fluorescence images of infiltrated microspheres. (B) Fluorescence intensity of infiltrated microspheres by diameter. (C) Microsphere retention rate after 72 h. Data are represented as mean ± SD (n=3). Scale bars: 1.2 mm. Reprinted with permission from *Society for Laboratory Automation and Screening*, Copyright 2015, doi: 10.1177/2211068214551826.

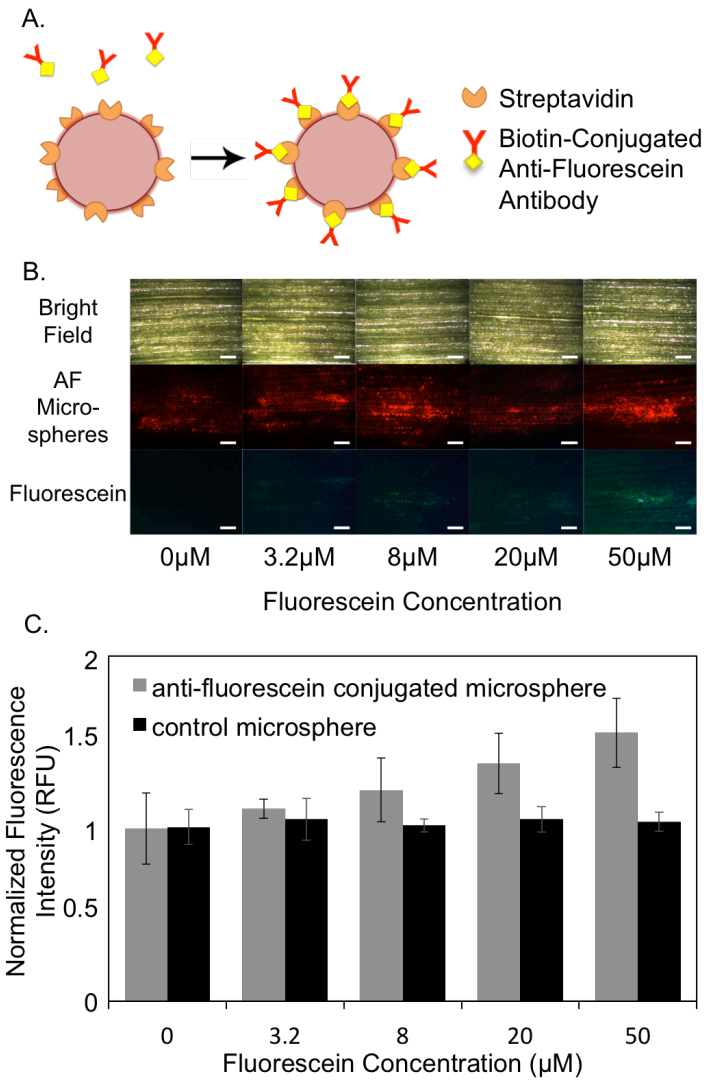

Figure 6.3. Lateral flow detection of fluorescein in live maize plants after 72 h growth in fluorescein solutions. (A) Immobilization of anti-fluorescein antibody onto red fluorescent microspheres. (B) Infiltration of anti-fluorescein coated red fluorescent microspheres in leaves followed by antibody capture of fluorescein from plants grown in fluorescein solutions of varying concentrations. (C) Relative fluorescence intensity of fluorescein captured by anti-fluorescein conjugated microspheres and control (non-coated) microspheres. Data are represented mean ± SD (n=3). Scale bars: 500 µm. Reprinted with permission from *Society for Laboratory Automation and Screening*, Copyright 2015, doi: 10.1177/2211068214551826.

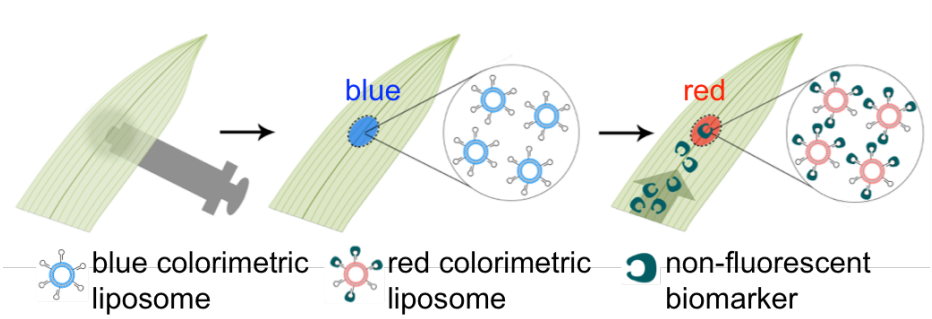

Figure 6.4. Proposed method of colorimetric, one-step lateral flow detection of pathogens in maize leaves for future development. Infiltrated stimuli-sensitive, colorimetric liposomes respond to analyte binding to aptamers or antibodies conjugated on the vesicle surface via a blue to red color shift visible to the naked eye. Reprinted with permission from *Society for Laboratory Automation and Screening*, Copyright 2015, doi: 10.1177/2211068214551826.

References

[1] E.T. Nuss, S.A. Tanumihardjo, Maize: a paramount staple crop in the context of global nutrition, *Compr Rev Food Sci Food Saf,* 9(2010) 417-46.

[2] G. Farre, R.M. Twyman, C. Zhu, *et al*., Nutritionally enhanced crops and food security: scientific achievements versus political expediency, *Curr Opin Biotechnol* 2(2011) 245-51.

[3] M. Smale, D. Byerlee, T. Jayne, Maize revolutions in sub-Saharan Africa, World Bank*,* 2011.

[4] R. Mumford, N. Boonham, J. Tomlinson, *et al.*, Advances in molecular phytodiagnostics–new solutions for old problems, *Eur J Plant Pathol*, 116(20060) 1-19.

[5] J.A. Tomlinson, M.J. Dickinson, N. Boonham, Rapid detection of Phytophthora ramorum and P. kernoviae by two-minute DNA extraction followed by isothermal amplification and amplicon detection by generic lateral flow device, *Phytopathology*, 100(2010) 143-9.

[6] K.K. Mondal, V. Shanmugam, Advancements in the diagnosis of bacterial plant pathogens: an overview, *Biotechnol Mol Biol Rev* 8(2013), 1-11.

[7] B. Ngom, Y. Guo, X. Wang, *et al*., Development and application of lateral flow test strip technology for detection of infectious agents and chemical contaminants: a review, *Anal Bioanal Chem* 397(2010) 1113-35.

[8] Q. Chen, H. Lai, J. Hurtado, *et al*., Agroinfiltration as an effective and scalable strategy of gene delivery for production of pharmaceutical proteins, *Adv Tech Biol Med* 1(2013) 1000103.

[9] H. Schob, C. Kunz, F. Meins Jr., Silencing of transgenes introduced into leaves by agroinfiltration: a simple, rapid method for investigating sequence requirements for gene silencing, *Mol Gen Genet*, 256(1997) 581-5.

[10] P. Annamalai, A.L.N. Rao, Delivery and expression of functional viral RNA genomes *in planta* by agroinfiltration, *Curr Protoc Microbiol*, (2006) 16B2.1-5.

[11]T. Wroblewski, A. Tomczak, R. Michelmore, Optimization of agrobacterium-mediated transient assays of gene expression in lettuce, tomato and Arabidopsis, *Plant Biotechnol J*, 3(2005) 259-73.

[12] M. Santos-Rosa, A. Poutaraud, D. Merdinoglu, *et al.*, Development of a transient expression system in grapevine via agro-infiltration, *Plant Cell Rep*, 27(2008) 1053-63.

[13] J.R. Kikkert, J.R. Vidal, B.I. Reisch, Stable transformation of plant cells by particle bombardment/biolistics, *Methods Mol Biol*, 286(2004) 61-78.

[14] S. Wolf, W.J. Lucas, C.M. Deom, *et al.*, Movement protein of tobacco mosaic virus modifies plasmodesmatal size exclusion limit, *Science*, 246(1989) 377-9.

[15] R. Jelinek, M. Ritenberg, Polydiacetylenes–recent molecular advances and applications, *RSC Adv*, 3(2013) 21192-201.

[16] Y.K. Jung, T.W. Kim, H.G. Park, *et al.*, Specific colorimetric detection of proteins using bidentate aptamer-conjugated polydiacetylene (PDA) liposomes, *Adv Funct Mater*, 20(2010) 3092-7.

[17] D.A. Armbruster, T. Pry, Limit of blank, limit of detection and limit of quantitation, *Clin Biochem Rev*, 20(2009) S49-52.

[18] S.D. Jayasena, Aptamers: an emerging class of molecules that rival antibodies in diagnostics, *Clin Chem*, 45(1999) 1628-50.

CHAPTER 7:

POLYDIACETYLENE LIPOSOMES FOR IMMUNOCHROMATIC DETECTION OF *P. STEWARTII*

Abstract

This chapter reports the development of polydiacetylene liposomes that transition from blue to red in the presence of *P. stewartii*, the causal agent of Stewart's wilt in sweet corn. The liposomes are conjugated with anti-*P. stewartii* antibodies for specific detection of the pathogen. Our sensor exhibited three color transitions and four distinct colors, blue, purple, pink, and red, that were distinguishable by the naked eye. Additionally, we report successful visibility of red PDA liposomes *in vivo* when injected into an intact corn leaf. This study suggests that this sensor is appropriate for the ongoing development of an *in vivo* platform for continuous monitoring and early detection plant pathogens.

1. INTRODUCTION

Pantoea stewartii subsp. *stewartii* is a gram-negative bacterium and causal agent of Stewart's wilt in sweet corn [1, 2]. Stewart's wilt is indigenous to the United States and has been responsible for severe economic losses in the 1930's, which prompted intensive research into the causal bacterium and development of resistant corn hybrids [1, 3-5]. Transmission of the disease occurs primarily through the corn flea beetle, *Chaetocnema pulicaria*, although a low frequency of seed-borne transmission has also been reported [6]. Symptoms of the disease include water-soaked lesions, leaf blight and stunted growth in mature plants. Systemic spread of the pathogen in young seedlings also leads to wilting and premature death [3]. Movement of the pathogen in the plant begins with colonization of the apoplast (intercellular spaces) of the leaf and xylem tissues. Proliferation and expansion of the bacteria in the xylem block water flow and eventually rupture the pit membrane resulting in systemic virulence of the pathogen via movement into the pith and intercellular spaces of other plant organs [1]. In this report, *P. stewartii* is selected for sensor development as a well-studied, model plant pathogenic bacterium.

Current methods for *P. stewartii* detection and diagnosis include field inspection, seed grow-out testing, and enzyme-linked immunosorbant assay (ELISA) [4, 7]. However, field inspection and seed grow-out tests are inefficient and unreliable and ELISA testing requires a laboratory setting with trained operators. Recently, protocols for the detection of *P. stewartii* through polymerase chain reaction (PCR) have been reported for improved detection sensitivities of the pathogen [8-10], nonetheless PCR procedures are even more complicated and time-consuming than ELISA tests. Alternatively, the

recent development of immunochromatic strips for lateral flow detection for *P. stewartii* detection has provided an equipment-free and rapid testing method for the pathogen [11]. Indeed, an *in vivo* lateral flow test for naked-eye detection of *P. stewartii* would be a further improvement to the strip detection method in foregoing the need for plant processing and user-initiated action for testing. In particular, an *in vivo* system would enable continuous monitoring of the disease for early detection and prevention of additional transmission.

In this study, we report the development of *P. stewartii*-sensing polydiacetylene (PDA) liposomes for future implementation into an *in vivo* lateral flow detection system for the pathogen in sweet corn [12]. PDA materials undergo unique optical transitions from blue to red in response to environmental stimuli such as pH [13, 14], temperature [15-17] and molecular binding events [18, 19]. These chromatic properties have resulted in the recent popularity of PDA for use in a range of biosensor applications [20-24]. Additionally, the ease of chemical modification and photopolymerization of PDA has made the material advantageous in the development of biocompatible liposomes for *in vivo* drug delivery systems [25-29]. The PDA liposomes reported in this study are conjugated with anti-*P. stewartii* antibodies for specific detection of the bacterium in liquid cultures. The liposomes displayed colorimetric transitions from blue to red in solutions of increasing concentration with the pathogen. Finally, injection of unconjugated PDA liposomes into live maize plants was demonstrated.

2. MATERIALS AND METHODS

2.1 Materials

Diacetylene (DA) monomer, 10,12-pentacosadiynoic acid (PCDA) was purchased from Spectrum Chemicals (Gardena, CA, USA) and 1,2-dimyristoyl-*sn*-glycero-3-phosphocholine (DMPC) was obtained from Avanti Polar Lipids, Inc. (Alabaster, AL, USA). Organic solvents were purchased from Fisher Scientific (Pittsburgh, PA, USA). Anti-*P. stewartii* antibody was from Agdia, Inc. (Elkhart, IN, USA). Luria Agar and Luria Broth were from Difco Laboratories (Detroit, MI, USA). Peters Excel 21-5-20 Mutli Purpose fertilizer solution was purchased from Everris (Dublin, OH, USA). All other compounds are research grade and were from Sigma Aldrich (St. Louis, MO, USA). Sweet corn (*Zea mays* var. Jubilee) seeds were obtained from Syngenta (Hemet, CA, USA).

2.2 Preparation of PDA Liposomes for P. stewartii Detection

A PDA liposome solution (188 nmol PCDA-N-hydroxysuccinimide (NHS), nmol PCDA 8813, and 6000 nmol DMPC) was prepared and incubated with 1 mg/mL anti-*P. stewartii* antibody before photopolymerization (Chapter 3, Section 2). Dynamic light scattering (DLS, Malvern Zetasizer Nano ZS90) analysis indicated the mean diameter of the liposomes was approximately 125 nm (Figure 7.S1).

2.3 Preparation of PDA Liposomes for In Vivo Injection

A 4.5 mM PDA liposome solution (13.5 mmol PCDA and 9 mmol DMPC) was used for *in vivo* injection into sweet corn. A solution of red PDA liposomes was produced by heat treatment above 60 ºC.

2.4 Bacterial Cultures

P. stewartii subsp. *stewartii* (DC283), *Xylella fastidiosa* subsp. *fastidiosa* (Temecula-1), and *Escherichia coli* BL21(DE3) were used in this study (Chapter 3, Section 5).

2.5 P. stewartii Detection and Sensor Analysis

PDA liposomes were incubated in solutions containing various concentrations of *P. stewartii* from 0 to 9.5 x 10^7 cells/mL in LB media at room temperature. Absorbance measurements were recorded by a spectrophotometer after 2 and 24 h incubation in bacterial cultures. Color Response (CR) was calculated as previously described [30] (Chapter 3, Section 4.1).

2.6 Sweet Corn Growth

Readers are referred to Chapter 3 (Section 6) for a detailed protocol for sweet corn growth.

2.7 Injection of PDA Liposomes into Sweet Corn

A laser-cut, light-impenetrable mask (Epilogue Zing 16 Laser) was placed on the adaxial (front) side of intact sweet corn leaves. The abaxial (back) side was additionally shielded from light with a square piece of aluminum foil. This induced artificial chlorosis on the leaf to increase the contrast between the leaf background and injected liposomes. 7 days following mask placement, blue and red PDA liposomes (4.5 mM) were injected into the abaxial side of an intact corn leaf via previously reported needleless syringe method [12]. The liposome-injected leaf was imaged using a Nikon D5100 digital camera every 24 h for 72 h. The mask was replaced each time after imaging to maintain color contrast and protect liposomes from non-specific transitioning due to sunlight exposure.

3. RESULTS AND DISCUSSION

Anti-*P. stewartii* antibody-conjugated PDA liposomes were incubated in solutions of varying concentrations from 0 to 9.5 x 10^7 cells/mL of *P. stewartii* at room temperature. After 2 h, the liposomes exhibited a range of colors from blue to red respective to increasing concentrations of *P. stewartii* (Figure 7.1A). The color shifts of the liposomes are reflected in their absorbance spectra as the absorption peak at 647 nm (PDA blue phase) decreases and the peak at 537 nm (PDA red phase) increases with increasing concentrations of *P. stewartii* (Figure 7.1B). CR analysis was performed to quantify the chromatic shifts of the liposomes in response to *P. stewartii* detection (Figure 7.1C). Previous reports have indicated that a CR of approximately 10-15% or greater is readily

discernable by the naked eye [21, 31]. Accordingly, three transitions and four colors were exhibited by the liposomes, blue, purple, pink, and red (Figure 7.1A, 7.1C). The first transition was at 4.2 x 10^7 cells/mL (15.9% CR, detection limit of the sensor), at which a blue to purple transition occurred. The second transition occurred at 6.3 x 10^7 cells/mL (49.1% CR), at which a purple to pink transition is denoted by a 33.2% CR difference between liposomes incubated in 4.2 and 6.3 x 10^7 cells/mL *P. stewartii*. The third pink to red transition was observed at 9.5 x 10^7 cells/mL (74.6% CR), at which a 25.5% CR increase occurred between liposomes in 6.3 and 9.5 x 10^7 cells/mL *P. stewartii*. The liposomes continued to transition over a 24-hour period (Figure 7.S2).

The detection limit of the strips at 4.2 x 10^7 cells/mL after 2 h is comparable to the bacterial load found in *P. stewartii*-infected corn leaf tissue at early stages of disease infection. Specifically, the bacterial load of infected leaf tissue approximately 6 days after transmission is ~1 x 10^{10} cfu/g plant tissue [32]. While the detection limit of current ELISA tests for the pathogen is in the range of 10^5 cells/mL [4, 33], the limit of detection for this sensor remains significant because it is well within the range of *in vivo* bacterial load one week after transmission. Additionally, the user-friendly advantage of the proposed *in vivo* sensor platform provides greater potential for the adoption of this sensor despite higher detection limits. This is reflected in the current preference of ELISA testing over PCR (detection limit ~10^2) for plant pathogen diagnostics due to the complicated protocols involved in PCR assays [7, 34, 35]. Consequently, the detection limit demonstrated by the current sensor suggests its relevance for early detection of *P. stewartii in vivo*, which is critical for disease management and prevention.

To evaluate the specificity of the sensor, the liposomes were incubated in solutions containing 9.5 x 10^7 cells/mL *X. fastidiosa* (causal agent of Pierce's disease in grapevine [36]) and *E. coli.* CR analysis of the liposomes after 2 h indicate that significant liposome transitions did not occur in solutions containing bacteria other than *P. stewartii* (Figure 7.2). Specifically, CR of liposomes incubated in 9.5 x 10^7 cells/mL *P. stewartii* are 25 times higher than those incubated in 9.5 x 10^7 cells/mL *E. coli* and 14 times higher than those in 9.5 x 10^7 cells/mL *X. fastidiosa* respectively.

Finally, unconjugated PDA liposomes were injected into an intact corn leaf to observe the visibility of the liposomes *in vivo*. First, we placed a light-impenetrable mask onto the leaf surface to induce artificial chlorosis and enhance the contrast between the color of injected PDA liposomes and the green leaf background (Figure 7.3). Liposomes were imaged immediately after injection and every 24 h over a 72 h period (Figure 7.4A). From visual observation, injected red liposomes in masked leaves were more distinguishable from the leaf background as compared to those injected in unmasked leaves (Figure 7.4B). Even more, the color of injected red liposomes remained visible after 72 h in the leaf. While the color of blue injected liposomes was not readily discernable from the green leaf background, a distinction between the red and blue injected liposomes can be distinguished. These observations demonstrate the visibility of a "positive" pathogen test by the unaided eye.

4. CONCLUSIONS

We have demonstrated a PDA liposome sensor for immunochromatic detection of *P. stewartii*. The detection limit of our sensor after 2 h is 4.2 x 10^7 cells/mL, which is in the range of the bacterial load inside infected leaf tissue within 6 days of disease transmission [32]. Additionally, we report the *in vivo* visibility of red PDA liposomes injected in an intact corn leaf over a 72 h period. These results indicate that this sensor is appropriate for the future development of an *in vivo* lateral flow detection platform for the disease.

5. FIGURES

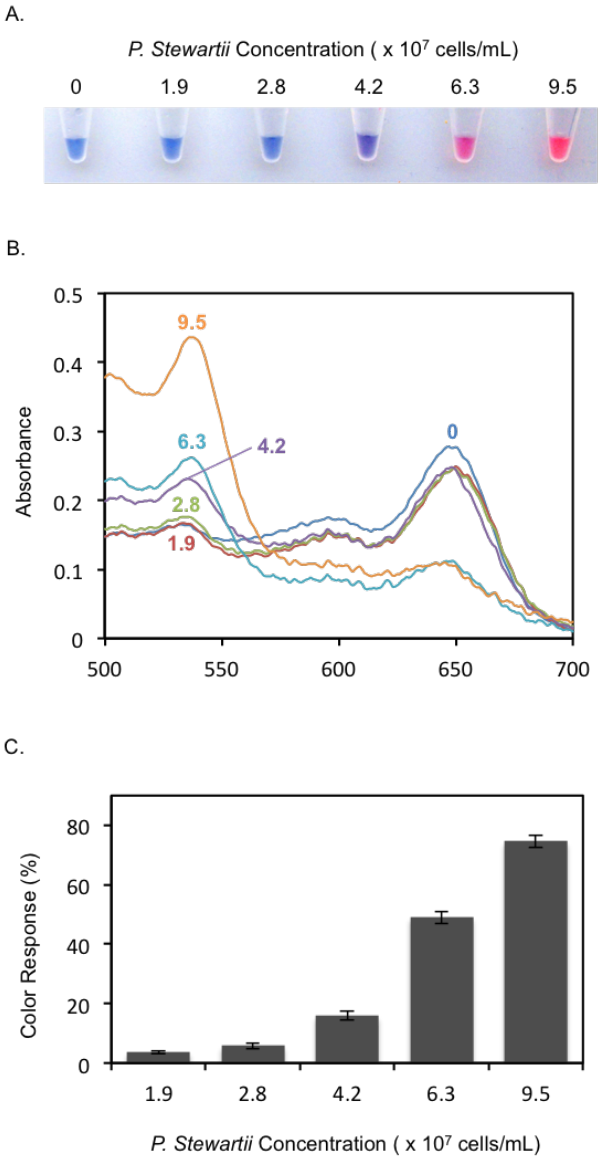

Figure 7.1. Color transitions (A), UV-Vis absorabance spectra (B) and color response (C) of PDA liposomes conjugated with anti-*P. stewartii* antibodies after 2 h incubation in *P. stewartii* solution. Color response data are represented as mean ± SD (n = 9).

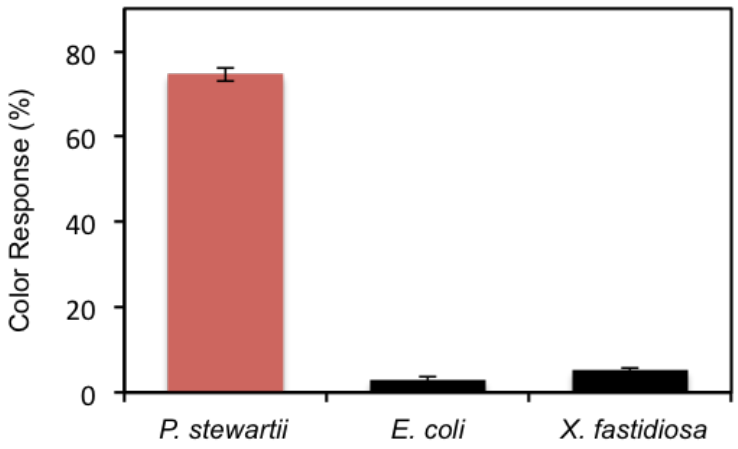

Figure 7.2. Color response of PDA liposomes after 2 h incubation in solutions containing 9.5 x 10^7 cells/mL *P. stewartii, E. coli, and X. fastidiosa.* All data are represented as mean ± SD (n = 3).

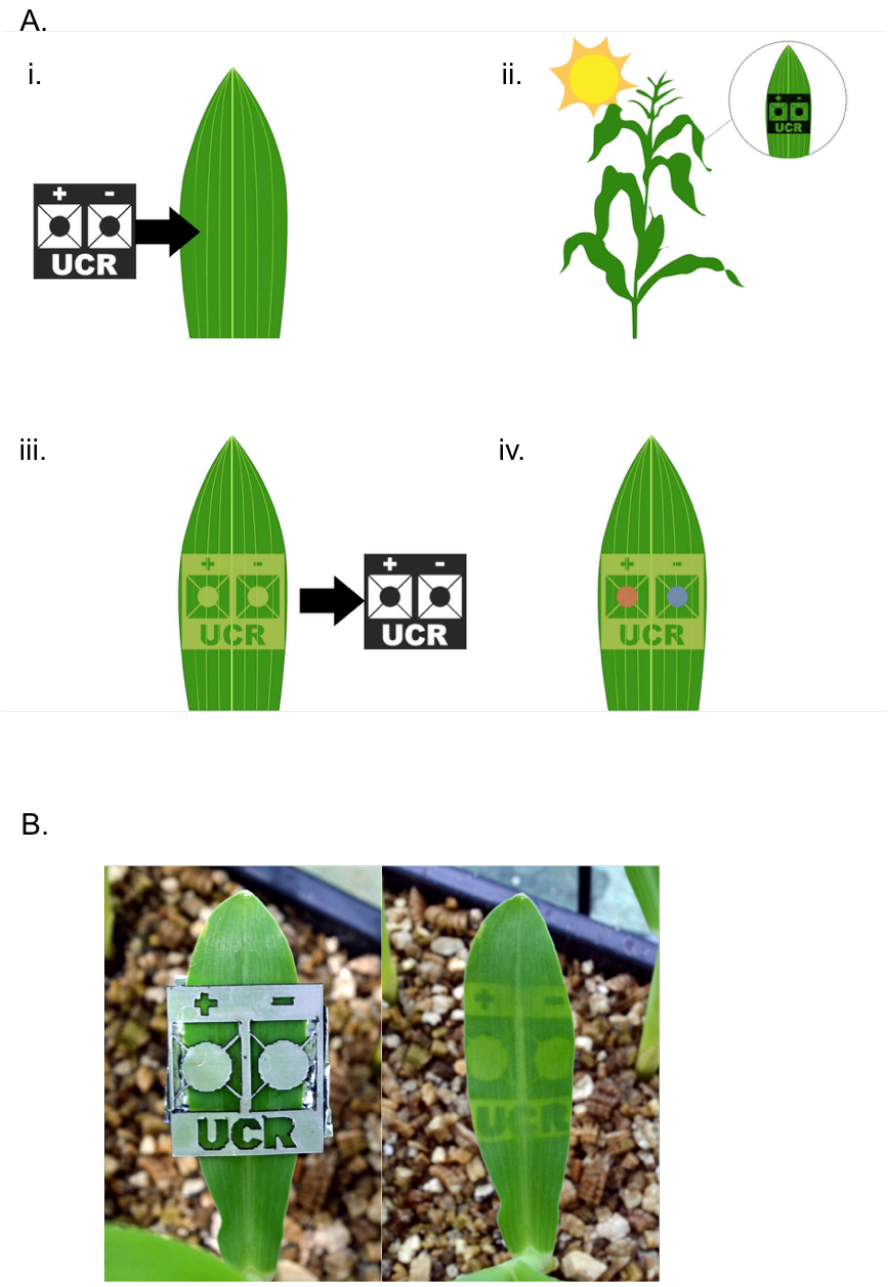

Figure 7.3. Injection of PDA liposomes in sweet corn leaf. (A) Process of patterned artificial chlorosis using a mask to enhance the contrast of injected colored liposomes. (B) Image of mask on leaf (left) and patterned chlorosis 7 days after mask placement (right).

A.

B.

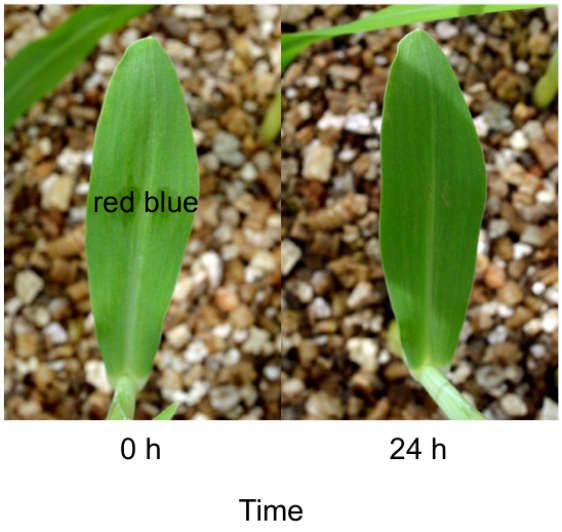

Figure 7.4. Images of injected liposomes. (A) Images of injected red (left side of leaf) and blue (right side of leaf) liposomes in a patterned (masked) leaf over 72 h. (B) Images of injected red (left side of leaf) and blue (right side of leaf) liposomes in a non-patterned (un-masked) leaf over 24 h.

References

[1] M.C. Roper, Pantoea stewartii subsp. stewartii: lessons learned from a xylem-dwelling pathogen of sweet corn, *Mol Plant Pathol*, 12(2011) 628-37.

[2] C. Block, J. Hill, D. McGee, Relationship between late-season severity of Stewart's bacterial wilt and seed infection in maize, *Plant Dis*, 83(1999) 527-30.

[3] E.H. Pepper, Stewart's bacterial wilt of corn: American Phytopathology Society; 1967.

[4] G.L. Lamka, J. Hill, D. McGee, E. Braun, Development of an immunosorbent assay for seedborne Erwinia stewartii in corn seeds, *Phytopathology*, 81(1991) 839-46.

[5] N.D. Freeman, J.K. Pataky, Levels of Stewart's wilt resistance necessary to prevent reductions in yield of sweet corn hybrids, *Plant Dis*, 85(2001) 1278-84.

[6] P. Michener, J. Pataky, D. White, Rates of transmitting Erwinia stewartii from seed to seedlings of a sweet corn hybrid susceptible to Stewart's wilt, *Plant Dis*, 86(2002) 1031-5.

[7] D.L. Coplin, D.R. Majerczak, Y. Zhang, W.-S. Kim, S. Jock, K. Geider, Identification of Pantoea stewartii subsp. stewartii by PCR and strain differentiation by PFGE, *Plant Dis*, 86(2002) 304-11.

[8] A. Wensing, S. Zimmermann, K. Geider, Identification of the corn pathogen Pantoea stewartii by mass spectrometry of whole-cell extracts and its detection with novel PCR primers, *Appl Envrion Microb*, 76(2010) 6248-56.

[9] J. Tambong, K. Mwange, M. Bergeron, T. Ding, F. Mandy, L. Reid, *et al.*, Rapid detection and identification of the bacterium Pantoea stewartii in maize by TaqMan® real-time PCR assay targeting the cpsD gene, *J Appl Microb*, 104(2008) 1525-37.

[10] S.P. Thapa, D.H. Park, C. Wilson, J.H. Hur, C.K. Lim, Multiplex PCR assay for the detection of Pantoea stewartii subsp. stewartii using species-specific genetic markers, *Australasian Plant Pathol*, 41(2012) 559-64.

[11] Y. Sun, S.-Z. Feng, X.-J. Guo, L.-W. Zhu, B. Zhou, J. Liu, *et al.*, Development of immunochromatographic strip for detection of enterohemorrhagic Escherichia coli O157, *Chin J Zoonoses*, 24(2008) 356-9.

[12] J.T. Wen, C. Castro, H. Tsutsui, *In planta* microsphere-based lateral flow leaf biosensor in maize, *J Lab Autom*, 20(2015) 500-5.

[13] Q. Cheng, R.C. Stevens, Charge-induced chromatic transition of amino acid-derivatized polydiacetylene liposomes, *Langmuir*, 14(1998) 1974-6.

[14] J. Song, Q. Cheng, S. Kopta, R.C. Stevens, Modulating artificial membrane morphology: pH-induced chromatic transition and nanostructural transformation of a bolaamphiphilic conjugated polymer from blue helical ribbons to red nanofibers, *J Am Chem Soc*, 123(2001) 3205-13.

[15] H. Beckham, M. Rubner, On the origin of thermochromism in cross-polymerized diacetylene-functionalized polyamides, *Macromolecules*, 26(1993) 5198-201.

[16] R. Chance, G. Patel, J. Witt, Thermal effects on the optical properties of single crystals and solution-cast films of urethane substituted polydiacetylenes, *J Chem Phys*, 71(1979) 206-11.

[17] R.R. Chance, R.H. Baughman, H. Muller, C.J. Eckhardt, Thermochromism in a Polydiacetylene Crystal, *J Chem Phys*, 67(1977) 3616-8.

[18] D.H. Charych, J.O. Nagy, W. Spevak, M.D. Bednarski, Direct colorimetric detection of a receptor-ligand interaction by a polymerized bilayer assembly, *Science*, 261(1993) 585-8.

[19] D.H. Charych, W. Spevak, J.O. Nagy, M.D. Bednarski, Specific interaction of influenza-virus with organized assemblies of polydiacetylenes, *Mater Res Soc Symp P*roc, 292(1993) 153-61.

[20] J. Lee, H.-J. Kim, J. Kim, Polydiacetylene liposome arrays for selective potassium detection, *J Am Chem Soc*, 13 (2008) 5010-1.

[21] Y.-l. Su, J.-r. Li, L. Jiang, Chromatic immunoassay based on polydiacetylene vesicles, *Colloid Surface B*, 38(2004) 29-33.

[22] M.-C. Lim, Y.-J. Shin, T.-J. Jeon, H.-Y. Kim, Y.-R. Kim, Microbead-assisted PDA sensor for the detection of genetically modified organisms, *Anal Bioanal Chem*, 400(2011) 777-85.

[23] M.A. Reppy, B.A. Pindzola, Biosensing with polydiacetylene materials: structures, optical properties and applications, *Chem Commun*, (2007) 4317-38.

[24] R. Jelinek, M. Ritenberg, Polydiacetylenes–recent molecular advances and applications, *RSC Adv* 3 (2013) 21192-201.

[25] E. Gravel, J. Ogier, T. Arnauld, N. Mackiewicz, F. Ducongé, E. Doris, Drug delivery and imaging with polydiacetylene micelles, *Chemistry*, 18(2012) 400-8.

[26] C. Guo, S. Liu, Z. Dai, C. Jiang, W. Li, Polydiacetylene vesicles as a novel drug sustained-release system, *Colloid Surface B*, 76(2010) 362-5.

[27] C. Guo, S. Liu, C. Jiang, W. Li, Z. Dai, H. Fritz, *et al*., A promising drug controlled-release system based on diacetylene/phospholipid polymerized vesicles, *Langmuir*, 25(2009) 13114-9.

[28] N. Mackiewicz, E. Gravel, A. Garofalakis, J. Ogier, J. John, D.M. Dupont, *et al*., Tumor-targeted polydiacetylene micelles for *in vivo* imaging and drug delivery, *Small*, 7(2011) 2786-92.

[29] X. Yan, X. An, Multifunctional polydiacetylene-liposome with controlled release and fluorescence tracing, *RSC Advances*, 4(2014) 18604-7.

[30] S. Okada, S. Peng, W. Spevak, D. Charych, Color and chromism of polydiacetylene vesicles, *Acc Chem Res*, 31(1998) 229-39.

[31] S. Kolusheva, L. Boyer, R. Jelinek, A colorimetric assay for rapid screening of antimicrobial peptides, *Nat Biotechnol*, 18(2000) 225-7.

[32] M.C. Roper, L.P. Burbank, K. Williams, P. Viravathana, H.-Y. Tien, S. von Bodman, A Large Repetitive RTX-Like Protein Mediates Water-Soaked Lesion Development, Leakage of Plant Cell Content and Host Colonization in the Pantoea stewartii subsp. stewartii Pathosystem, *Mol Plant Microbe Interact*, 28(2015) 1374-82.

[33] Y. Zhao, L. Liu, D. Kong, H. Kuang, L. Wang, C. Xu, Dual Amplified Electrochemical Immunosensor for Highly Sensitive Detection of Pantoea stewartii sbusp. stewartii, *ACS Appl Mater Interfaces*, 6(2014) 21178-83.

[34] Q. Huang, J. Bentz, J. Sherald, Fast, easy and efficient DNA extraction and one-step polymerase chain reaction for the detection of Xylella fastidiosa in potential insect vectors, *J Plant Pathol*, 88(2006) 77-81.

[35] N. Schaad, D. Opgenorth, P. Gaush, Real-time polymerase chain reaction for one-hour on-site diagnosis of Pierce's disease of grape in early season asymptomatic vines, *Phytopathology*, 92(2002) 721-8.

[36] J. Janse, A. Obradovic, Xylella fastidiosa: its biology, diagnosis, control and risks, *J Plant Pathol*, 92(2010) S1.35-48.

6. SUPPLEMENTARY DATA

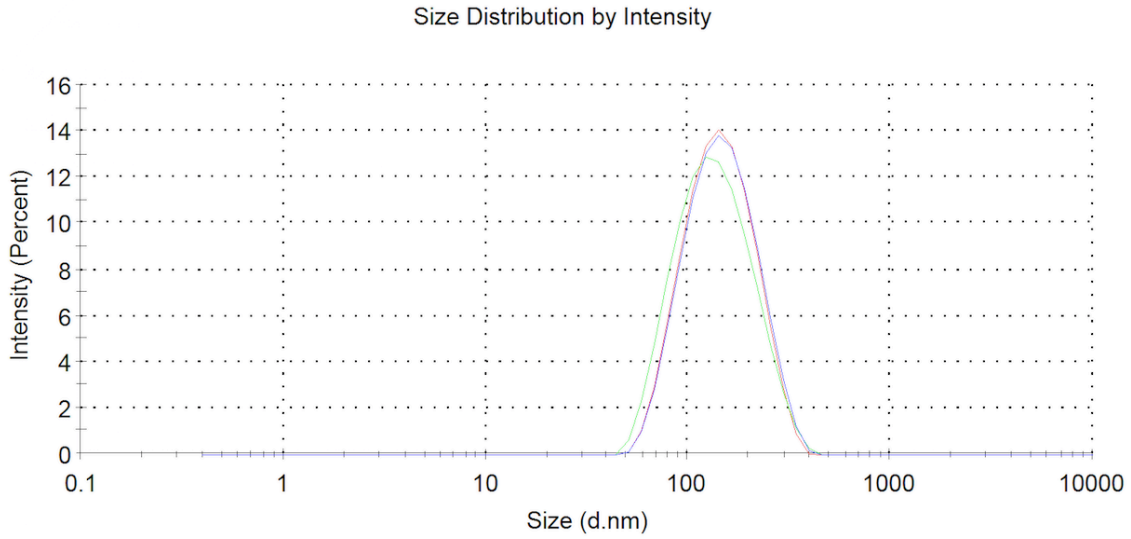

Figure 7.S1. DLS graph of PDA liposome size. All lines represent data recorded from a single sample.

6.1. Analysis of PDA liposomes after 24 h in X. fastidiosa Culture

PDA liposomes were incubated with varying concentrations of *X. fastidiosa* from 0 to 9.5 x 10^7 cells/mL for 24 h and absorption measurements were recorded by a spectrophotometer. CR analysis of the liposomes after 24 h indicate that the liposomes exhibited four colors and three color transitions discernable by the naked eye (Figure 7.S2). The limit of detection after 24 h was 2.8 x 10^7 cells/mL (20.6% CR), at which a blue to purple transition occurred. This detection limit is 1.5 times lower than that of liposomes after 2 h incubation in *P. stewartii* cultures (Figure 7.1). After 24 h, the second purple to pink transition was observed at 4.2 x 10^7 cells/mL (40.6% CR) and the third pink to red transition at 6.3 x 10^7 cells/mL (76.9% CR).

From an application perspective, this continual transition of the liposomes over 24 h is significant. Because the liposomes are expected to become implemented as injectable *in vivo* sensors, they will be embedded inside the leaf epidermis for periods of 24 h or more. This suggests that the detection limit and color transitions exhibited by the liposomes after 24 h are relevant for the purpose of developing an *in vivo* platform for plant pathogen detection.

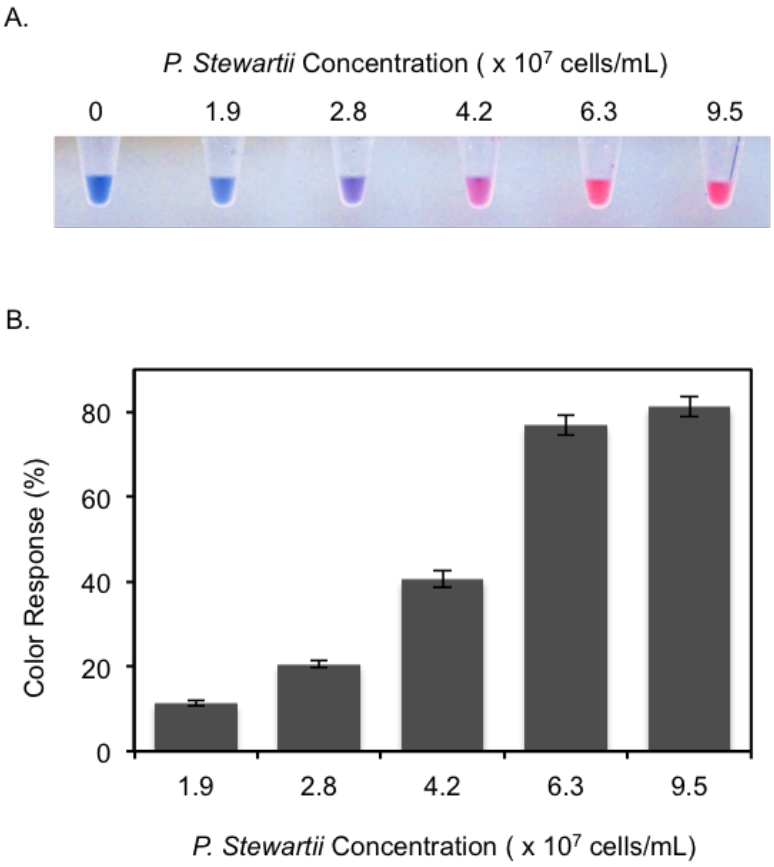

Figure 7.S2. Color transitions of PDA liposomes after 24 h incubation in *P. stewartii* cultures. Color response data are represented as mean ± SD (n = 9).

CHAPTER 8:

CONCLUSION

1. RESEARCH CONCLUSIONS

This research focused on the development of both *in vitro* and *in vivo* polydiacetylene (PDA)-based sensors for plant diagnostic applications. In particular, the *in vitro* devices reported in this work included PDA-coated polyvinylidene fluoride (PVDF) strips for equipment-free, naked-eye detection of plant nutrient, Zn^{2+}, and xylem-limited plant bacterium, *Xylella fastidiosa.* Furthermore, an *in vivo* pathogen detection platform was presented that utilizes the plant leaf itself as the substrate for a lateral flow detection system in maize. Lastly, injectable PDA liposome sensors were developed for the detection of apoplast-colonizing bacterium, *Pantoea stewartii*.

The Zn^{2+}-sensing strips were conjugated with Zn^{2+}-specific DNA hairpin aptamers. These strips exhibited two color transitions and three colors, blue, purple and pink/red, after 4 h in Zn^{2+} solutions. The first blue to purple transition occurred at 125 μM Zn^{2+} (detection limit), which aligns with the lower limit of critical Zn^{2+} levels for many healthy food crops [1]. In addition, the second transition occurred at 500 μM Zn^{2+}, which aligns with the upper limit of critical Zn^{2+} levels in many food crops.

PDA-coated PVDF strips were additionally conjugated with anti-*X. fastidiosa* antibodies for immunochromatic detection of *X. fastidiosa*. These strips exhibited three color transitions and four colors, blue, indigo, purple, and pink. After 4 h in solutions containing the bacterium, the detection limit of the sensor was at 0.8×10^8 cells/mL. This threshold is comparable to bacterial load found in grapevine leaf tissue approximately 18 days following *X. fastidiosa* transmission [2]. Consequently, the detection limit of these strips is appropriate for early detection of *X. fastidiosa* infection of grapevine.

Next, a proof-of-concept study was demonstrated prior to the development of an *in vivo* detection system for apoplast-colonizing plant bacterial pathogens. Specifically, 0.5 μm anti-fluorescein antibody-conjugated fluorescent microspheres were injected into the abaxial leaf apoplast of maize plants. Then, plants were grown in solutions containing fluorescein (mock pathogen) for 72 h and the injected microspheres were analyzed for fluorescein capture. A positive correlation was observed between the levels of fluorescein captured and plants grown in increasing concentrations of fluorescein solution.

Finally, PDA liposome sensors were fabricated for the colorimetric detection of model apoplast-colonizing bacterium, *P. stewartii*. The liposomes were conjugated with anti-*P. stewartii* antibodies for specific detection of the bacterium in solution. After 2 h, the detection limit of this sensor was at 4.2×10^7 cells/mL, which is under the threshold of bacterial loads found in infected sweet corn leaf tissues approximately 6 days after disease transmission [3]. Subsequently, unconjugated liposomes were injected into sweet corn plants. Patterned artificial chlorosis of corn leaves was induced with a light-imprenetrable mask to enhance contrast between the color of injected liposomes and the leaf background. The visibility of injected red liposomes in chlorosis-patterned leaves was observed and distinguished from injected blue liposomes.

2. FUTURE DIRECTIONS

Future improvements for the pathogen-sensing strips and liposomes include an expansion of the detection range of the sensor. The current strips and liposomes detect pathogen

levels within the range of ~10^8 and ~10^7 cells/mL respectively. However, since bacterial loads can vary widely from 0 to 10^{10} cells/mL in the first 30 days after disease transmission [2, 4], it would be advantageous for the sensors to exhibit a wider detection range for more precise discriminations of disease progression. Accordingly, a decrease in the detection limit of both sensors is additionally desirable. In particular, a detection limit comparable or lower than that of current ELISA assays for plant pathogens (~10^5 cells/mL [5, 6]) is needed.

Future advancements for the *in vivo* detection platform include the injection and analysis of *P. stewartii*-sensing liposomes in sweet corn plants inoculated with the pathogen. A long-term research plan includes the fabrication of a user-friendly device for quick and easy injection of the sensor accompanied by the development of a simple and efficient disease diagnostics protocol for the detection system (Figure 8.1). The success of the proposed future endeavors for both the diagnostic strips and the *in vivo* pathogen detection system has great potential to provide a lasting impact and improve plant disease diagnostics not only in developing countries, but also across the agricultural industry worldwide.

3. FIGURES

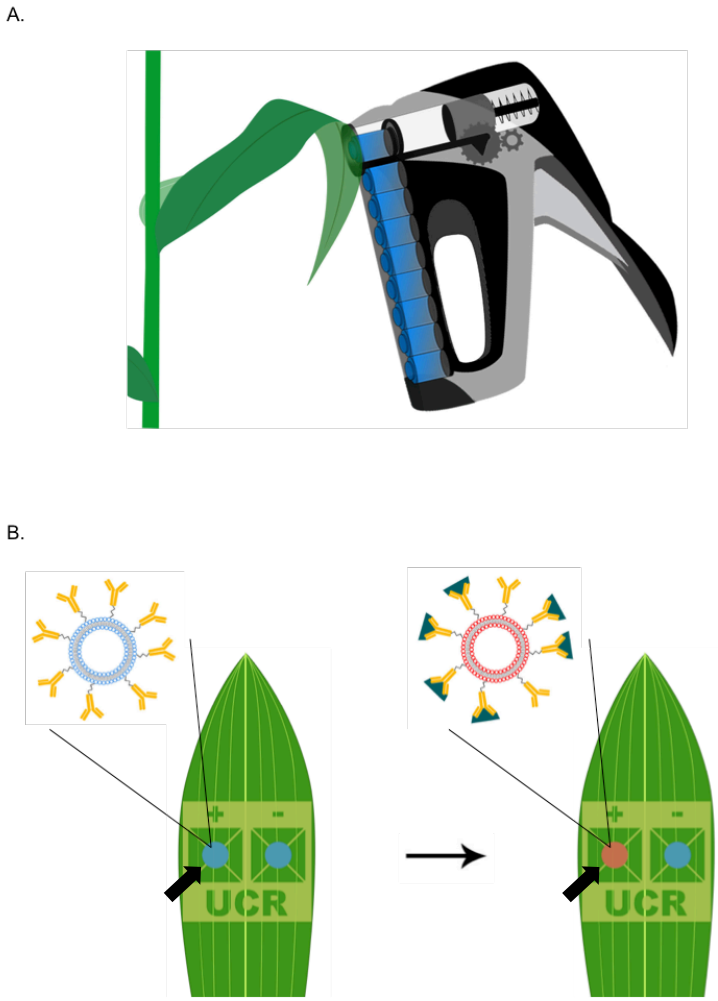

Figure 8.1. Future directions for the *in vivo* pathogen detection system. (A) A user-friendly device facilitates the injection of PDA liposome sensors into the plant leaf apoplast. (B) A healthy plant (left) is indicated by a blue spot in the detection zone (black arrows), whereas a pathogen-infected plant (right) is indicated by a red spot in the detection zone.

References

[1] B.J. Alloway, Zinc in soils and crop nutrition, Brussels, Belgium: International Zinc Association 2004.

[2] B. Hill, A. Purcell, Multiplication and movement of Xylella fastidiosa within grapevine and four other plants, *Phytopathology*, 85(1995) 1368-72.

[3] M.C. Roper, L.P. Burbank, K. Williams, P. Viravathana, H.-Y. Tien, S. von Bodman, A Large Repetitive RTX-Like Protein Mediates Water-Soaked Lesion Development, Leakage of Plant Cell Content and Host Colonization in the Pantoea stewartii subsp. stewartii Pathosystem, *Mol Plant Microbe Interact*, 28(2015) 1374-82.

[4] B. Hill, A. Purcell, Populations of Xylella fastidiosa in plants required for transmission by an efficient vector, *Phytopathology*, 87(1997) 1197-201.

[5] D. Carbajal, K.A. Morano, L.D. Morano, Indirect immunofluorescence microscopy for direct detection of Xylella fastidiosa in xylem sap, *Curr Micrbiol*, 49(2004) 372-5.

[6] G.L. Lamka, J. Hill, D. McGee, E. Braun, Development of an immunosorbent assay for seedborne Erwinia stewartii in corn seeds, *Phytopathology*, 81(1991) 839-46.